

THERMAL PERFORMANCE AND DESIGN GUIDELINES OF THERMO-ACTIVE FOUNDATIONS

By

BYUNG CHANG KWAG

B.S., Architectural Engineering, Hanyang University, 2009

M.S., Civil, Environmental, and Architectural Engineering, University of Colorado, 2012

A thesis submitted to the

Faculty of the Graduate School of the

University of Colorado in partial fulfillment

Of the requirement for the degree of

Doctor of Philosophy

Department of Civil, Environmental, and Architectural Engineering

2015

This thesis entitled:

THERMAL PERFORMANCE AND DESIGN GUIDELINES OF THERMO-ACTIVE FOUNDATIONS

Written by Byung Chang Kwag

has been approved for the Department of Civil, Environmental, and Architectural Engineering

by

Moncef Krarti (Advisor)

Michael J. Brandemuehl, Ph.D

John Z. Zhai, Ph.D

Wil V. Srubar III, Ph.D

Junghyon Mun, Ph.D (UNT)

Date

The final copy of this thesis has been examined by the signatories, and we find that both the content and the form meet acceptable presentation standards of scholarly work in the above mentioned discipline.

Kwag, Byung Chang (PhD., Civil, Environmental, and Architectural)

THERMAL PERFORMANCE AND DESIGN GUIDELINES OF THERMO-ACTIVE FOUNDATION SYSTEMS

A thesis directed by Professor Moncef Krarti, Ph.D., PE, LEEP® AP

A thermo-active foundation system can be a cost-effective technology to utilize ground thermal energy to heat and cool buildings. Indeed, thermo-active foundations, also known as thermal piles, integrate heat exchangers with the foundation elements and thus eliminate the need of drilling deep boreholes typically required by the conventional ground source heat pumps. In order to properly design thermo-active foundation systems, their thermal performance under various operating and climatic conditions are evaluated as part of this study using detailed modeling and simulation analyses. In particular, a transient three-dimensional finite difference numerical model has been developed and validated to analyze thermal performances of thermo-active foundations. The numerical model is then used to assess the impact of design parameters such as foundation depth, shank space, fluid flow rate, and the number of loops on the effectiveness of thermal piles to exchange heat between the building and the ground. Moreover, thermal response factors have been developed to integrate the performance of thermo-active foundations within detailed whole-building simulation programs. In this study, response factors specific to thermo-active foundations are implemented into EnergyPlus to investigate the impact of design and operating conditions. The results from the detailed simulation analysis are then used to develop a set of guidelines to properly design thermo-active foundation to meet heating and cooling loads of commercial buildings.

This paper develops the design guide chart for TAF systems. The design guide chart provides the determination of required heat exchanger pipe length per water-to-water heat pump capacity for

certain annual average ground temperature and for certain targeted maximum entering water temperature to a heat pump. Using an example application, this paper presents the usage of the design guide chart as well as shows the potential of the design guide chart for designing TAF system.

ACKNOWLEDGEMENT

I would like to thank to my advisor professor Moncef Krarti for his guidance and support for this research. He gave me encouragement not only for this research, but also for my general academic achievements at University of Colorado at Boulder. His knowledge, patience, comments and suggestions throughout my research were always invaluable.

I also want to thank my all committee members: Michael J. Brandemuehl, John Z. Zhai, Wil Srubar, and Junghyon Mun. As my committee, they provided me insights and suggestions for this research. In addition, John S. McCartney was my former committee member, and he also provided me valuable experimental data and good suggestions for my research. I really appreciate their willingness to serve on my committee as well as their encouragement throughout this research.

Last but not least, I would like to express the greatest gratitude to my family who has supported me throughout my long and endless journey towards the degree. Especially my wife Namhee Kim and my son Isaac Moongyu Kwag always showed me their love, and so I was always happy with them. I also special thank my parents, parents in law, my brother and his wife, and my sister-in law and her family for their valuable advice and supports.

TABLE OF CONTENTS

TABLE OF CONTENTS	vi
TABLES	ix
FIGURES	xii
CHAPTER 1. INTRODUCTION.....	1
CHAPTER 2. BACKGROUND AND LITERATURE REVIEW	7
2.1. Ground Coupled Heat Exchanger.....	7
2.2. Existing Ground-Coupled Heat Exchanger Models	13
2.2.1. Analytical Methods	13
2.2.2. Numerical Methods.....	22
2.3. Thermo-active Foundation Systems	24
2.4. Summary.....	28
CHAPTER 3. TRANSIENT THREE-DIMENSIONAL NUMERICAL MODELING	29
3.1. Model Description.....	29
3.2. Three-dimensional Finite Difference Method in Cartesian Coordinates	32
3.3. Analysis of impact of grid discretization	37
3.4. Validation Analysis of the Three-Dimensional Numerical Model	39
3.4.1. Validation Method Description	39
3.4.2. Results	41
3.5. Comparison Analysis –Cartesian Model vs. Cylindrical Model.....	45
3.6. Sensitivity Analysis.....	48
3.6.1. Impact of foundation depth.....	51
3.6.2. Impact of fluid velocity	52
3.6.3. Impact of the shank space	54
3.6.4. Impact of the thermal conductivity of ground.....	55
3.6.5. Impact of the thermal conductivity of concrete	56
3.6.6. Impact of insulation level of slab-on floor	58
3.6.7. Thermal Interferences of neighboring thermal pile.....	58
3.7. Summary.....	66

CHAPTER 4.	ANALYSIS FOR THERMAL COUPLING	69
4.1.	Introduction.....	69
4.2.	Simulation Settings	70
4.2.1.	Description of numerical model	70
4.2.2.	Grid sensitivity analysis.....	71
4.2.3.	Sensitivity analysis	73
4.3.	Correlation between Design Parameters and Performance of TAFs Piles	74
4.3.1.	Formularization of the correlation between design parameters.....	74
4.3.2.	Verification of the new formularization for heat transfer through thermal piles.....	81
4.4.	Ground-Coupled Heat Transfer Caused by TAFs System	82
4.4.1.	Formularization of the correlation between design parameters.....	82
4.4.2.	Verification of the new formularization of heat transfer through ground floor	87
4.5.	Summary.....	89
CHAPTER 5.	THERMAL RESPONSE FACTOR MODEL.....	90
5.1.	Introduction.....	90
5.2.	Modification of the G-function Calculation for Several Configurations of a Pile Foundation91	
5.2.1.	Circular Sectional Foundation.....	92
5.2.2.	Rectangular Sectional Foundation.....	95
5.2.3.	Equilateral Triangular Sectional Foundation.....	98
5.2.4.	The Modified G-function Equations	99
5.2.5.	The Fractional Shape Factor for the Modified Thermal Response Factor.....	100
5.2.6.	Verification Analysis of the Modified Thermal Response Factor Model	103
5.3.	The Effect of Indoor Air Temperature on the G-function	107
5.3.1.	Develop of the G-function Calculation for the Effect of Indoor Air Temperature	107
5.3.2.	Comparative Analysis of Modified G-functions	110
5.3.3.	Sensitivity Analysis of the G-function Calculation	115
5.4.	Summary.....	120
CHAPTER 6.	INTEGRATION OF THERMO-ACTIVE FOUNDATION MODELING IN ENERGYPLUS 123	
6.1.	Introduction.....	123

6.2.	Application to Medium Sized Office Building	124
6.2.1.	Building Description	125
6.2.2.	Modeling Approach.....	127
6.2.3.	Discussion of Selected Results	128
6.3.	Application to Residential Building	131
6.3.1.	Building Description	131
6.3.2.	Modeling Approach.....	133
6.3.3.	Discussion of Selected Results	135
6.4.	Summary.....	138
CHAPTER 7.	DESIGN GUIDELINES FOR THERMO-ACTIVE FOUNDATIONS	139
7.1.	Background.....	139
7.2.	Description of the Case Model Simulated in EnergyPlus.....	140
7.3.	Description of the Climate Conditions	143
7.4.	Design Guide Chart for Thermo-Active Foundations	144
7.4.1.	Evaluation of Heat Exchanger Pipe Length per Heat Pump Capacity	144
7.4.2.	Example Applications.....	147
7.5.	Summary and conclusions	155
CHAPTER 8.	SUMMARY AND FUTURE WORK	157
8.1.	Summary.....	157
8.2.	Future work	160
REFERENCES	162	

TABLES

Table 2-1: Common Heat Pump Sources and Sinks (ASHRAE Handbook – HVAC Systems and Equipment 2008).....	10
Table 3-1: The characteristics of the ground domain and foundation	30
Table 3-2: Features of U-tube pipes	30
Table 3-3: Features of the fluid circulating in the U-tube pipes	31
Table 3-4: Thermal properties of the floor insulation material	31
Table 3-5: The impact of grid node numbers of both CPU time and RMSE values for the numerical solution	37
Table 3-6: Basic dimensions of the small-scale thermo-active foundation model used in the experimental analysis	40
Table 3-7: Coordinates of the probe locations for the experiment test.....	40
Table 3-8: Thermal conductivities of the materials used in the experimental set-up.....	41
Table 3-9: RMSE values between model predictions and measurements during five hours	42
Table 3-10: The RMSE results of the calibrations	43
Table 3-11: Boundary Conditions.....	46
Table 3-12: Probe locations for validation analysis	47
Table 3-13: RMSE results of validation analysis.....	47
Table 3-14: The boundary conditions and the initial conditions of the base case in the sensitivity analyses.....	50
Table 3-15: Summary of boundary and initial conditions of the numerical model for a thermo-active foundation with multiple thermal piles.....	59
Table 4-1: Description of sizes of the numerical model	70
Table 4-2: Description of inputs of numerical model	70
Table 4-3: The impact of grid node numbers on both CPU time and RMSE values for numerical simulations.....	72
Table 4-4: Description of settings for sensitivity analysis.....	73

Table 4-5: Description of foundation sizes for sensitivity analysis	73
Table 5-1: The modified G-function equations for different cross-sectional configurations of thermo-active foundation.....	100
Table 5-2: The hydraulic diameters for different configurations of foundation section	102
Table 5-3: Summary of specifications of the energy foundation.....	111
Table 5-4: Summary of assumptions in thermal properties of the model	112
Table 5-5: Typical soil thermal conductivity values (ASHRAE Fundamental, SI & IP, 2009)	119
Table 6-1: The description of the base prototypical multi-family residential building	125
Table 6-2: The peak demand of the baseline for different U.S. climate conditions	126
Table 6-3: Cooling/heating energy savings associated with plants	129
Table 6-4: Average utility rate of different states of U.S. (U.S. Energy Information Administration, 10/2014).....	129
Table 6-5: Energy costs and percent energy cost savings.....	129
Table 6-6: Overview of initial costs of cooling/heating systems	130
Table 6-7: The description of the base prototypical multi-family residential building	132
Table 6-8: The peak demand of the baseline for different U.S. climate conditions	133
Table 6-9: Cooling/heating energy savings associated with plants	136
Table 6-10: Average utility rate of different states of U.S. (U.S. Energy Information Administration, 10/2014).....	136
Table 6-11: Energy costs and percent energy cost savings.....	136
Table 6-12: Overview of initial costs of cooling/heating systems	137
Table 7-1: The input data used for modeling TAF system in EnergyPlus.....	142
Table 7-2: Specifications of geothermal heat pump systems (Manufacturer of NSW model – WaterFurnace, and Manufacturer of RWXW model – Johnson Controls)	142
Table 7-3: Summary of selected US sites and associated ASHRAE climate zones used in the energy analysis (ASHRAE Standard 90.1-2004).....	143
Table 7-4: Simulation results in maximum entering water temperature for Chicago, IL.	149

Table 7-5: Comparison of linear interpolation result of the simulations and the prediction of design guide chart.....	150
Table 7-6: Simulation results in maximum entering water temperature for New York, NY	152
Table 7-7: Comparison of linear interpolation result of the simulations and the prediction of design guide chart.....	153
Table 7-8: Simulation results in maximum entering water temperature for Chicago, IL.	155
Table 7-9: Comparison of linear interpolation result of the simulations and the prediction of design guide chart.....	155

FIGURES

Figure 1-1: Horizontal GSHP systems with parallel pipes (left) and with series pipes (right).....	2
Figure 1-2: Typical configuration for vertical GSHP systems	3
Figure 1-3: Schematic configuration for a TAF system	3
Figure 2-1: Typical vapor compression cycle (a) schematic and (b) P-h diagram (Energy Audit 2nd edition, Krarti)	8
Figure 2-2: Closed Vapor Compression Cycle (ASHRAE Handbook HVAC Systems and Equipment 2008).....	9
Figure 2-3: Ground-Coupled Heat Pump System for cooling season (left) and for heating season (right)	11
Figure 2-4: Temperature response factors (G-functions) for multiple borehole configurations (Spitler 2000).....	23
Figure 2-5: A schematic image of pie-sector approach: the borehole region on the numerical model domain is discretized using the pie-sector approximation for the U-tube pipes (left), the pie-sector representation of the U-tube pipes (right).....	24
Figure 3-1: Simplified three-dimensional Cartesian numerical model	29
Figure 3-2: The boundary conditions for numerical modeling	30
Figure 3-3: Schematic drawing of non-uniform grids	32
Figure 3-4: Control Volume of a regular node	32
Figure 3-5: Variation of CPU time and RMSE value associated with the numerical solution as functions of the number of the grid nodes.....	38
Figure 3-6: A scale-model for a thermo-active foundation set-up (Stewart et al., 2012)	39
Figure 3-7: The variations of the fluid inlet and outlet temperatures, and the ambient temperature of the experimental data, (Stewart et al., 2012)	41
Figure 3-8: The results of sensitivity analyses of validation analysis for individual variable	43
Figure 3-9: The temperature variations of the calibrated numerical model and the experiment at the probe around the foundation (radius = 50.8mm, depth = 190.5mm)	44

Figure 3-10: The temperature variations of the calibrated numerical model and the experiment at the probe within the foundation (radius = 0mm, depth = 190.5mm)	44
Figure 3-11: Variation of fluid outlet temperature with time based on model predictions and testing measurements	45
Figure 3-12: 3D numerical models for validation analysis: (left) Cartesian model, and (right) Cylindrical model.....	46
Figure 3-13: The scheme of the floor heat transfer.....	49
Figure 3-14: The impact of foundation depth for various normalized fluid velocities on the U-tube heat transfer	52
Figure 3-15: The impact of foundation depth for various normalized fluid velocities on the floor heat transfer	52
Figure 3-16: The impact of fluid velocity for various normalized foundation depth on the U-tube heat transfer	53
Figure 3-17: The impact of fluid velocity for various normalized foundation depth on the floor heat transfer	53
Figure 3-18: The impact of shank space ratio for various foundation radii on the U-tube heat transfer.....	54
Figure 3-19: The impact of shank space ratio for various foundation radii on the floor heat transfer.....	55
Figure 3-20: The impact of the thermal conductivity of ground for various thermal conductivity of concrete on the U-tube heat transfer	56
Figure 3-21: The impact of the thermal conductivity of ground for various thermal conductivity of concrete on the floor heat transfer	56
Figure 3-22: The impact of the thermal conductivity of concrete for various thermal conductivity of ground on the U-tube heat transfer	57
Figure 3-23: The impact of the thermal conductivity of concrete for various thermal conductivity of ground on the floor heat transfer	57
Figure 3-24: Effect of insulation level of above-grade floor on ground-coupled floor heat transfer.....	58

Figure 3-25: Temperature isotherms of different thermo-active foundations with variable number of thermal piles during the winter season; the center-to-center distance between piles is (a) 3.3m, (b) 5m, (c) 10m, and (d) 20m, $T_{out}=0.28^{\circ}\text{C}$, $T_{in}=22^{\circ}\text{C}$	62
Figure 3-26: Temperature isotherms of different thermo-active foundations with variable number of thermal piles during the summer season; the center-to-center distance between piles is (a) 3.3m, (b) 5m, (c) 10m, and (d) 20m, $T_{out}=29.7^{\circ}\text{C}$, $T_{in}=22^{\circ}\text{C}$	65
Figure 3-27: Thermal interactions between adjacent thermal piles for several pile aspect ratios	66
Figure 4-1: Schematic image of numerical model	70
Figure 4-2: Variations of CPU time and RMSE values associated with the numerical solutions as functions of the number of the grid nodes.....	72
Figure 4-3: Configurations of number of foundations	74
Figure 4-4: The variation of pipe heat transfer for different distance between piles for different pile depth: (a) depth=3m, (b) depth=5m, (c) depth=10m, (d) depth=15m, (e) depth=20m	76
Figure 4-5: The variation of pipe heat transfer for different distance between piles, for different diameter of thermal pile: (a) $F_x, F_y=0.5\text{m}$, (b) $F_x, F_y=0.6\text{m}$, (c) $F_x, F_y=0.7\text{m}$, (d) $F_x, F_y=0.8\text{m}$, (e) $F_x, F_y=1.0\text{m}$	78
Figure 4-6: Comparison analysis between actual data from a numerical model and predicted data from a simplified model.....	80
Figure 4-7: Verification analysis by comparing actual data from a numerical model and predicted data from a simplified model	81
Figure 4-8: Scatter diagram to compare the predictions of the annual average heat transfer through heat exchanger pipes with the actual data from a numerical model	82
Figure 4-9: The variation of floor heat transfer for different distance between piles for different pile depths: (a) depth=5m, (b) depth=10m, (c) depth=15m, (d) depth=20m.....	84
Figure 4-10: The effect of foundation depth for ground floor heat transfer.....	85
Figure 4-11: Comparison analysis between actual data from a numerical model and predicted data from a simplified model.....	86
Figure 4-12: Verification analysis by comparing actual data from a numerical model and predicted data from a simplified model	88

Figure 4-13: Scatter diagram to compare the predictions of the annual average heat transfer through ground floor with the actual data from a numerical model	88
Figure 5-1: Superposition of piece-wise linear step heat inputs (Spitler, 2000)	90
Figure 5-2: Configurations of a circular sectional foundation	94
Figure 5-3: Configurations of a rectangular sectional foundation.....	95
Figure 5-4: Configurations of an equilateral triangular sectional foundation	98
Figure 5-5: Long-time step G-function variation (with $t_s = H^2/9\alpha$)	105
Figure 5-6: Short-time step G-function variation.....	106
Figure 5-7: Long-time step and short-time step G-function obtained from the 3-D numerical model	107
Figure 5-8: The scheme of thermal response factor model for TAF systems	108
Figure 5-9: Foundation wall temperature variations and G-function curves of the cases with/without thermal effect of indoor air temperature, AR=5.0	110
Figure 5-10: The inlet fluid temperatures, and outlet fluid temperatures of actual data, and of predicted data for typical week in the summer season	113
Figure 5-11: The inlet fluid temperatures, and outlet fluid temperatures of actual data, and of predicted data for typical week in the winter season	113
Figure 5-12: Scatter diagram to compare the predictions of the outlet fluid temperature and actual outlet fluid temperature for winter season	114
Figure 5-13: Scatter diagram to compare the predictions of the outlet fluid temperature and actual outlet fluid temperature for summer season	114
Figure 5-14: Foundation wall temperature variations of single TAF pile for different aspect ratios (ARs) without consideration of indoor air temperature (above) and with consideration of indoor air temperature (down)	116
Figure 5-15: G-function curves of single TAF pile for different aspect ratios (ARs) without consideration of indoor air temperature (above) and with consideration of indoor air temperature (down)	117
Figure 5-16: G-function curves of single TAF pile for different indoor air temperature settings for the aspect ratio of a thermal pile AR=20 with annual average ground temperature of 9.7°C	118

Figure 5-17: Apparent thermal conductivity for moist soils (Source: ASHRAE Fundamental, 2009)	119
Figure 5-18: G-function curves for different soil thermal conductivities (ksoil).....	120
Figure 6-1: Example medium-sized office building modeled in EnergyPlus	125
Figure 6-2: Monthly average outdoor air dry-bulb temperature of Boulder, CO., Chicago, IL, and New York, NY. (Sources: Boulder TMY2 724699, Chicago TMY3 725300, New York TMY3 744860)	126
Figure 6-3: Schematic drawings for (a) cooling system loop, and (b) heating system loop coupled with water-to-water heat pump and ground coupled heat exchangers modeled in EnergyPlus.....	127
Figure 6-4: Foundation locations of the prototypical multi-family residential building.....	128
Figure 6-5: Example multi-family residential building modeled in EnergyPlus	131
Figure 6-6: Monthly average outdoor air dry-bulb temperature of Boulder, CO., Chicago, IL, and New York, NY.....	133
Figure 6-7: Schematic drawings for (a) cooling system loop, and (b) heating system loop coupled with water-to-water heat pump and ground coupled heat exchangers modeled in EnergyPlus.....	134
Figure 6-8: Foundation locations of the prototypical multi-family residential building.....	135
Figure 7-1: Schematic 3D image and floor plan of the medium sized office building	141
Figure 7-2: Schematic HVAC system with ground heat exchangers and a geothermal heat pump as modeled in EnergyPlus	141
Figure 7-3: US ASHRAE Climate zones (ASHRAE Standard 90-1-2004)	143
Figure 7-4: Average heat transfer rate per heat exchanger pipe length [W/m] as a function of entering water temperature for an annual average ground temperature of 7.3°C (45.1°F) representing Cheyenne, WY.	145
Figure 7-5: Average heat transfer rate per heat exchanger pipe length [W/m] as a function of entering water temperature for an annual average ground temperature of 9.7°C (49.5°F) representing Boulder, CO.....	145
Figure 7-6: Average heat transfer rate per heat exchanger pipe length [W/m] as a function of entering water temperature for an annual average ground temperature of 12.4°C (54.3°F) representing New York, NY.	146

Figure 7-7: Design guide chart for thermo-active foundations ($k_{soil}=1.3 \text{ W/m-K}$, $k_{conc}=1.8 \text{ W/m-K}$)	147
Figure 7-8: Foundation locations for the example of the medium sized office building	148
Figure 7-9: Example of using design guide chart for thermo-active foundations ($k_{soil}=1.3 \text{ W/m-K}$, $k_{conc}=1.8 \text{ W/m-K}$)	149
Figure 7-10: Linear relationship between water-to-water heat pump capacity and maximum EWT for the example model with 77-10m thermal piles in Chicago, IL	150
Figure 7-11: Linear relationship between water-to-water heat pump capacity and minimum COP for cooling mode for the example model with 77-10m thermal piles in Chicago, IL.	150
Figure 7-12: Location of foundation piles for the case study office building in New York, NY.	151
Figure 7-13: Design guide for thermo-active foundation system for small sized office building in New York, NY ($k_{soil}=1.3 \text{ W/m-K}$, $k_{conc}=1.8 \text{ W/m-K}$)	152
Figure 7-14: Location of foundation piles for the multi-family residential building in Chicago, IL	154
Figure 7-15: Design guide for thermo-active foundation system for the multi-family residential building in Chicago, IL ($k_{soil}=1.3 \text{ W/m-K}$, $k_{conc}=1.8 \text{ W/m-K}$)	154

CHAPTER 1. INTRODUCTION

1.1. Introduction

The global energy crisis and the increasing interest in environmental impact of greenhouse emissions have led to the need to explore alternatives of low-cost and clean energy sources. While distribution generation technologies such as applications of solar energy, wind power, and biomass have been considered and integrated with the built environment, geothermal energy provides a proven source to heat and cool buildings.

In particular, one of the common applications for buildings of geothermal energy system is the ground source heat pump (GSHP) system using heat exchangers embedded in boreholes. GSHP system allows heat to be extracted and rejected into the soil medium depending on the building thermal loads without a significant reliance on any external energy source. GSHPs take advantage of the uniform ground temperature, which is in most climates higher than outside air temperature during winter and lower than outside air temperature during summer. According to the U.S. Department of Energy (DOE, 2011), ground temperatures range between 10 and 16°C (50 and 60°F) at 10 ft. or higher depth throughout the US climates.

In general, ground acts as a heat source or heat sink for GSHP systems. Heat is extracted from the ground to heat exchanger pipes during the heating season, and ground removes heat from the heat exchanger pipes during the cooling season. GSHPs are categorized by type of heat source and by ground heat exchanger pipe design. Types of ground heat sources are ground, groundwater, and surface water. In terms of the types of ground heat sources, GSHPs are subdivided into ground-coupled heat pumps, groundwater heat pumps, and surface water heat pumps, respectively. In addition, GSHPs are subdivided into horizontal systems and vertical systems in terms of ground heat exchanger pipe design.

Horizontal GSHP systems (Figure 1-1) uses horizontal heat exchanger pipes embedded large ground area at relatively shallow deep, generally 4ft deep. The advantage of this system is less expensive because of the low-installation costs. Disadvantage of this system is obviously that large ground area is required for the horizontal heat exchanger pipes. This may important because it may be hard to obtain 100% thermal performance of the system for commercial buildings and residential buildings where have not large enough space enough to install the horizontal heat exchanger pipes. In addition, since the depth which pipes are buried is also not much deep for the mild ground temperature, so that the ground temperature is easily affected by varying outside air temperature, sunlight, rainfall, snowfall, etc. (ASHRAE, 2007).

Meanwhile, vertical GSHP systems (Figure 1-2) utilize deep boreholes where heat exchanger pipes are placed. The depth of these boreholes ranges from 50 ft. (15m) to 600 ft. (183m). Compared to horizontal GSHPs, vertical GSHPs do not require an extended area to install pipes. In addition, the deep heat exchanger pipes are contact with the ground medium with mild, steady, and uniform temperatures. However, the vertical GSHPs require high initial costs due to expensive digging costs (ASHRAE, 2007).

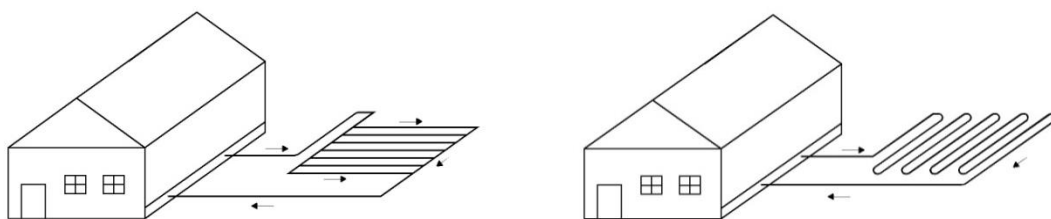


Figure 1-1: Horizontal GSHP systems with parallel pipes (left) and with series pipes (right)

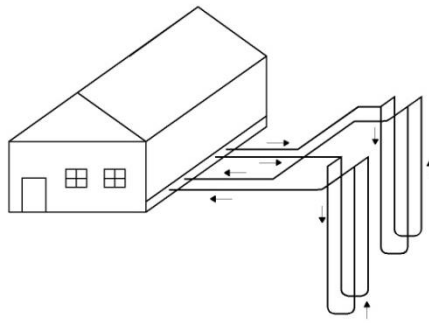


Figure 1-2: Typical configuration for vertical GSHP systems

It is important to pinpoint that vertical ground source heat pump (GSHP) systems can have high installation costs due to the drilling work needed for the boreholes. In other words, even though GSHP systems can take advantage of the mild ground temperature, the high installation costs would make this system less cost-effective compared to other more conventional systems. In fact, horizontal systems have been more widely installed more than the vertical systems for this reason. Therefore, alternative systems or methods are desired to reduce the high installation costs of GSHP vertical systems associated with digging process for deep boreholes. Thermo-active foundation (TAF) systems represent a viable solution to reduce the installation costs related drilling work associated with deep boreholes of vertical GSHPs.

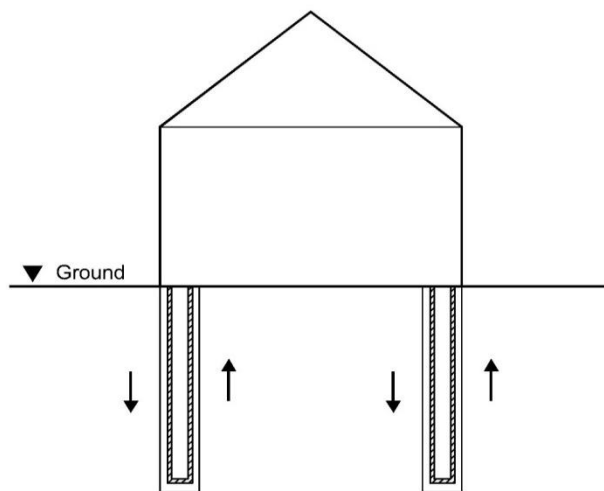


Figure 1-3: Schematic configuration for a TAF system

A thermo-active foundation (TAF) system (Figure 1-3) provides an option to integrate vertical ground heat exchanger pipes into building foundations. Since TAF systems take advantage of the vertical building foundation piles, they are able to eliminate the need for any digging work required for deep boreholes. Therefore, the installation costs associated with TAF systems can be significantly reduced compared to those of vertical GSHPs.

1.2. Definition of the Problem and Objectives

There have been several studies related to vertical GSHP systems, but only limited analyses and research studies have been reported for TAF systems especially for the US. In addition, these research studies have been mostly focused on the evaluation of the thermal and structural impacts of single thermal pile independently on building energy use. Indeed, there have been no detailed studies to evaluate the performances of TAF systems using whole-building building energy simulation programs as well as no design guidelines for TAF systems to ensure their proper sizing and operation. Therefore, a detailed analysis of the TAF systems integrated with other building components is needed in order to optimize their design and their performance especially in US climates.

There are several types of building foundations including but not limited to spread footing as a shallow foundation which is usually about a meter deep, drilled shafts, caissons, helical piles, and earth stabilized columns as deep foundations. However, considering the better and easier construction of TAF systems as well as achieving the more general solutions for TAF systems, pile foundation and vertical footing can be the types for TAF systems. Thus, the scope of the study presented in this thesis is to evaluate the thermal performance of TAF systems integrated as part of concrete pile foundations.

- One of the objectives of this research is to estimate thermal performance of a thermo-active foundation as part of a prototypical building. For this analysis, a transient three-dimensional finite-difference numerical model is first developed to analyze heat transfer rate between the ground and the heat exchanger pipes.
- The second objective is to improve the existing equation for calculating thermal response factors to be associated with thermo-active foundations considering different cross-sectional configurations (i.e. a circular section, a square section, a rectangular section, and an equilateral triangular section), based on mathematical methods and heat conduction theory. In addition, the improved equations should also be able to take the additional boundary conditions into account.
- The third objective is to develop set of thermal response factors of thermo-active foundations, based on three-dimensional numerical model and the modified new equations of thermal response factor. Using the thermal response factors, the impact of design and operating parameters on the thermo-active foundations is evaluated.
- The fourth objective is to integrate thermal models of TAF systems in a detailed whole-building energy simulation program, EnergyPlus, in order to assess their impact on building energy consumption.
- The last objective is to establish general design guidelines for a thermo-active foundation system to lead an appropriate system designing and sizing for several US climates.

The results from the research study presented in this thesis will be useful for thermo-active foundation designers or installers to ensure optimal design and operation of TAF systems. In addition, the integration of thermal models of TAF systems into EnergyPlus allows designers and modelers to

assess the potential energy savings and the cost-effectiveness associated with these novel heating and cooling systems.

CHAPTER 2. BACKGROUND AND LITERATURE REVIEW

2.1. Ground Coupled Heat Exchanger

Ground coupled heat exchanger is the mean to transfer heat between ground and buildings for GSHP systems. During the cooling season, ground absorbs heat from the fluid circulating in the heat exchanger pipes, and during the heating season, the reverse heat flow occurs with heat extracted from the ground. Heat pumps and air conditioners are mechanical devices that facilitate heat transfer from low temperature mediums to high temperature mediums. This heat transfer mechanism which is against the natural flow energy (from hot to cold medium) requires energy (in the form of electrical work) to be used by the heat pump systems and air conditioners. The principles for these two devices are the same, but the purposes are different: an air conditioner is a cooling system, and a heat pump system can provide both heating and cooling. Both air conditioner and heat pump systems have basically four components; condenser, compressor, evaporator, and expansion device. These components are connected within a closed loop as illustrated in Figure 2-1(a). The cycle used by air conditioners and heat pumps is vapor compression cycle. Ideally, it is assumed that there are no heat losses and no heat transfer by pipes between components. The overall process of this system is similar to that of the reverse Carnot cycle, in which the fluid absorbs and releases heat while flowing through the heat exchanger components absorbing heat from surroundings through the evaporator, and releasing heat to surroundings through the condenser. The processes of an ideal vapor compression cycle are summarized below (Cengel, 2005):

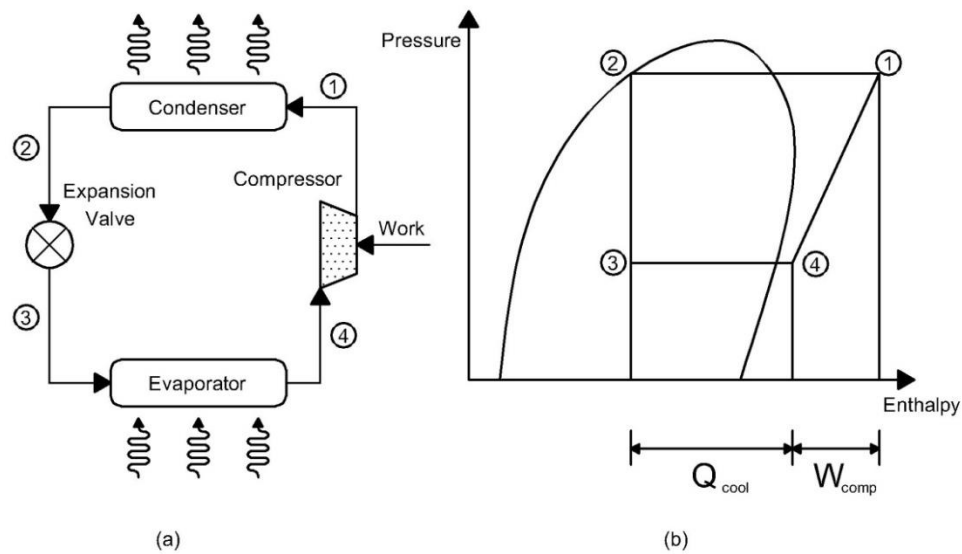


Figure 2-1: Typical vapor compression cycle (a) schematic and (b) P-h diagram (Energy Audit 2nd edition, Krarti)

- Compressor: Isentropic compression
- Condenser: constant pressure heat rejection
- Expansion device: throttling the saturated circular medium
- Evaporator: constant pressure heat absorption

According to basic principles of thermodynamics (Cengel, 2005), the refrigerant fluid at state 4 has low pressure and low temperature with a saturated vapor. This vapor enters the compressor and is compressed to a higher pressure during the compression process (i.e., the process from state 4 to state 1). The fluid becomes superheated vapor with the higher pressure and higher temperature. The temperature of the refrigerant at state 1 is typically higher than the surrounding temperature. The next stage at a condenser is the heat exchange. The superheated vapor of the circular medium rejects heat to

the surrounding medium that is lower temperature than the refrigerant. During this stage (state 1 – state 2), the refrigerant becomes saturated liquid.

The saturated liquid (state 2) is still high pressure. However, in order for better phase change and heat transfer at evaporator, the high pressure of the saturated vapor needs to drop its pressure. This is based on the basic principle of phase changes: at lower pressure, liquid can be vaporized at lower temperature (Figure 2-1(b)). Thus, in the ideal vapor-compression cycle, expansion device expands the refrigerant by throttling, so that the pressure of the circular medium is dropped as well as its temperature is decreased. During this stage (state 2 – state 3), the saturated liquid becomes low-quality saturated mixture. The final step of the cycle is the heat exchange at an evaporator. When the low-quality saturated mixture (state 3) passes through an evaporator, the low pressure, low temperature circular refrigerant absorbs heat from the surrounding medium, and is vaporized (state 3 – state 4). Thus, the circular refrigerant leaves the evaporator as saturated vapor state (state 4). And, then the cycle is repeated.

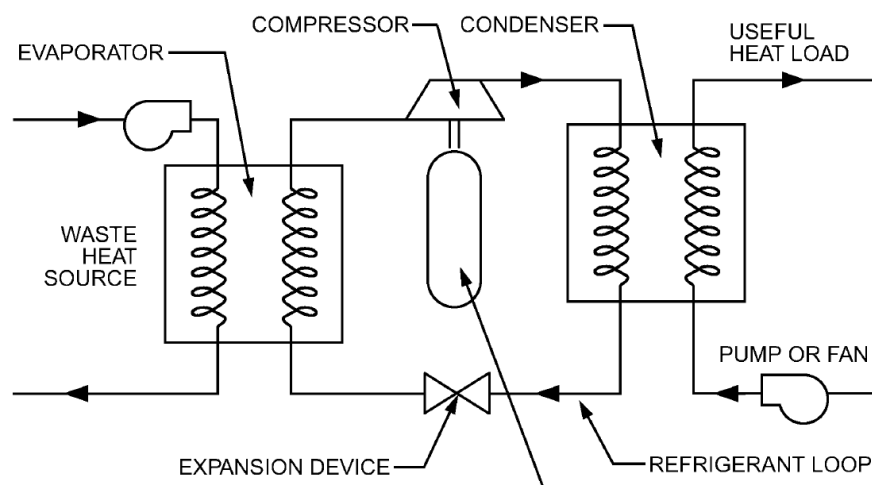


Figure 2-2: Closed Vapor Compression Cycle (ASHRAE Handbook HVAC Systems and Equipment 2008)

According to the ASHRAE Handbook (ASHRAE, 2008), heat pump systems are categorized by the type of heat sources/sinks: air, water, ground, solar energy, and industrial process. The overall features of heat sources/sinks are summarized in Table 2-1. Air source is widely used for heat pumps, since air is readily available in the ambient environment. However, as the outside air temperature varies with time, the site outdoor air temperature must be considered when designing air-source heat pumps. When air temperature varies, it can result in a substantial decrease of the efficiency and capacity of a heat pump system. Specifically, the efficiency and the capacity of a heat pump decreases with a decreasing ambient air temperature during the heating mode. However, during the cooling mode, the efficiency and capacity of a heat pump can decrease as ambient air temperature increases. In addition, air source heat pump systems must consider the problems associated with frost formation, which affects the efficiency of a heat pump system because frost on an outdoor air coil causes a reduction in heat transfer.

Table 2-1: Common Heat Pump Sources and Sinks (ASHRAE Handbook – HVAC Systems and Equipment 2008)

Medium	Suitability	Availability	Cost		Temperature
			Installed	Operation and Maintenance	
Air	Good	Universal	Low	Moderate	Variable
Groundwater well	Excellent	Varies by depth and location	Varies by depth	Low, periodic maintenance	Generally excellent, varies by location
Surface water	Excellent for large water bodies or high flow rates	limited: depends on proximity	Depends on proximity and water quality	Depends on proximity and water quality	Usually satisfactory
Ground-coupled	Good if ground is moist; otherwise poor	Depends on soil suitability	High to moderate	Low	Usually good
Ground -Direct expansion	Varies with soil conditions	Varies with soil conditions	High	High	Varies by design
Solar Energy	Fair for heat source, poor for heat sink	Universal	Extremely high	Moderate to high	Varies by design

Meanwhile, compared to air source, water source provides an alternative to take advantage of an almost year-round constant temperature of groundwater (ASHRAE, 2007). However, when using water source, some additional considerations are required including testing of water quality and local soil and groundwater conditions. Indeed, groundwater and surface water temperature and depth depend on the site for each building. In order to use groundwater for GSHPs, accurate estimation of its depth is important not only for thermal performance, but also for determining the installation costs.

A ground source heat pump (GSHP) system uses ground as heat source or heat sink (Figure 2-3). Below a certain depth, the ground temperature is generally mild and remains constant throughout the year. However, in order to design ground-coupled heat pump system and analyze its performance, knowledge of soil composition and its thermal properties is critical (ASHRAE, 2007). Particularly, thermal conductivity is an important factor for estimating heat transfer rates. Moreover, moisture content affects thermal properties of soil (ASHRAE, 2008). In addition, the installation cost due to drilling work for boreholes depend on the soil type and is a significant factor to determine the cost-effectiveness of ground source heat pump systems, especially vertical loop systems.

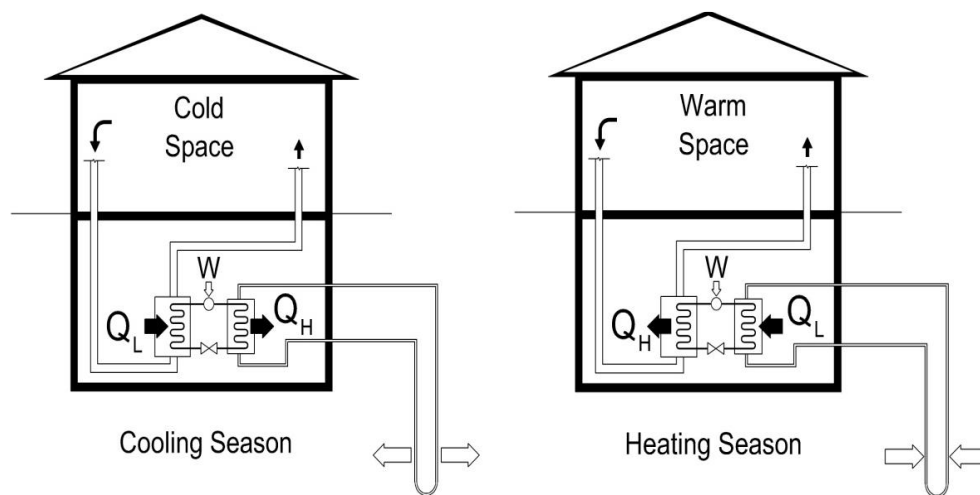


Figure 2-3: Ground-Coupled Heat Pump System for cooling season (left) and for heating season (right)

$$(\text{Refrigerator}) \text{ COP}_R = \frac{Q_L}{w_{\text{net,in}}} = \frac{h_4 - h_3}{h_1 - h_4} \quad \text{Equation 2-1}$$

$$(\text{Heat Pump}) \text{ COP}_{\text{HP}} = \frac{Q_H}{w_{\text{net,in}}} = \frac{h_1 - h_2}{h_1 - h_4} = \frac{Q_L}{w_{\text{net,in}}} + 1 = \text{COP}_R + 1 \quad \text{Equation 2-2}$$

where

Q_L = Heat flow rate at an evaporator = $(h_4 - h_3) \cdot \dot{m}$

Q_H = Heat flow rate at a condenser = $-(h_1 - h_2) \cdot \dot{m}$

h = Enthalpy

w = The rate of energy input = $(h_1 - h_4) \cdot \dot{m}$

\dot{m} = Mass flow rate of circular medium (refrigerant)

As shown in the above equations, heat pumps' COP is always higher than 1 because of $\text{COP}_R > 0$. Thus, even in the worst cases, heat pumps provide heat into the space at least as the same amount of energy as they consume. It should be noted, however, that in reality the COP of heat pumps can be lower than the values provided by Equations 2-1 and 2-2 due various heat losses associated with both pipes and other devices. In particular, in the case of air-to-air heat pump systems, when outdoor temperature is too cold, it is possible for COP_{HP} to be less than 1 (Cengel, 2005). This possibility makes ground-coupled heat pumps more attractive due to the rather constant ground temperatures. Indeed, while outdoor air temperatures can vary significantly with time and seasons, deep ground temperature is almost constant year-round. In addition, air-to-air heat pump systems can be subjected to frost conditions that inhibit heat transfer through evaporators, and thus additional systems and energy are required to defrost.

2.2. Existing Ground-Coupled Heat Exchanger Models

Since thermo-active foundations are essentially a type of vertical ground coupled heat exchangers, the benefits associated with vertical ground source heat pumps are applicable to the thermo-active foundations. The performance of ground coupled heat exchanger systems is determined based on its ability of heat transfer over several time periods ranging from few minutes to 100 years between the heat exchanger pipes and the ground. So, in order to design thermo-active foundations, computationally efficient and accurate design models are required like conventional vertical GSHP system. Many researchers have been studied using empirical, analytical and numerical approaches to compute efficiently heat rejected to the ground from the heat exchanger pipes or extracted from the ground to the heat exchanger pipes.

2.2.1. Analytical Methods

Analytical solutions for ground coupled heat exchangers are based on several simplified assumptions. The primary assumptions include ‘cylindrical heat source’ (Carslaw and Jaeger 1959; Ingersoll and Zobel 1954), ‘infinite line source’ (Carslaw and Jaeger 1959; Gehlin 1998; Witte et al. 2002; Pesl et al. 2007; Philippe et al. 2009), and ‘finite line source’ (Eskilson, 1987; Zeng et al. 2002; Philippe et al. 2009; Kozak et al. 2009; Bandos et al. 2009).

Cylindrical-source model

Kavanaugh (1985) used cylindrical source approximation to determine the temperature distribution and the heat transfer rate around a pipe embedded in the ground medium. The cylindrical source method was based on the Carslaw and Jaeger’s solution (1959). Kavanaugh’s cylindrical model

used a finite cylinder in an infinite solid medium which has constant and uniform properties. The proposed solution is specific for a constant pipe surface temperature or for a constant heat transfer rate between the pipe and its surroundings. The thermal interference between boreholes is neglected in this solution.

The solution of Kavanaugh's cylindrical model is based on constant heat transfer rates and is given by the following equations:

$$T_{ff} - T_{ro} = \frac{Q'}{k} G(z, p) \quad \text{Equation 2-3}$$

$$G(z, p) = \frac{1}{\pi^2} \int_0^\infty \frac{e^{-\beta^2 z} - 1}{J_1^2(\beta) + Y_1^2(\beta)} [J_0(p\beta)Y_1(\beta) - J_1(\beta)Y_0(p\beta)] \frac{1}{\beta^2} d\beta \quad \text{Equation 2-4}$$

where

$$z = \frac{\alpha t}{r^2}, \quad p = \frac{r}{r_0}, \quad r_0 = \text{Outer pipe radius}$$

T_{ff} = Far – field temperature [°C]

T_{ro} = Temperature of outer pipe surface [°C]

Meanwhile, in order to represent the number of legs of U-tube pipes in this solution, it is necessary to modify the diameter of the pipe. So, the equivalent pipe diameter is estimated as follows:

$$D_{eq} = \sqrt{n} D_0 \quad \text{Equation 2-5}$$

where n is the number of U-tube legs in one borehole, D_0 is the original diameter of one U-tube leg, and D_{eq} is the equivalent diameter of a single pipe.

Using this solution, using the energy balance, the outlet water temperature (T_{wo}) can be computed by the following equations:

$$T_{wo} = \frac{Q' L}{2 \cdot m_w c_{pw}} + T_{avgw} \quad \text{Equation 2-6}$$

$$T_{wo} - T_{wi} = \frac{Q' L}{m_w c_{pw}} \quad \text{Equation 2-7}$$

$$T_{avgw} = \frac{T_{wo} - T_{wi}}{2} \quad \text{Equation 2-8}$$

$$T_{avgw} = T_{ff} + \left[\frac{Q'}{k} G(z, p) \right] + \Delta T_p \quad \text{Equation 2-9}$$

$$\Delta T_p = \frac{Q'}{C \cdot N_i \cdot 2\pi r_0 \cdot h_{eq}} \quad \text{Equation 2-10}$$

where

T_{avgw} = Average water temperature [°C]

T_{wo} = Outlet water temperature [°C]

T_{wi} = Inlet water temperature [°C]

T_{ff} = Far – field ground temperature [°C]

ΔT_p = Temperature difference between outer pipe surface and fluid [°C]

N_i = Number of U – tubes

C = Correction factor for non – uniform heat flow
($C = 0.85$ when $N_i = 2$; $C = 0.6 - 0.7$ when $N_i = 4$)

Infinite Line-source model

Ingersoll (1954) applied the line source theory to vertical ground coupled heat exchangers to calculate the temperature at any point in the infinite medium. One of the approaches by Philippe et al. (2009) was the infinite line-source model using the same formula as that used by Ingersoll. Ingersoll's solution for ground temperature involves source heat transfer rate, distance from center line of pipe,

and ground thermal properties. Specifically Ingersoll's solution assumes that heat flow is radial as depicted by Equations 2-11 and 2-12.

$$T - T_0 = \frac{Q'}{2\pi k} \int_x^\infty \frac{e^{-\beta^2}}{\beta} d\beta = \frac{Q'}{2\pi k} I(X) \quad \text{Equation 2-11}$$

$$X = \frac{r}{2\sqrt{\alpha t}} \quad \text{Equation 2-12}$$

where

T = Temperature of ground at any selected distance from the line source [$^{\circ}\text{C}$]

T_0 = Initial temperature of the ground [$^{\circ}\text{C}$]

Q' = Heat transfer rate over the source [W/m]

r = Distance from center line of pipe [m]

k = Thermal conductivity of the ground [W/(m · $^{\circ}\text{C}$)]

α = Thermal diffusivity of the ground = $k/(\rho \cdot c)$

ρ = Density of the ground [kg/m^3]

β = Integration variable = $\frac{r}{2\sqrt{\alpha(t - t')}}$

t = Time

The Ingersoll solution is valid for a case of true line source. However, Ingersoll suggested that Equation 2-11 can be used for the case of small pipes of 2 inches or less in diameter without resulting in significant errors. Specifically, it is determined that the dimensionless term $\frac{\alpha t}{r^2}$ must be greater than 20 for practical applications to ensure small computational errors.

Hart and Couvillion (1986) developed another solution to estimate temperature distribution around a line source. They also used line source theory and considered an undisturbed far field

temperature for better prediction of ground temperature distribution. In their solution, Hart and Couvillion assumed that the ground temperature is constant and undisturbed when the ground radius is greater than the far field radius. The proposed far field radius is defined as follows:

$$r_{\infty} = 4\sqrt{\alpha t} \quad \text{Equation 2-13}$$

And, the temperature distribution around a line source is given by the following equation:

$$T - T_0 = \frac{Q'}{2\pi k} \left[\ln \frac{r_{\infty}}{r} - 0.9818 + \frac{4r^2}{2r_{\infty}^2} - \frac{1}{4 \times (2!)} \left(\frac{4r^2}{r_{\infty}^2} \right)^2 + \dots + \frac{(-1)^{N+1}}{2N \times (N!)} \left(\frac{4r^2}{r_{\infty}^2} \right)^N \right] \quad \text{Equation 2-14}$$

Where, r is the radial distance from the line source. Hart and Couvillion suggested that this equation applies for pipes when $\frac{r_{\infty}}{R}$ is greater than or equal to 15, where R is the pipe radius. The accuracy of Equation 2-6 depends on the ratio of $\frac{r_{\infty}}{R}$. When the value of this ratio is greater than or equal to 3, only 2 power series terms are needed, but for cases with a ratio of less than 3, the number of required power series terms is increased.

The infinite line-source of Carslaw and Jaeger (1959) was for the continuous constant heat liberated per unit time per unit length of a line (x' , y' , z') parallel to the z -axis with the initial solid temperature of zero. So the temperature at time t , at (x, y, z) is:

$$T(r, z, t) = \frac{q}{4\pi k} \int_{r^2/4\pi k}^{\infty} \frac{e^{-u} du}{u} = -\frac{q}{4\pi k} \text{Ei} \left(-\frac{r^2}{4\pi k t} \right) \quad \text{Equation 2-15}$$

$$\text{where} \quad -\text{Ei}(-x) = \int_x^{\infty} \frac{e^{-u}}{u} du \quad \text{and} \quad r^2 = (x - x')^2 + (y - y')^2$$

For small x

$$\begin{aligned} \text{Ei}(-x) &= \gamma + \ln(x) - x + \frac{1}{4}x^2 + O(x^3) \\ \gamma &= 0.5772 \text{ (Euler's constant)} \end{aligned} \quad \text{Equation 2-16}$$

Thus, for large t

$$T(r, z, t \rightarrow \infty) = \frac{q}{4\pi k} \ln\left(\frac{4kt}{r^2}\right) - \frac{\gamma q}{4\pi k} \quad \text{Equation 2-17}$$

Finite Line-source model

Eskilson (1987) presented that the seasonal temperature variations had less impact on the underground temperature below a ground depth of 10m. For this reason, the temperature disturbance caused by the ground surface temperature was neglected, and thus the ground surface temperature was assumed as a constant far-field ground temperature. Based on the Eskilson's approach, Zeng et al. (2002), Lamarche et al. (2007) and Philippe et al. (2009) also used the 'mirror image technique' in order to consider the constant ground surface boundary condition.

Zeng et al. (2002) derived an analytical solution of the transient temperature response in a semi-infinite solid using a finite line-source. Using the finite line-source model, Zeng et al. estimated and compared two representative steady-state borehole wall temperatures: the middle point temperature, and the integral mean temperature. Before deriving the analytical solution, Zeng et al. made several assumptions:

- (1) The ground is a homogeneous semi-infinite medium, and its thermophysical properties do not change with temperature.
- (2) The medium has a uniform initial temperature, $T(t = 0) = T_0$.
- (3) The ground surface keeps a constant temperature throughout the period considered.

- (4) The radial dimension of the borehole is neglected, so that the borehole can be approximated as a finite line source.
- (5) The heating rate per length of the source is constant q_l since the starting instant ($t=0$).

The temperature variation at the time (t) in the point (m) of an infinite medium due to the point source can be expressed in Equation 2-18. And then, the solution of the temperature excess can be computed by integrating the point sources on a closed interval $[0, H]$ (Equation 2-19). It was found that by using the mean integral temperature the better solution was achieved than the solution of the mid-point of the borehole that overestimated the steady-state temperature.

$$d\theta = \frac{q_l dh}{4\pi k} \frac{\operatorname{erfc}\left(\frac{\sqrt{r^2 + (z-h)^2}}{2\sqrt{at}}\right)}{\sqrt{r^2 + (z-h)^2}} \quad \text{Equation 2-18}$$

$$\theta = \frac{q_l}{4\pi k} \int_0^H \left\{ \frac{\operatorname{erfc}\left(\frac{\sqrt{r^2 + (z-h)^2}}{2\sqrt{at}}\right)}{\sqrt{r^2 + (z-h)^2}} - \frac{\operatorname{erfc}\left(\frac{\sqrt{r^2 + (z+h)^2}}{2\sqrt{at}}\right)}{\sqrt{r^2 + (z+h)^2}} \right\} dh \quad \text{Equation 2-19}$$

$$\theta_s = \frac{q_l}{4\pi k} \operatorname{Ln} \left[\frac{(H-z) + \sqrt{r^2 + (H-z)^2}}{(H+z) + \sqrt{r^2 + (H+z)^2}} \cdot \frac{2z^2 + r^2 + 2z\sqrt{r^2 + z^2}}{r^2} \right] \quad \text{Equation 2-20}$$

$$\theta_{b,m} = \frac{q_l}{2\pi k} \operatorname{Ln} \frac{H}{\sqrt{3}r_b} \quad \text{Equation 2-21}$$

$$\bar{\theta}_b = \frac{1}{H} \int_0^H \theta(r_b, z) dz = \frac{q_l}{2\pi k} \operatorname{Ln} \frac{H}{2.2r_b} \quad \text{Equation 2-22}$$

$$\theta = T - T_0 \text{ (The temperature excess)}$$

$$\theta_s = \text{The steady - state distribution}$$

- $\theta_{b,m}$ = The temperature excess at the middle of a borehole wall
 $\bar{\theta}_b$ = The integral mean temperature of a borehole wall
 dh = A differential increment
 k = The thermal conductivity of the medium
 a = The thermal diffusivity of the medium

Lamarche et al. (2007) proposed a modified analytical solution for G-function to make it numerically efficient (Equation 2-23). The analytical solution of Lamarche et al. was mainly based on the analytical solution of Zeng et al. (2002). So, the main assumption of this model was also using the method of mirror images to ensure zero temperature at the ground surface like the previous researches by Eskilson (1987) and Zeng et al. (2002). It was found that the analytical solution of Lamarche et al. led to the same value as the infinite line source.

$$g(t^*, \beta) = \int_{\beta}^{\sqrt{\beta^2+1}} \frac{\text{erfc}(\gamma z)}{\sqrt{z^2 - \beta^2}} dz - D_A - \int_{\sqrt{\beta^2+1}}^{\sqrt{\beta^2+4}} \frac{\text{erfc}(\gamma z)}{\sqrt{z^2 - \beta^2}} dz - D_B \quad \text{Equation 2-23}$$

where

$$\begin{aligned}
 D_A &= \int_{\beta}^{\sqrt{\beta^2+1}} \text{erfc}(\gamma z) dz \\
 D_B &= \frac{1}{2} \times \left(\int_{\beta}^{\sqrt{\beta^2+1}} \text{erfc}(\gamma z) dz + \int_{\sqrt{\beta^2+1}}^{\sqrt{\beta^2+4}} \text{erfc}(\gamma z) dz \right) \\
 \beta &= \frac{r_b}{H} \\
 \gamma &= \frac{3}{2\sqrt{t^*}} \\
 t^* &= \frac{t}{t_s}
 \end{aligned}$$

Philippe et al. (2009) presented three analytical solutions to transient heat transfer around boreholes. The analytical solutions were the infinite line-source, the infinite cylindrical source, and the finite line source models. Especially, from the comparison analysis between the infinite line source and the finite line source models it was found that the temperature difference of the borehole wall between the infinite line source and the finite line source models decreased as the borehole length increased.

Using the three-dimensional finite line-source model for a borehole heat exchanger Bandos et al. (2009) presented an analytical solution. Particularly, Bandos et al. not only considered a finite line-source, but also took into account the vertical z-axis with a constant temperature gradient in the semi-infinite medium and a variable ground surface temperature. This model consisted of three contributions to the temperature of a point in the medium. The temperature can be expressed as a sum of the solution of the inhomogeneous, v_d , and the solution of the homogeneous, v_0, v_s . Bandos et al. mentioned that v_0, v_s solutions did not vary with the radial coordinate, while v_d varied with r.

$$T(r, z, t) = v_0(z, t) + v_s(z, t) + v_d(r, z, t) \quad \text{Equation 2-24}$$

$$v_0(z, t) + v_s(z, t) = \frac{2}{\sqrt{\pi}} \int_{z/\sqrt{4\alpha t}}^{\infty} f\left(t - \frac{z^2}{4\alpha u^2}\right) e^{-u^2} du + T_0 \operatorname{erf}\left(\frac{z}{\sqrt{4\alpha t}}\right) + zk_{geo} \quad \text{Equation 2-25}$$

$$v_d(r, z, t) = \frac{Q_z}{4\pi k} \int_{r/\sqrt{4\alpha t}}^{\infty} \left[2 \operatorname{erf}\left(\frac{z}{r} u\right) - \operatorname{erf}\left(\frac{H+z}{r} u\right) + \operatorname{erf}\left(\frac{H-z}{r} u\right) \right] \frac{e^{-u^2}}{u} du \quad \text{Equation 2-26}$$

where

T = Temperature of ground at any selected distance from the line source [°C]

T_0 = The undisturbed ground temperature [°C]

v_0 = The contribution to temperature by the initial condition [°C]

v_s = The contribution to temperature induced by the ground surface [°C]

v_d = The contribution to temperature by the heat source [°C]

$f(t)$ = A variable ground surface temperature

α = The ground thermal diffusivity (m^2/s)

k_{geo} = The geothermal gradient, $k_{geo} = \nabla_z T_{geo}$, ($^{\circ}\text{C}/\text{m}$)

2.2.2. Numerical Methods

As noted in the previous section, the analytical solutions described above are based on several simplifying assumptions to model ground coupled heat exchangers. In particular, these solutions ignore the effects of leg-to-leg thermal interferences as well as local geometries of the embedded heat exchangers. In order to consider these limitations of the analytical solutions, numerical methods have been utilized by several researchers to help estimate the performance of ground-coupled heat exchangers. Particularly, Eskilson (1987) developed one of the first numerical solutions. This solution is the basis of several other numerical solutions reported for ground coupled heat exchangers. Eskilson's solution estimates the thermal performance of the ground loop heat exchangers using non-dimensional temperature response factors, called G-functions. In order to determine the response factors, both numerical and analytical models are employed.

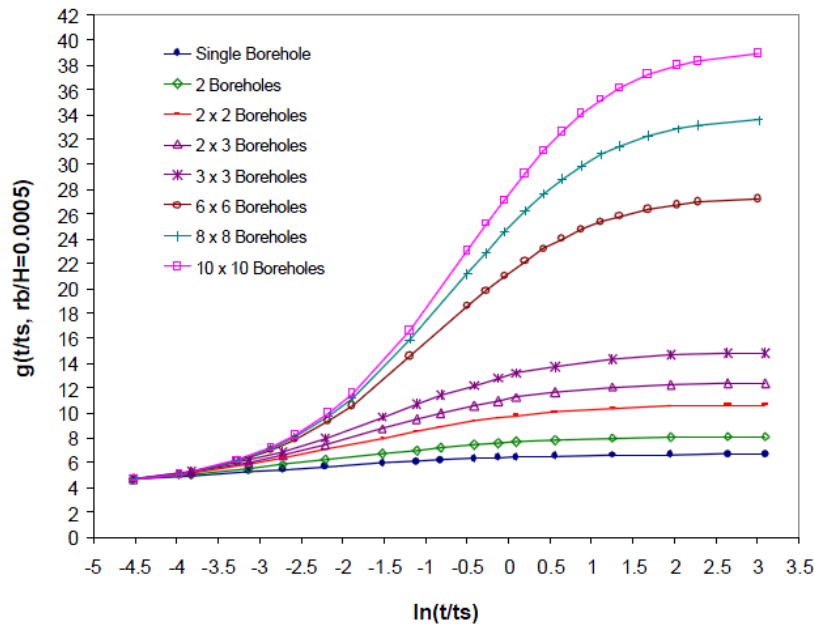


Figure 2-4: Temperature response factors (G-functions) for multiple borehole configurations (Spitler 2000)

Using a two-dimensional (radial-axial) explicit transient finite-difference method, the numerical solution for the Eskilson's determines the response to a unit step function heat pulse. In the Eskilson's method, the thermal capacitances of the individual borehole elements are neglected in the numerical analysis. By setting the temperature response of the borehole field to be dimensionless, the resulting non-dimensional ground temperatures and dimensionless times are G-functions (Figure 2-4).

However, even though the G-functions were developed for various borehole configurations, Eskilson's approach is only valid for long time steps. Thus, for short time steps, additional response function is required. Yavuzturk (1999) developed short time step response factors using two-dimensional implicit finite volume method applied to a cylindrical coordinate system. In this approach, the three-dimensional effects and the end of the U-tube are neglected. Compared to Eskilson's approach, Yavuzturk's model accounted for individual borehole elements, and the effects of changing pipe temperature with depth are approximated.

Meanwhile, in cylindrical coordinates it is hard to model circular pipe. In order to represent the circular pipe of U-tube legs on polar grid, Yavuzturk employed a 'Pie-Sector' approximation (Figure 2-5). This discretization approach was also used by Rottmayer et al. (1997) for the quasi-three dimensional numerical U-tube heat exchanger model (Yavuzturk, 1999), (Rottmayer et al. 1997). In the method of pie-sector, a circular pipe is modeled as a pie-shaped pipe by defining the inside perimeter boundaries of the pie-sector as that estimated from the circular pipes with identical heat flux and resistance conditions used. In order to validate this approach, Yavuzturk used other cylindrical model which was an infinite cylinder model. It is concluded that the Pie-Sector approach was validated with an average relative error of less than 1%.

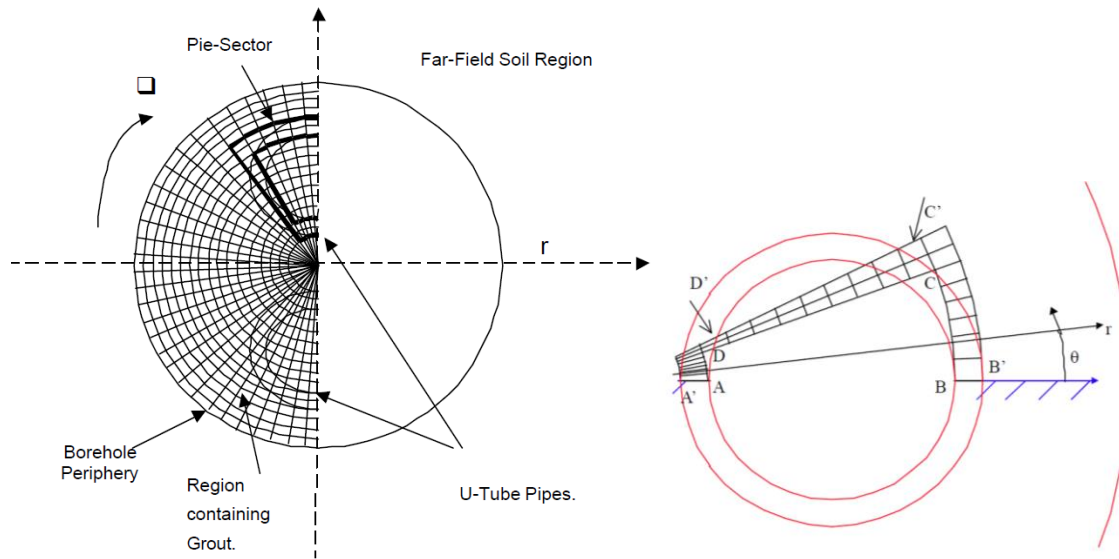


Figure 2-5: A schematic image of pie-sector approach: the borehole region on the numerical model domain is discretized using the pie-sector approximation for the U-tube pipes (left), the pie-sector representation of the U-tube pipes (right)

2.3. Thermo-active Foundation Systems

Thermo-active foundation (TAF) systems is the combination of ground loop heat exchanger pipes and building foundations used to heat and cool either partially or fully buildings. TAFs utilize

building foundation elements (i.e., footings) in order to reduce the excavation costs associated with digging the boreholes for ground coupled heat exchange systems. TAF systems are also known as energy piles and foundation heat exchangers. Currently, there is a keen interest in installing TAF systems to meet heating and cooling requirements of a wide range of buildings especially in Europe and Japan (Brandl 2006, Laloui et al. 2006, Ooka et al. 2007). However, compared to vertical ground source heat pump systems, the performance of thermo-active foundation systems have not been widely studied and evaluated. Nevertheless, there have been some limited studies on the effectiveness of energy piles in extracting and rejecting heat in the ground medium using both numerical and empirical analyses (Adam et al. 2009). Some studies have analyzed both the thermal and mechanical performances of the thermo-active foundation systems (Brandl, 2006; McCartney et al., 2010). Using a wide range of case studies, Brandl discusses the performance of thermo-active ground structures including energy foundations in terms of both thermal and mechanical responses. Brandl concluded that concrete has good thermal properties that enhance heat transfer between the ground and heat exchanger pipes, and that for general thermo-active ground structures, low-permeability soil and low hydraulic gradient of groundwater are favorable.

Some researchers have reported the results of in-situ field experimental analysis using full-scale pile-foundation heat exchanger systems. In particular, Laloui et al. (2006) performed the experiment for 97 piles of 25m length for a building in Switzerland to validate the predictions of their numerical model. Hamada et al. (2007) monitored the performance of thermo-active foundation installed in a building located in Sapporo, Japan. From the Hamada et al.'s research, it was found that the TAF system reduced the primary energy rates for heating and cooling the building by 23.2%. Similar experimental analyses have been reported by Sekine et al. in 2007 for a cast-in-place concrete pile foundation for a building in Japan, by Wood et al. (2010) for a TAF system in UK, and by Jalaluddin et al. (2011) for 20m depth steel

pile foundations with three types of ground heat exchangers (single U-tube type, double-tube type, and multi-tube type). From the analysis, Jalaluddin et al. found that the pile with double-tube exhibited the highest heat exchange rate, followed by the multi-tube and U-tube type.

In addition to in-situ field test, McCartney et al. (2010) and Stewart et al. (2012) performed a controlled laboratory experimental analysis using a centrifuge set-up to evaluate the soil-foundation interactions for geothermal foundations. The test was developed to evaluate the thermal and mechanical behavior of a small-scale thermo-active building foundation. From the resulting thermal responses of the test, it was observed that heat was transferred effectively to the ground through the fluid circulating in the pipes embedded in the thermo-active foundation.

Some research evaluate thermal performances of TAF system, and found that several factors can affect how heat is transferred between the soil medium and the fluid circulating in the heat exchanger pipes within a thermal foundation pile. Using analytical method, Bozts et al. (2011) evaluated the effects of the number of pipes, the type and dimensions of pipes, and the heat/flow characteristics in the pipes on the temperature difference between the fluid and the pile. Kaltreider (2011, Roussi et al. (2011), Abdelaziz et al. (2011), and Kwag et al. (2013) used numerical methods to evaluate the effects of design and operational parameters on the thermal performances of energy piles. Particularly, Kaltreider (2011) and Roussi et al. (2011) used the test results of McCartney et al. (2010), and Kwag et al. (2013) used the data of the experimental analysis performed by Stewart et al. (2012) to validate the predictions of their finite difference numerical models for a thermo-active foundation. Using the validated two-dimensional numerical models, Kaltreider (2011) and Roussi et al. (2011) found that several physical parameters can have a significant impact on the heat transfer rate between a thermo-active foundation and the ground medium, including foundation depth, flow velocity, and shank space. Abdelaziz et al. (2011) and Kwag et al. (2013) also found that the thermal conductivity of soil and foundation material

had an effect on the performance of energy pile, and that turbulent flow conditions had larger effects on the heat transfer through energy pile than laminal flow condition. In addition, Kwag et al. (2013) showed that foundation depth had a profound effect on the performance of energy pile.

However, Kaltreider and Roussi et al. also found that there are potential thermal interactions between the building heating and cooling loads (through the foundation heat loss or gain) and the TAF system. Specifically, when compared to the standard foundations (i.e., without embedded heat exchangers), TAF systems increase ground-coupled slab heat transfer. Kaltreider and Roussi et al. found that TAF systems can increase heat losses during the heating season, and heat gains during cooling season.

In addition to thermal performance analysis, some research studied about thermal response factor method for TAF system. Recently, Loveridge (2012a), Loveridge et al. (2013) and Kwag et al. (2013) have developed three-dimensional numerical solutions for thermal performance of TAF systems. Loveridge developed a new G-function to simulate transient thermal behavior within a single foundation. Using the numerical solution in cylindrical coordinates, Kwag et al. (2013) developed a set of thermal response factors specific to a standalone TAF pile. The response factors developed by Kwag et al. were then used to assess the impact of various design parameters on thermal performances of TAF systems using a whole-building energy simulation program, EnergyPlus. However,

However, even though Loveridge (2012a), Loveridge et al. (2013) and Kwag et al. (2013) developed the new G-functions for simulating thermal behavior within thermal pile accurately, in those G-functions the heat transfer through an above-grade floor and the impact of indoor air temperature on the ground heat exchangers was not taken into account.

2.4. Summary

In this chapter, the reported thermal performance for both ground coupled heat exchangers and thermo-active foundation (TAF) systems are briefly summarized. For a conventional ground heat exchanger system, several analytical and numerical models have been developed to investigate heat exchanger rate and thermal performance associated to several TAF design and operating parameters. Based on the literature review for a conventional ground heat exchanger system, a detailed transient numerical model needs to be developed to evaluate the performance of thermo-active foundations. Analytical solutions while useful to provide some physical insights are not sufficient to develop design guidelines for TAF systems. Although some previous researches briefly studied about the effects of design and operational parameters of a thermo-active foundation, these researches only dealt with few design parameters and with simplified boundary conditions, and didn't analyze the effects of a building above foundations. So, for the accurate analysis of performances of a thermo-active foundation the detail analyses with three-dimensional modeling and with detail boundary condition would be required.

CHAPTER 3. TRANSIENT THREE-DIMENSIONAL NUMERICAL MODELING

3.1. Model Description

A three-dimensional numerical model for a rectangular slab-on-grade floor equipped with thermal piles is considered as illustrated in Figure 3-1. The 3-D numerical model is consisted of floor, full-covered floor insulation, foundation piles (3 by 3), and ground medium. Because of the difficulties of modeling due to the Cartesian coordinates, two heat exchanger pipes are simplified as two lines representing pipes, and foundation configuration is square shape. The thermal piles are embedded into the concrete foundation elements, and include heat exchanger pipes.

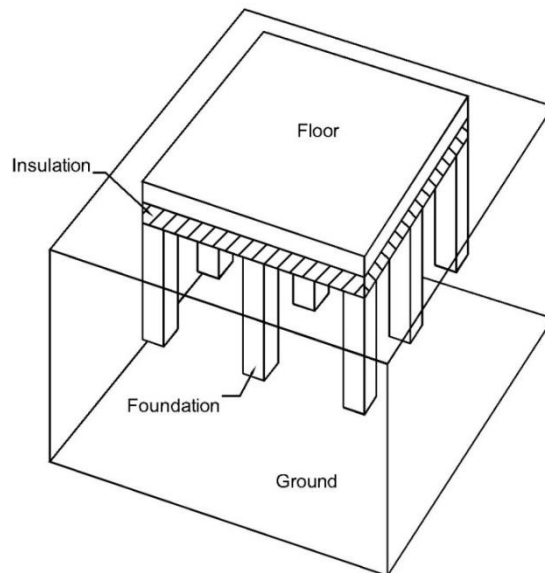


Figure 3-1: Simplified three-dimensional Cartesian numerical model

Figure 3-2 illustrates the sectional image of the 3D model and boundary conditions. The outer edge of the domain is assumed to be adiabatic, and the bottom boundary condition is constant temperature representing groundwater. The top boundary condition is constant temperatures standing

for outdoor air temperature and indoor air temperature. The size of the domain ground is assumed to be large enough to set the undisturbed ground temperature as boundary conditions for the model.

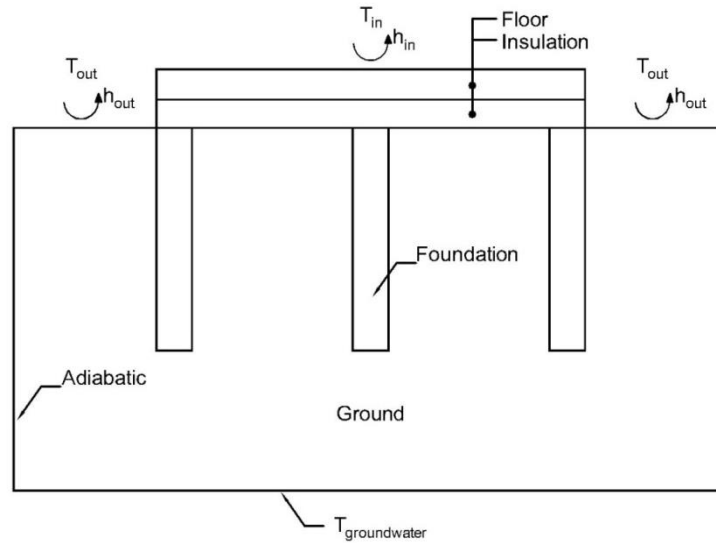


Figure 3-2: The boundary conditions for numerical modeling

Table 3-1 provides a summary of the typical geometric and thermal characteristics of the ground medium, foundation domain, and slab-on-grade floor. The characteristics of the commonly used heat exchanger U-tube pipes are summarized in Table 3-2. Table 3-3 lists the thermal properties of the circular fluid flowing in the heat exchanger pipes.

Table 3-1: The characteristics of the ground domain and foundation

	Domain	Foundation	Floor
Material	Soil	Concrete	Concrete
Length & Width & Depth (m)	40 x 40 x 20	0.5 x 0.5 x 10	10 x 10 x 0.25
Thermal Conductivity (W/m-K)	1.00	1.73	1.73
Density (kg/m³)	2240	2600	2600
Specific Heat (J/kg-K)	837	880	880

Table 3-2: Features of U-tube pipes

Pipe Diameter (m)	0.025
Pipe Depth (m)	9.95
Shank Space (m)	0.300
Space between Foundation to Pipe	0.050
Thermal Conductivity (W/m-K)	0.360

Table 3-3: Features of the fluid circulating in the U-tube pipes

Thermal Conductivity (W/m-K)	0.58
Density (kg/m³)	1000
Specific Heat (J/kg-K)	4181

Table 3-4 presents the thermal properties of the floor insulation material. The floor insulation material is rigid polyurethane foam (PUR/PIR) insulation.

Table 3-4: Thermal properties of the floor insulation material

Insulation Material	Rigid Polyurethane Insulation
Thickness (m)	0.105
Thermal Conductivity (W/m-K)	0.025
Density (kg/m³)	30
Specific Heat (J/kg-K)	1500

In this paper, it is assumed that the ground medium has uniform soil thermal properties, which is a common assumption to evaluate thermal performance of ground source heat pumps (GSHPs), building foundations, and TAF systems (Krarti, 1999, Yavuzturk, 1999, Kavanaugh, 2010, EnergyPlus, 2010).

3.2. Three-dimensional Finite Difference Method in Cartesian Coordinates

The transient three-dimensional numerical model developed in this research, uses an implicit finite difference method associated with the Cartesian coordinates. In order to reduce consuming time, non-uniform grids in X-, Y-, and Z-axis were employed as shown in Figure 3-3. The control volume used to solve the transient heat conduction equation within and around the embedded TAF pipes is described by Figure 3-4.

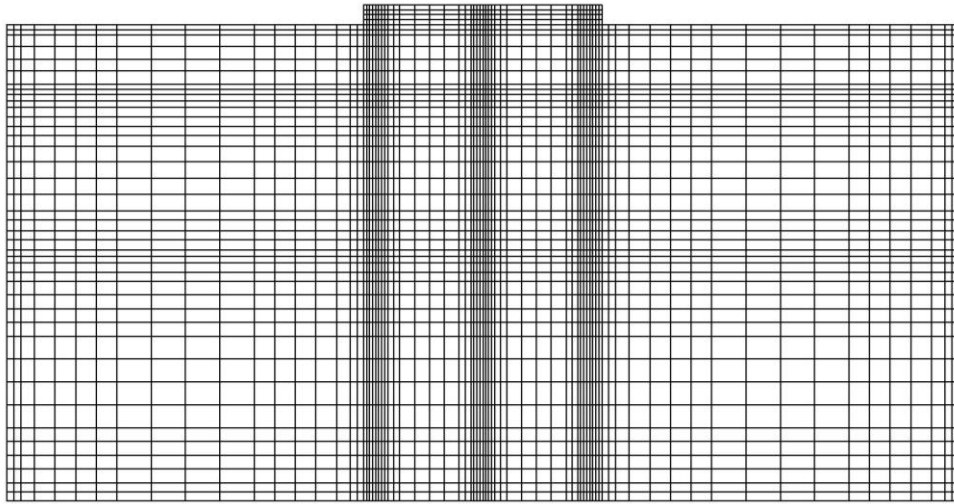


Figure 3-3: Schematic drawing of non-uniform grids

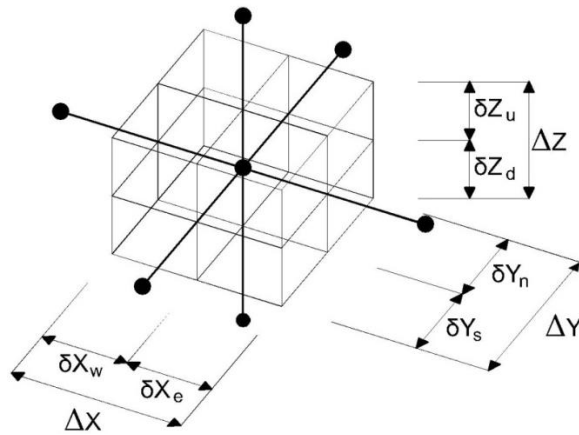


Figure 3-4: Control Volume of a regular node

In this study, the heat transfer in both the ground medium and thermal foundation is estimated assuming only conduction. The transient conduction equation in Cartesian coordinates can be expressed as follows:

$$\frac{1}{\alpha} \frac{\partial T}{\partial t} = \frac{\partial^2 T}{\partial x^2} + \frac{\partial^2 T}{\partial y^2} + \frac{\partial^2 T}{\partial z^2} \quad \text{Equation 3-1}$$

The resulting implicit discretized equations for the heat conduction equation defined above are provided below. It is assumed that there is no heat source in the ground. Thus, the conductive heat transfer equation is reduced to the following relationship between the temperatures of various nodes:

$$a_P T_P = a_E T_E + a_W T_W + a_N T_N + a_S T_S + a_U T_U + a_D T_D + b \quad \text{Equation 3-2}$$

where,

$$a_P = a_E + a_W + a_N + a_S + a_U + a_D + a_P^0 \quad \text{Equation 3-3}$$

$$a_E = \frac{k_e \Delta y \Delta z}{\delta x_e} \quad \text{Equation 3-4}$$

$$a_W = \frac{k_w \Delta y \Delta z}{\delta x_w} \quad \text{Equation 3-5}$$

$$a_N = \frac{k_n \Delta x \Delta z}{\delta x_n} \quad \text{Equation 3-6}$$

$$a_S = \frac{k_s \Delta x \Delta z}{\delta x_s} \quad \text{Equation 3-7}$$

$$a_U = \frac{k_u \Delta x \Delta y}{(\delta z)_u} \quad \text{Equation 3-8}$$

$$a_D = \frac{k_d \Delta x \Delta y}{(\delta z)_d} \quad \text{Equation 3-9}$$

$$a_P^0 = \frac{(\rho c)_P \Delta V}{\Delta t} \quad \text{Equation 3-10}$$

$$b = S_c \Delta V + a_P^0 T_P^0 \quad \text{Equation 3-11}$$

Since the vertical U-tube pipes have typically narrow diameter and a long depth, thermal properties are set as constant; such as thermal conductivity, density, specific heat, dynamic viscosity, and Prandtl Number of the circulating fluid within the pipes. The dominant heat transfer mechanisms for the fluid circulating within the heat exchanger pipes are convection and diffusion. Therefore, the advection heat transfer equations are used, and Equation 3-12 through Equation 3-36 describe the discretization schemes for these equations.

$$a_p T_p = a_W T_W + a_E T_E + a_N T_N + a_S T_S + a_U T_U + a_D T_D + b \quad \text{Equation 3-12}$$

where,

$$a_W = D_W * (A_{Pe_W}) + \max(F_W, 0) \quad \text{Equation 3-13}$$

$$a_E = D_E * (A_{Pe_E}) + \max(-F_E, 0) \quad \text{Equation 3-14}$$

$$a_S = D_S * (A_{Pe_S}) + \max(F_S, 0) \quad \text{Equation 3-15}$$

$$a_N = D_N * (A_{Pe_N}) + \max(-F_N, 0) \quad \text{Equation 3-16}$$

$$a_U = D_U * (A_{Pe_U}) + \max(F_U, 0) \quad \text{Equation 3-17}$$

$$a_D = D_D * (A_{Pe_D}) + \max(-F_D, 0) \quad \text{Equation 3-18}$$

$$a_p^0 = \frac{\rho_{\text{fluid}} * C_{p\text{fluid}} * \Delta V}{dy} \quad \text{Equation 3-19}$$

$$\Delta V = \Delta x * \Delta y * \Delta z \quad \text{Equation 3-20}$$

$$b = a_p^0 * T_p^0 \quad \text{Equation 3-21}$$

With the conductance terms are defined as follows:

$$\text{(West)} \quad D_W = k_{\text{fluid}} * \frac{\Delta y * \Delta z}{\delta x_w} \quad \text{Equation 3-22}$$

$$\text{(East) } D_E = k_{\text{fluid}} * \frac{\Delta y * \Delta z}{\delta x_e} \quad \text{Equation 3-23}$$

$$\text{(North) } D_N = k_{\text{fluid}} * \frac{\Delta x * \Delta z}{\delta y_n} \quad \text{Equation 3-24}$$

$$\text{(South) } D_S = k_{\text{fluid}} * \frac{\Delta x * \Delta z}{\delta y_s} \quad \text{Equation 3-25}$$

$$\text{(Up) } D_U = k_{\text{fluid}} * \frac{\Delta x * \Delta y}{\delta z_u} \quad \text{Equation 3-26}$$

$$\text{(Down) } D_D = k_{\text{fluid}} * \frac{\Delta x * \Delta y}{\delta z_d} \quad \text{Equation 3-27}$$

While the flow rate terms are expressed as follows:

$$F_{W,E} = \rho_{\text{fluid}} * C_{p\text{fluid}} * U_{W,E} * \Delta y * \Delta z \quad \text{Equation 3-28}$$

$$F_{N,S} = \rho_{\text{fluid}} * C_{p\text{fluid}} * U_{N,S} * \Delta x * \Delta z \quad \text{Equation 3-29}$$

$$F_{U,D} = \rho_{\text{fluid}} * C_{p\text{fluid}} * U_{U,D} * \Delta x * \Delta y \quad \text{Equation 3-30}$$

The Peclet Number terms are defined:

$$Pe_{W,E} = F_{W,E} / D_{W,E} \quad \text{Equation 3-31}$$

$$Pe_{N,S} = F_{N,S} / D_{N,S} \quad \text{Equation 3-32}$$

$$Pe_{U,D} = F_{U,D} / D_{U,D} \quad \text{Equation 3-33}$$

The $A(|Pe|)$ function is described using the Power Law Scheme:

$$APe_{W,E} = \max \left(0, \left(1 - 0.1 * |Pe_{W,E}|^5 \right) \right) \quad \text{Equation 3-34}$$

$$APe_{N,S} = \max \left(0, \left(1 - 0.1 * |Pe_{N,S}|^5 \right) \right) \quad \text{Equation 3-35}$$

$$AP_{e_{U,D}} = \max\left(0, \left(1 - 0.1 * |P_{e_{U,D}}|^5\right)\right) \quad \text{Equation 3-36}$$

While convective coefficients are used to compute convection heat transfer as described in the above equations, it is difficult to determine adequate convective coefficients for the analysis since these coefficients depend on the flow rate, pipe size, and fluid temperature. However, the effect of the fluid temperature on convective coefficient is relatively small. In this analysis, the impact of temperature is neglected, and the fluid is assumed to be at constant temperature. Thus, by using these values, Reynolds Number and Nusselt Number can be defined:

$$Re = \frac{(U * D)}{v} \quad \text{Equation 3-37}$$

where, D is pipe diameter, U is fluid velocity, and v is kinematic viscosity of fluid. Based on the Reynolds Number, Nusselt Number is calculated for both heating and cooling modes. For the case of turbulent flow ($Re \geq 2300$) in the pipes, Dittus-Boelter equation can be used.

$$\begin{cases} Nu = 3.36 & (\text{if } Re < 2300) \\ Nu = 0.023 * Pr^n * Re^{0.8} & (\text{if } Re \geq 2300) \\ n = 0.3 & (\text{for Cooling}) \\ n = 0.4 & (\text{for Heating}) \end{cases} \quad \text{Equation 3-38}$$

where Pr is Prandtl Number. Thus, using Nusselt Number, the convective coefficients of the fluid circulating within the pipes can be calculated:

$$h_{\text{fluid}} = \frac{(Nu * k_{\text{fluid}})}{D} \quad \text{Equation 3-39}$$

However, in order to account for the pipe thickness and pipe thermal properties, an effective convective coefficient is employed:

$$h_{\text{eff}} = \left(h_{\text{fluid}} + \frac{\text{pipe thickness}}{k_{\text{pipe}}} \right) \quad \text{Equation 3-40}$$

where k_{pipe} is the thermal conductivity of the pipe material.

3.3. Analysis of impact of grid discretization

Generally, finite difference models based on finer grids generate more accurate solutions. However, because of limitations in computing capabilities, finer grids require more simulation time. Thus, a sensitivity analysis to determine the adequate grid scheme to be utilized is required.

For the sensitivity analysis on the grid dependence, a very fine grid scheme is used as a reference against which all the other discretization schemes are compared. For the comparative analysis, Root Mean Square Error (RMSE) method is used to measure of the magnitude of the differences between the predictions using the reference and any other schemes as illustrated in Table 3-5:

$$\text{RMSE} = \sqrt{\frac{\sum_{i=1}^n (T_{1,i} - T_{2,i})^2}{n}} \quad \text{Equation 3-41}$$

$T_1 = [T_{1,1}, T_{1,2}, T_{1,3}, \dots, T_{1,n}]$ and $T_2 = [T_{2,1}, T_{2,2}, T_{2,3}, \dots, T_{2,n}]$

Table 3-5: The impact of grid node numbers of both CPU time and RMSE values for the numerical solution

Case	Grid	RMSE [°C]	Time [seconds]
1	52822	0.2208	0.5
2	64061	0.1941	57.1

3	75429	0.1700	57.6
4	81675	0.1570	149.5
5	109678	0.0974	270.8
6	154836	0.0370	640.7
7	207746	0.0171	5136.7
8	224147	0.0171	9416.2
9	262031	0.0102	15293.3
10	302867	0.0100	21295.0
11	371280	0.0056	60824.7
12	409728	0.0055	82315.8
13	464736	0.0000	98899.1

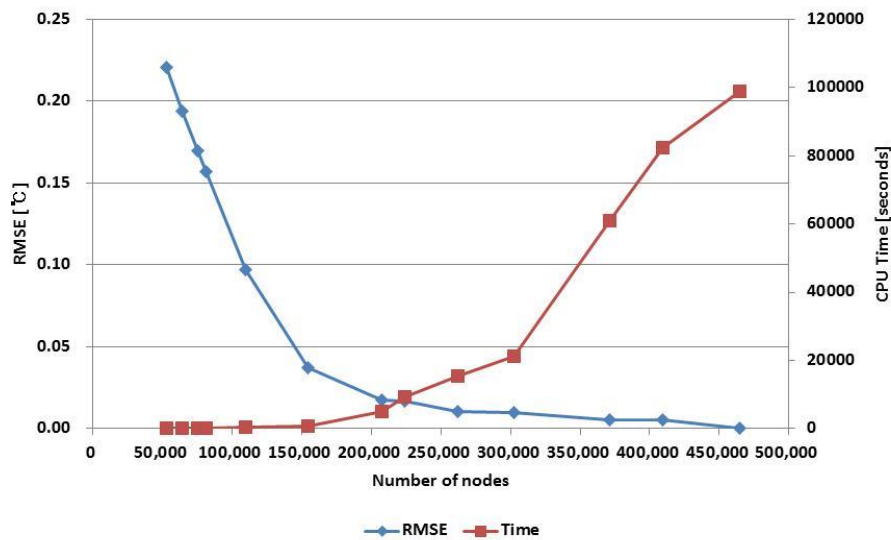


Figure 3-5: Variation of CPU time and RMSE value associated with the numerical solution as functions of the number of the grid nodes

The RMSE values are shown in Figure 3-5 for several grid schemes. As shown in Figure 3-5, the finer is the grid, the more accurate is the numerical solution characterized by lower RMSE values. However, the computational efforts defined by the CPU time required for the numerical solution increases with the number of grid nodes. Based on the results of Figure 3-5, an adequate number for the grid nodes is 224,147. Indeed, after this threshold number, the required simulation time increases

significantly as illustrated in Table 3-5 and Figure 3-5. In addition, the RMSE value for a grid made up of 224,147 nodes is relatively small (RMSE=0.017°C) attesting of the accuracy of the numerical solution. Therefore, a grid with 224,147 nodes will be in most of the analysis of the TAF system performance discussed in this research.

3.4. Validation Analysis of the Three-Dimensional Numerical Model

3.4.1. Validation Method Description

In order to validate the predictions from the developed three-dimensional transient numerical model, experimental data from the Centrifuge Lab of the Geotechnical Engineering and Geo-mechanics, the University of Colorado at Boulder. Specifically, the experimental set-up consisted of a scale-model thermo-active foundation (Table 3-6), which had three independent U-tube loops. The scale-model was around 24 times smaller than a typical real TAF foundation for a commercial building. The fluid used in the experiment is pure ethylene glycol heat transfer fluid. Table 3-6 shows the dimensions of the scaled experiment model.

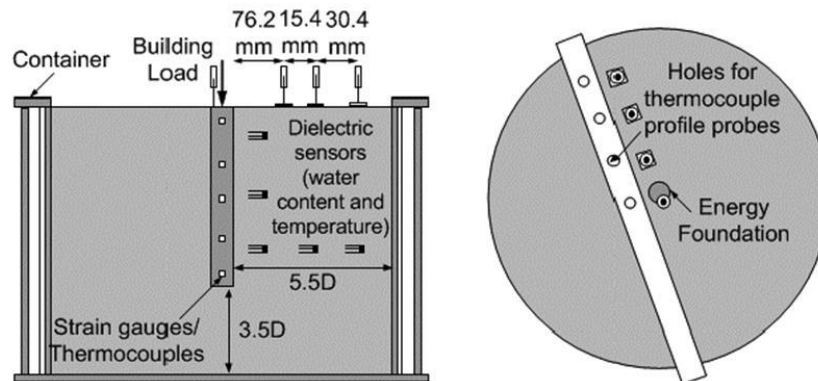


Figure 3-6: A scale-model for a thermo-active foundation set-up (Stewart et al., 2012)

Table 3-6: Basic dimensions of the small-scale thermo-active foundation model used in the experimental analysis

Domain Container	Diameter [mm]	600 mm
	Depth [mm]	540 mm
Foundation	Diameter [mm]	50.8 mm
	Depth [mm]	381 mm

The measured parameters from the test set-up include ground temperatures, foundation temperatures, and inlet/outlet flow temperatures. To monitor the outlet fluid temperature and the ground and foundation temperatures, several probes were used; 5 probes for the ground temperatures, 1 probe for the outlet fluid temperature, and 5 probes for the foundation temperatures.

Table 3-7: Coordinates of the probe locations for the experiment test

Ground	Radius	50.8mm	139.7mm	215.9mm	50.8mm	50.8mm
	Depth	190.5mm	190.5mm	190.5mm	114.3mm	38.1mm
Foundation (Radius = 0mm)	Depth	25.4mm	108.0mm	191.0mm	273.1mm	355.6mm

As part of the experimental set-up, four operation modes were considered to mimic operation of TAF system under various building thermal load conditions including: heating start-up, steady state heating, cooling start-up, and steady state cooling as shown in Figure 3-7 showing the heat exchanger fluid outlet temperature variation with time.

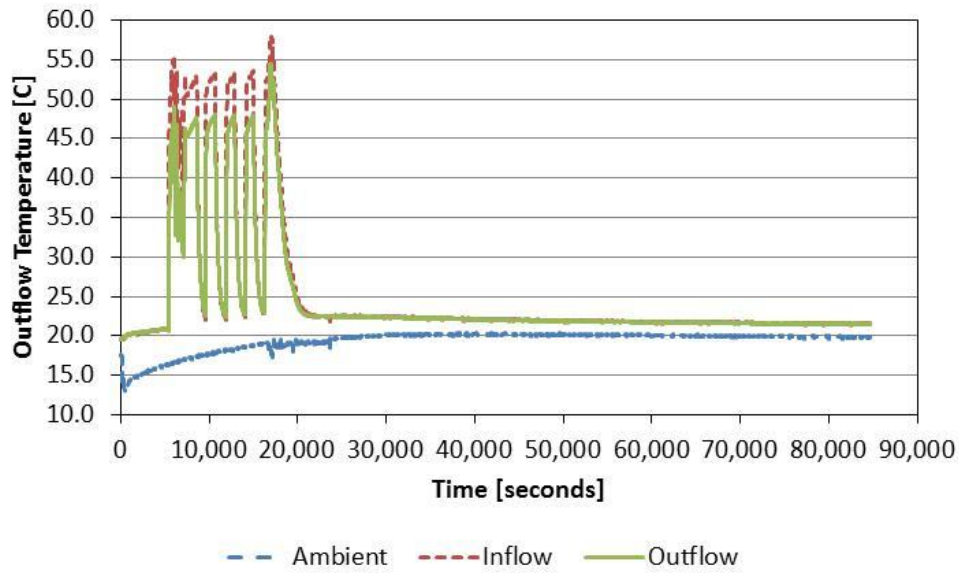


Figure 3-7: The variations of the fluid inlet and outlet temperatures, and the ambient temperature of the experimental data, (Stewart et al., 2012)

Since the specific thermal properties of various materials (such as soil and concrete) used in the experimental set-up were not given or tested, a sensitivity analysis was carried out. In addition, the bottom of the domain cylinder was not adiabatic surface, since it was not insulated and was on the metallic table exposed to the ambient air. The lower boundary condition in the numerical model had to be adjusted based on the ground temperature profiles measured during the experimental analysis.

Table 3-8: Thermal conductivities of the materials used in the experimental set-up

	Foundation	Soil
Thermal Conductivity (W/m K)	1.76	1.98

3.4.2. Results

In the experiment, type-k thermocouples (Omega fine wire Type K Model STC-TT-K-36 3C, and working temperature range -250°C to 400°C) were used to measure the variations of the fluid

temperature (inflow and outflow), the foundation temperature, and the ground temperature. According to the product catalogue, and ANSI and IEC codes, typically type-k thermocouples have tolerance range of $\pm 1.5^{\circ}\text{C}$ (IEC, -40°C to 375°C , the tolerance range of 3.0°C) or $\pm 2.2^{\circ}\text{C}$ (ANSI, -200°C to 1250°C , the tolerance range of 4.4°C). Therefore, it can be decided that the numerical model is validated when the temperatures predicted by the numerical model are within the tolerance range.

As a result, the overall root mean square error (RMSE) of the validation analysis is 2.32°C (Table 3-9). Although the result is within the tolerance range of the typical type-k thermocouples, the RMSE value is relatively high. The possible reason for this high RMSE result may be caused by the several unknown variables not provided from the experimental test (e.g. other thermal properties of soil and concrete like density and specific heat, etc.), or by the uncertain variables which cannot be measured (e.g. air convection coefficient, h_{out}). Additionally, it is possible that the thermal conductivity of soil was affected by the variation of moisture contents in the soil during the experiment. Indeed, during the experiment, the moisture contents in the soil were varied in different trends at the probes. So, the last possible reason is that ground domain in the numerical model was assigned to have thermally uniform properties during the simulation.

Table 3-9: RMSE values between model predictions and measurements during five hours

	Total	Ground	Foundation	Outflow
RMSE	2.32	2.47	2.24	1.40

So, for the better comparative analysis, the numerical model is calibrated based on a series of sensitivity analysis. Figure 3-8 shows results of the sensitivity analyses for the validation analysis. According to the results in Figure 3-8, the thermal conductivity of the foundation material (k_{conc}) has the significant impact on the RMSE result of the comparative analysis. The other variables also have the moderate impacts on the RMSE result of the validation analysis.

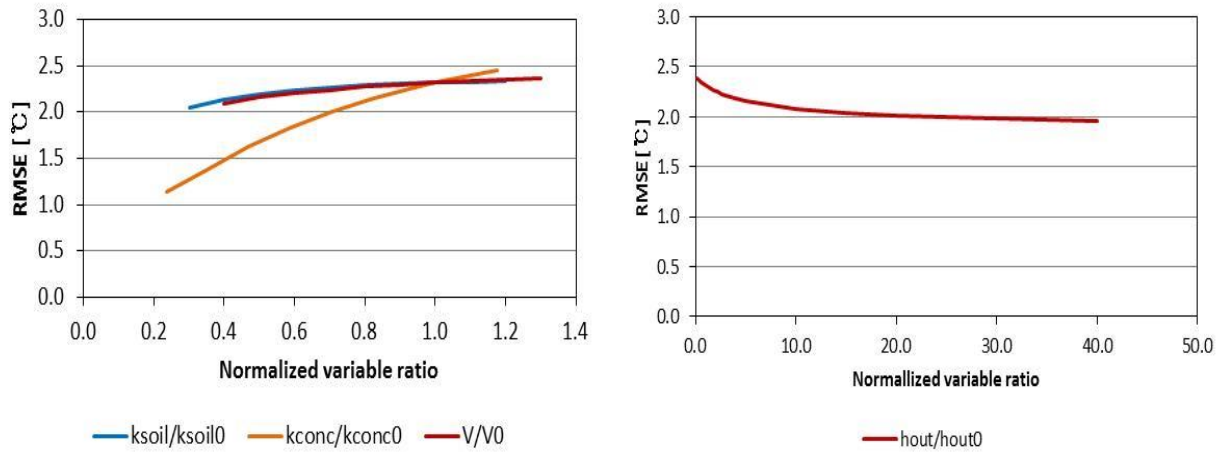


Figure 3-8: The results of sensitivity analyses of validation analysis for individual variable

The cases of calibrated numerical model have the lower RMSE results than the base case (Table 3-10), and generated the similar soil temperature, the foundation temperature, and the outflow fluid temperature to the experiment data (Figure 3-9, Figure 3-10, and Figure 3-11, respectively). The gray lines in these figures indicate the error bars with the tolerance of $\pm 1.5^{\circ}\text{C}$. The overall results of the numerical model are within the tolerance range with the low RMSE results.

Table 3-10: The RMSE results of the calibrations

	$\frac{k_{soil}}{k_{soil0}}$	$\frac{k_{conc}}{k_{conc0}}$	$\frac{h_{out}}{h_{out0}}$	$\frac{V}{V0}$	RMSE [°C]			
					Total	Ground	Foundation	Outflow
Base	1.0	1.0	1.0	1.0	2.32	2.47	2.24	1.40
Case 1	0.5	0.4	10.0	0.6	1.181	1.183	1.269	1.071
Case 2	0.3	0.2	40.0	0.4	1.066	0.983	1.406	1.068
Case 3	0.3	0.2	10.0	0.4	1.075	0.995	1.401	1.081
Case 4	0.3	0.2	1.0	0.4	1.123	1.066	1.382	1.113

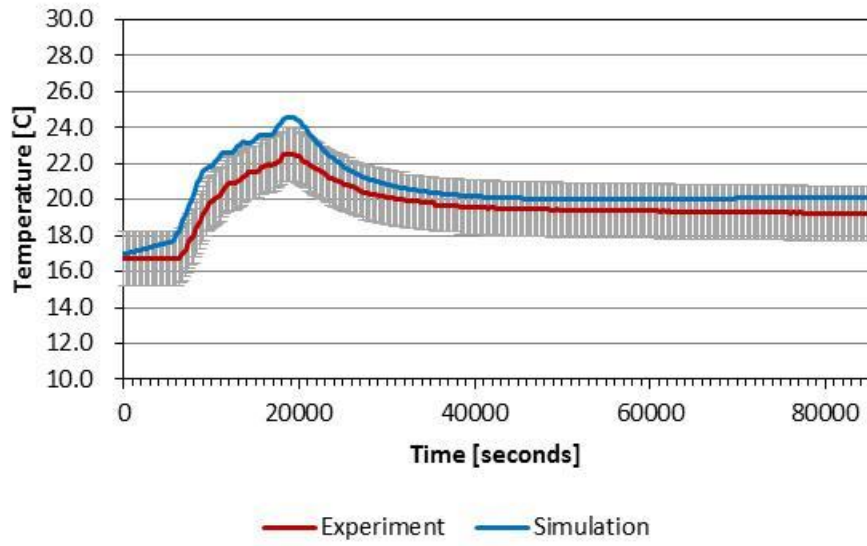


Figure 3-9: The temperature variations of the calibrated numerical model and the experiment at the probe around the foundation (radius = 50.8mm, depth = 190.5mm)

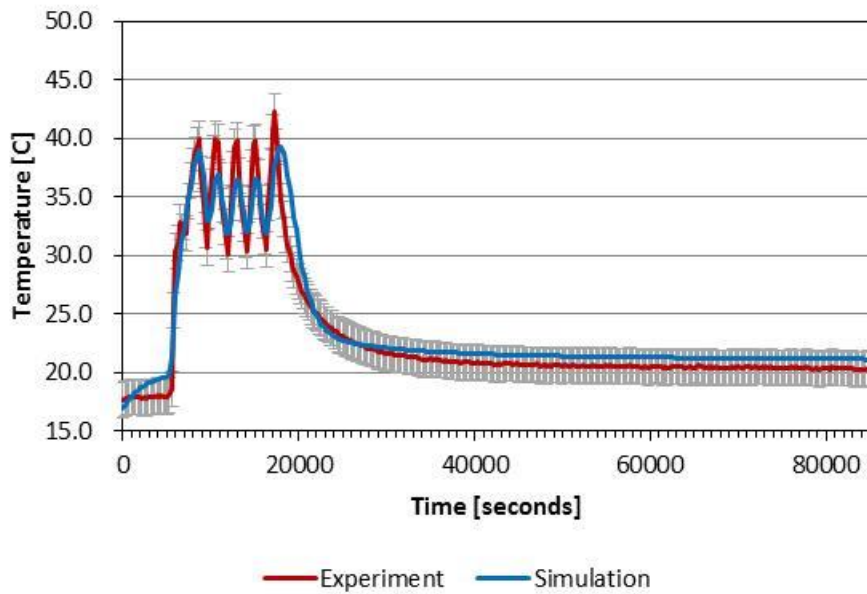


Figure 3-10: The temperature variations of the calibrated numerical model and the experiment at the probe within the foundation (radius = 0mm, depth = 190.5mm)

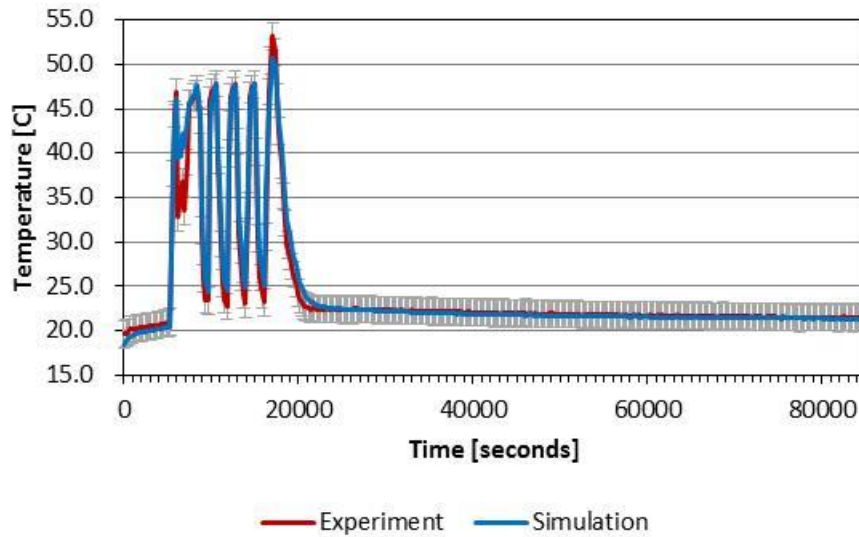


Figure 3-11: Variation of fluid outlet temperature with time based on model predictions and testing measurements

3.5. Comparison Analysis –Cartesian Model vs. Cylindrical Model

In this section, the numerical solution developed in the Cartesian coordinates (x, y, z) is compared to that of the numerical model in cylindrical coordinates (r, ω, z) (Figure 3-12). The cylindrical numerical model developed by Kwag et al. (2012) was validated with the small-scaled experimental test. For this comparative analysis, two numerical models have the same thermal properties and the same boundary conditions as presented in Table 3-11.

As shown in Figure 3-12, two numerical models had 31 probes logging temperature variations with time; 1 probe for outflow fluid temperature, and 30 probes for ground temperatures. Table 3-12 shows the probe locations for the validation analysis to log ground temperature variations used to calculate Root Mean Square Error (RMSE) values.

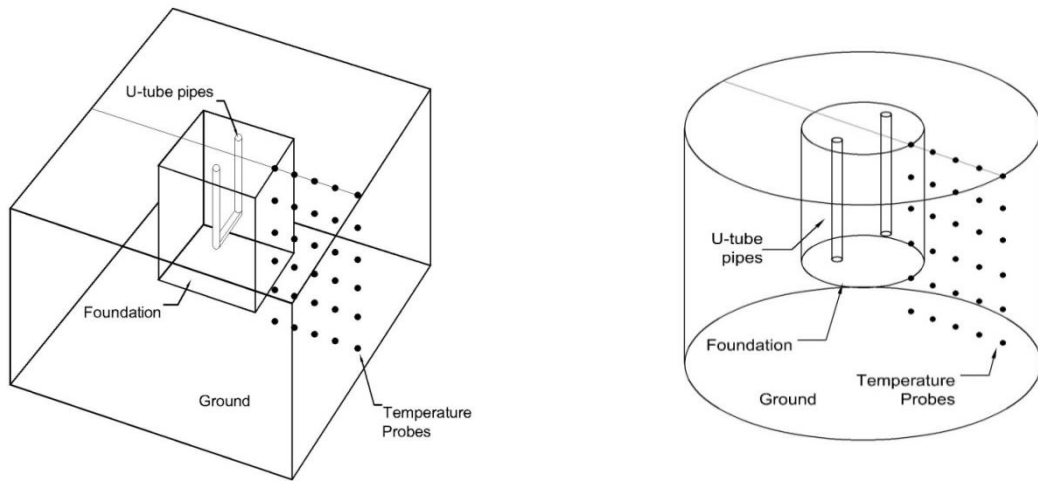


Figure 3-12: 3D numerical models for validation analysis: (left) Cartesian model, and (right) Cylindrical model

Table 3-11: Boundary Conditions

	Cartesian Model	Cylindrical Model
Domain Size	Length(X) = 18 (m) Width (Y) = 18 (m) Depth (Z) = 20 (m)	Diameter(r) = 18 (m) Depth(Z) = 20 (m)
Foundation Size	Length(X) = 1 (m) Width (Y) = 1 (m) Depth (Z) = 16 (m)	Diameter(r) = 1 (m) Depth(Z) = 16 (m)
Ground Thermal Properties	Thermal Conductivity = 1.0 (W/m·K) Density = 2240 (kg/m ³) Specific Heat = 837 (J/kg·K)	
U-tube Pipe Information	Depth = 15 (m) Diameter = 0.025 (m) Thermal Conductivity = 0.3 (W/m·K)	
Circular Fluid Information	Thermal Conductivity = 0.58 (W/m·K) Density = 1000 (kg/m ³) Specific Heat = 4181 (J/kg·K) Volumetric Flow Rate = 6.892E-5 (m ³ /seconds) Reynolds Number = 2700 (Turbulent Flow)	

Ambient Temperature	$T_{OA} = T_{OA,mean} - T_{OA,amp} \cdot \cos(w \cdot \text{time}) [^{\circ}\text{C}]$ $w = \text{angular frequency} = \frac{2\pi}{(3600 \times 24 \times 365)}$ $T_{OA,mean} = \text{mean outside air temperature } [^{\circ}\text{C}] = 15[^{\circ}\text{C}]$ $T_{OA,amp} = \text{amplitude of outside air temperature fluctuation } [^{\circ}\text{C}] = 17[^{\circ}\text{C}]$
Inlet Temperature	$T_{\text{Inlet Fluid}} = T_{\text{Inlet Fluid,mean}} - T_{\text{Inlet Fluid,amp}} \cdot \cos(w \cdot \text{time}) [^{\circ}\text{C}]$ $w = \text{angular frequency} = \frac{2\pi}{(3600 \times 24 \times 365)}$ $T_{\text{Inlet Fluid,mean}} = \text{mean inflow fluid temperature } [^{\circ}\text{C}] = 15.5[^{\circ}\text{C}]$ $T_{\text{Inlet Fluid,amp}} = \text{amplitude of inflow fluid temperature fluctuation } [^{\circ}\text{C}] = 13.5[^{\circ}\text{C}]$
Groundwater Temperature	$T_{\text{water}} = 10 (^{\circ}\text{C})$
Outer Edge Boundary Condition	Adiabatic

Table 3-12: Probe locations for validation analysis

X (m) \ Z (m)	9.5 m	12 m	14 m	16 m	18 m
0 m	Probe 1-1	Probe 2-1	Probe 3-1	Probe 4-1	Probe 5-1
3 m	Probe 1-2	Probe 2-2	Probe 3-2	Probe 4-2	Probe 5-2
6 m	Probe 1-3	Probe 2-3	Probe 3-3	Probe 4-3	Probe 5-3
9 m	Probe 1-4	Probe 2-4	Probe 3-4	Probe 4-4	Probe 5-4
12 m	Probe 1-5	Probe 2-5	Probe 3-5	Probe 4-5	Probe 5-5
15 m	Probe 1-6	Probe 2-6	Probe 3-6	Probe 4-6	Probe 5-6

Table 3-13 describes the RMSE results of validation results. The total RMSE result is 0.26 °C. This result indicates that even though two numerical models have different cross-sectional configurations, thermal performances of these models are similar. Indeed, both models has the same hydraulic diameter.

Table 3-13: RMSE results of validation analysis

Summary		RMSE Results of ground temperature (°C)									
Probe	RMSE	Probe 1	RMSE	Probe 2	RMSE	Probe 3	RMSE	Probe 4	RMSE	Probe 5	RMSE

T_outlet	0.13	Probe 1-1	0.00	Probe 2-1	0.00	Probe 3-1	0.00	Probe 4-1	0.00	Probe 5-1	0.00
Probe 1	0.53	Probe 1-2	0.28	Probe 2-2	0.19	Probe 3-2	0.03	Probe 4-2	0.02	Probe 5-2	0.02
Probe 2	0.23	Probe 1-3	0.35	Probe 2-3	0.26	Probe 3-3	0.04	Probe 4-3	0.03	Probe 5-3	0.03
Probe 3	0.04	Probe 1-4	0.35	Probe 2-4	0.27	Probe 3-4	0.05	Probe 4-4	0.04	Probe 5-4	0.04
Probe 4	0.03	Probe 1-5	0.37	Probe 2-5	0.29	Probe 3-5	0.05	Probe 4-5	0.03	Probe 5-5	0.03
Probe 5	0.03	Probe 1-6	1.11	Probe 2-6	0.24	Probe 3-6	0.04	Probe 4-6	0.02	Probe 5-6	0.02
Total	0.26										

3.6. Sensitivity Analysis

In order to evaluate the thermal performances of a thermo-active foundation, the impacts of several parameters are to be investigated using the validated numerical model. In general, the ground is a large medium and has high thermal capacitance, and the specific properties of the ground depend on a wide range of factors including type of soil, moisture content, soil layers, and groundwater level. In reality, however, it is very difficult to determine specific ground characteristics and properties with expensive testing set-up. Therefore, in this study, the ground is assumed to have uniform thermal properties neglecting the effect of groundwater flow.

The parameters that are studied in this section are foundation depth, fluid velocity in the heat exchanger loops, distance between U-tube pipes (also called shank space), and the number of U-tube loops in one pile. The impact of each parameter is evaluated in heat flux transferred between circulating fluid and the ground medium, and in the heat flux transferred through an above-grade floor. The heat flux between heat exchanger pipes and the ground medium is estimated using both inlet fluid and outlet fluid temperatures as indicated by Equations 3-42 and 3-43, while the heat flux through a floor is estimated using the Equations 3-44 and 3-45.

$$Q = \rho_{\text{fluid}} * cp_{\text{fluid}} * V * (T_{\text{outlet}} - T_{\text{inlet}}) \quad \text{Equation 3-42}$$

$$\text{Percent increase in heat transfer} = \frac{(Q - Q_{\text{base}})}{Q_{\text{base}}} \times 100\% \quad \text{Equation 3-43}$$

where

Q	=	Heat flux [w]
Q_{base}	=	Heat flux of the base case [w]
ρ_{fluid}	=	Density of fluid [kg/m ³]
cp_{fluid}	=	Specific heat of fluid [J/kg]
T_{outlet}	=	Outlet temperature of fluid [°C]
T_{inlet}	=	Inlet temperature of fluid [°C]
V	=	Volumetric flow rate [m ³ /sec]

In order to compute the heat flux transferred through a floor, the average floor top surface temperatures and the average floor bottom surface temperatures are employed (Figure 3-13). Floor heat transfer rates are computed by the equations below:

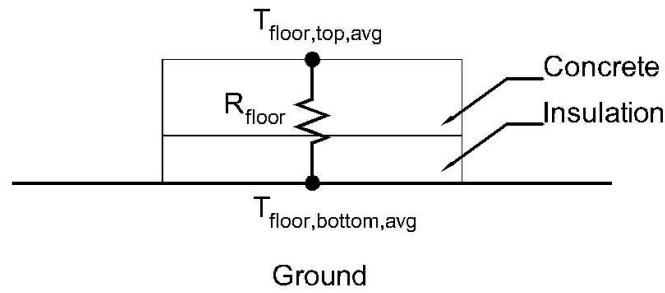


Figure 3-13: The scheme of the floor heat transfer

$$q_{\text{floor}} [\text{W/m}^2] = U \cdot \Delta T = U \cdot (T_{\text{floor,top,avg}} - T_{\text{floor,bottom,avg}}) \quad \text{Equation 3-44}$$

$$Q_{floor}, [W] = q_{floor} * Floor\ surface\ area$$

Equation 3-45

where U [W/m²K] is U-value, q_{floor} [W/m²] is floor heat transfer rate, $T_{floor,top,avg}$ is floor top surface temperature, $T_{floor,bottom,avg}$ is floor bottom surface temperature, and Q_{floor} [W] is total floor heat transfer rate accounting for floor surface area. Table 3-14 describes the boundary conditions and the initial conditions that are used in the sensitivity analysis.

Table 3-14: The boundary conditions and the initial conditions of the base case in the sensitivity analyses

Model Size			
	Length(X)	Width(Y)	Depth(Z)
Domain Size	Length(X) = 40 (m)	Width (Y) = 40 (m)	Depth (Z) = 20 (m)
Foundation Size	Length(X) = 01 (m)	Width (Y) = 01 (m)	Depth (Z) = 10 (m)
Slab Size	Length(X) = 10 (m)	Width (Y) = 10 (m)	Depth (Z) = 0.25 (m)
Thermal Properties			
	Thermal Conductivity	Density	Specific Heat
Ground Thermal Properties	1.3 (W/m·K)	2240 (kg/m3)	837 (J/kg·K)
Concrete Thermal Properties (Slab & Foundation)	1.8 (W/m·K)	2400 (kg/m3)	880 (J/kg·K)
U-tube Pipe Information	Depth = 9.8 (m) Diameter = 0.025 (m) Thermal Conductivity = 0.3 (W/m·K)		
Circular Fluid Information	Thermal Conductivity = 0.580 (W/m·K) Density = 1000 (kg/m3) Specific Heat = 4181 (J/kg·K) Volumetric Flow Rate = 6.892E-5 (m3/seconds) Reynolds Number = 2772 (Turbulent Flow)		
Temperature-based Boundary & Initial Conditions			
Ambient Temperature	$T_{OA} = T_{OA,mean} - T_{OA,amp} \cdot \cos(w \cdot time) [^{\circ}C]$ $w = \text{angular frequency} = \frac{2\pi}{(3600 \times 24 \times 365)}$ $T_{OA,mean} = \text{mean outside air temperature } [^{\circ}C] = 15[^{\circ}C]$ $T_{OA,amp} = \text{amplitude of outside air temperature fluctuation}[^{\circ}C] = 17[^{\circ}C]$		
Inlet Temperature	$T_{Inlet\ Fluid} = T_{Inlet\ Fluid,mean} - T_{Inlet\ Fluid,amp} \cdot \cos(w \cdot time) [^{\circ}C]$		

	$w = \text{angular frequency} = \frac{2\pi}{(3600 \times 24 \times 365)}$ $T_{\text{Inlet Fluid,mean}} = \text{mean inflow fluid temperature [}^{\circ}\text{C]} = 15.5[^{\circ}\text{C}]$ $T_{\text{Inlet Fluid,amp}} = \text{amplitude of inflow fluid temperature fluctuation [}^{\circ}\text{C]} = 13.5[^{\circ}\text{C}]$
Top & Bottom Boundary Conditions	$T_{\text{water}} = 10 (^{\circ}\text{C})$ (Groundwater temperature as a bottom boundary condition) $T_{\text{in}} = 22 (^{\circ}\text{C})$ (Indoor space temperature as a top surface of a slab)
Outer Edge Boundary Condition	Adiabatic

3.6.1. Impact of foundation depth

Similar to the vertical GSHPs, thermo-active foundation systems utilize geothermal energy. Therefore, the foundation depth can significantly affect the thermal performance of TAF systems. Figure 3-14 and Figure 3-15 illustrates the variations of the heat exchange rate through a U-tube and a floor, respectively (expressed in percent as defined by Equation 3-43) as a function of normalized foundation depths for various normalized fluid velocities. As shown in Figure 3-14, as the foundation pile is deeper more heat can be exchanged to or from the ground especially for higher fluid velocities. Therefore, when selecting a depth for a thermo-active foundation, it is important to also consider the fluid velocity within the geothermal exchanger loops. However, in Figure 3-15, it is observed that the foundation depth doesn't have impact on the heat transfer through an above-grade floor.

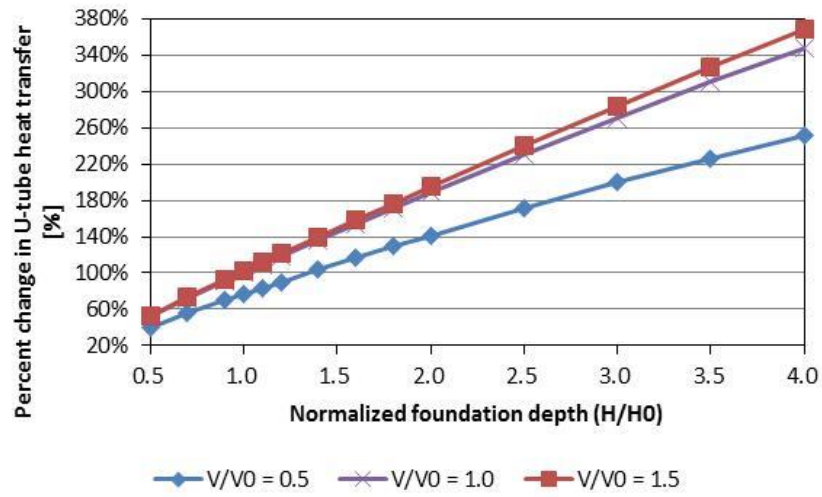


Figure 3-14: The impact of foundation depth for various normalized fluid velocities on the U-tube heat transfer

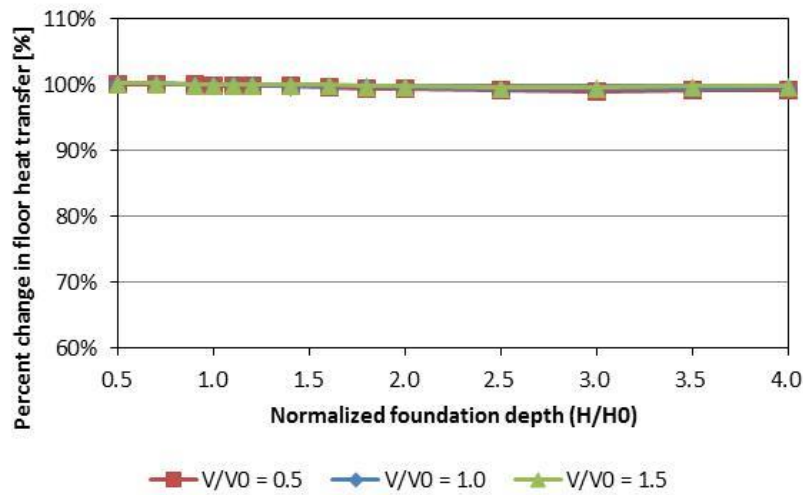


Figure 3-15: The impact of foundation depth for various normalized fluid velocities on the floor heat transfer

3.6.2. Impact of fluid velocity

The effect of fluid velocity in the U-tube loops on the performance of thermo-active foundation is shown in Figure 3-16 and Figure 3-17. As expected, the exchanged heat transfer increases as the fluid velocity increases. In addition, at the point that a shift from a laminar flow to a turbulent flow (i.e., when

$Re \geq 2300$) occurs, there is a sudden increase of the heat transfer rate. This change is due to the fact that turbulent flow increases the convective coefficient along the pipe walls, and therefore increases heat transfer through the pipe walls.

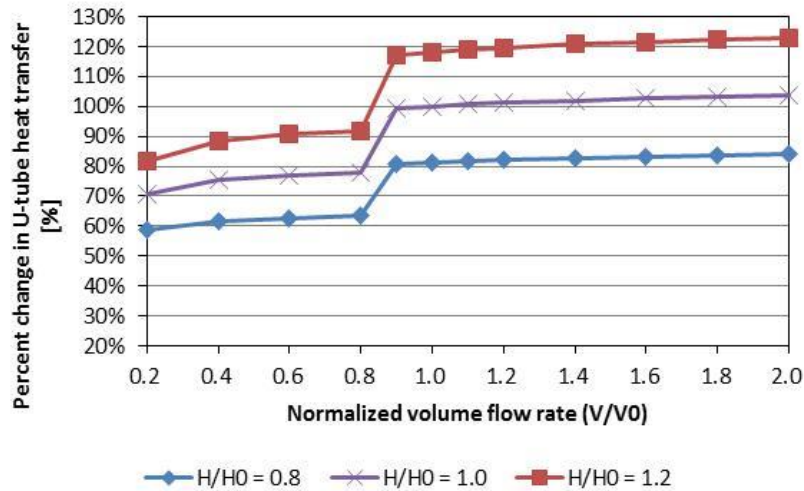


Figure 3-16: The impact of fluid velocity for various normalized foundation depth on the U-tube heat transfer

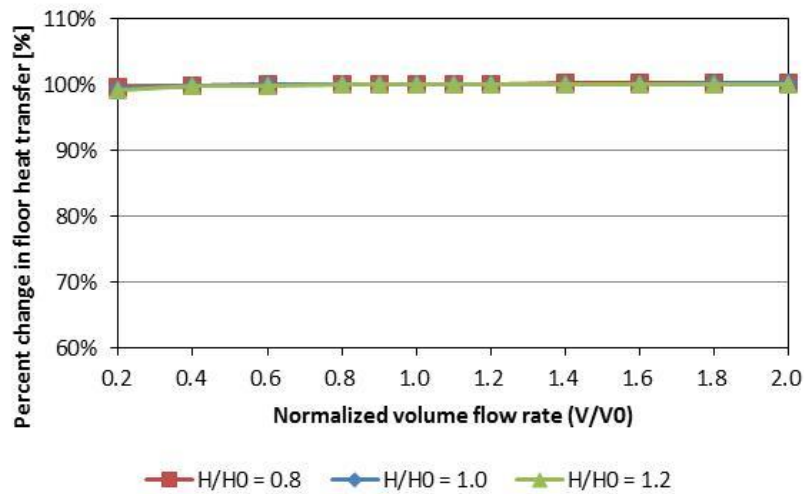


Figure 3-17: The impact of fluid velocity for various normalized foundation depth on the floor heat transfer

However and as shown in Figure 3-16, the increasing rate of heat transfer is rather slow after the shift from laminar flow to turbulent flow. Indeed, due to the higher fluid velocity there is not enough

time for heat exchanges between the fluid and the ground. Thus, the temperature differences between the inlet and outlet becomes rather small. Like the case of the foundation depth, the fluid flow rate doesn't have impact on the floor heat transfer (Figure 3-17).

3.6.3. Impact of the shank space

Within a thermo-active foundation, there is thermal interference between U-tube pipes. The impact of the distance between two loops, typically referred as the shank space, is evaluated. Figure 3-18 illustrates the percent increase in heat transfer between the thermo-active foundation and ground as a function of the ratio of shank space to the base shank space for various foundation radii. Figure 3-18 indicates that the heat transfer through the pipes increases as the shank space increases. A higher shank space implies that there are less thermal interactions between the U-tube pipes. In addition, larger foundation radius results in higher heat transfer by the thermo-active foundation due to larger surface area

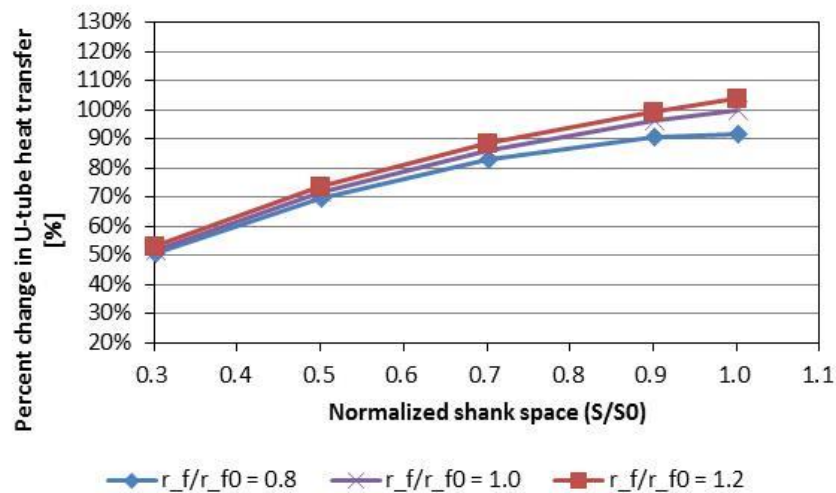


Figure 3-18: The impact of shank space ratio for various foundation radii on the U-tube heat transfer

Figure 3-19 illustrates the percent change in the floor heat transfer for various normalized shank space and various normalized foundation radii. As shown in Figure 3-19, shank space also doesn't have impact on the floor heat transfer. However, it can be shown that foundation radius has impact on the floor heat transfer. So, the wider foundation radius makes the more heat transfer through an above-grade floor.

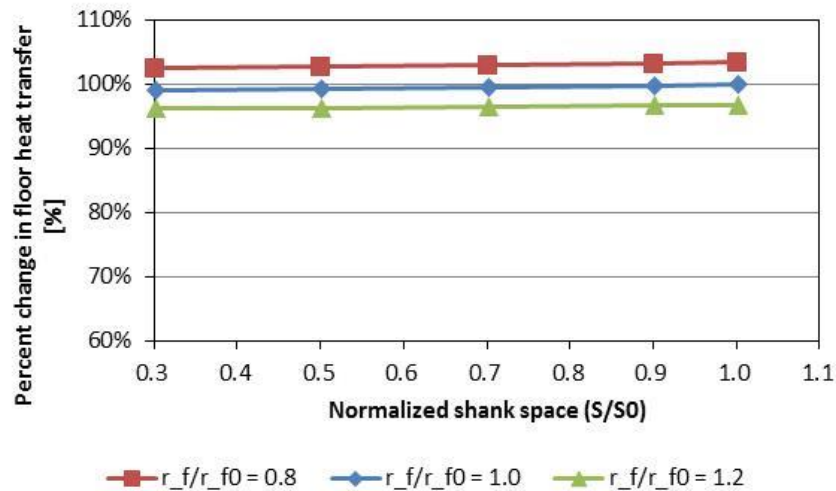


Figure 3-19: The impact of shank space ratio for various foundation radii on the floor heat transfer

3.6.4. Impact of the thermal conductivity of ground

To evaluate the effect of the thermal conductivity of ground on thermal performance of a thermo-active foundation, a sensitivity analysis was performed as shown in Figure 3-20 and Figure 3-21. As expected, increasing the thermal conductivity of ground increases the heat transfer between the foundation and the ground, and improves the thermal performance of a thermo-active foundation (Figure 3-20). In addition, increasing the thermal conductivity of ground causes the more heat transfer through a floor (Figure 3-21).

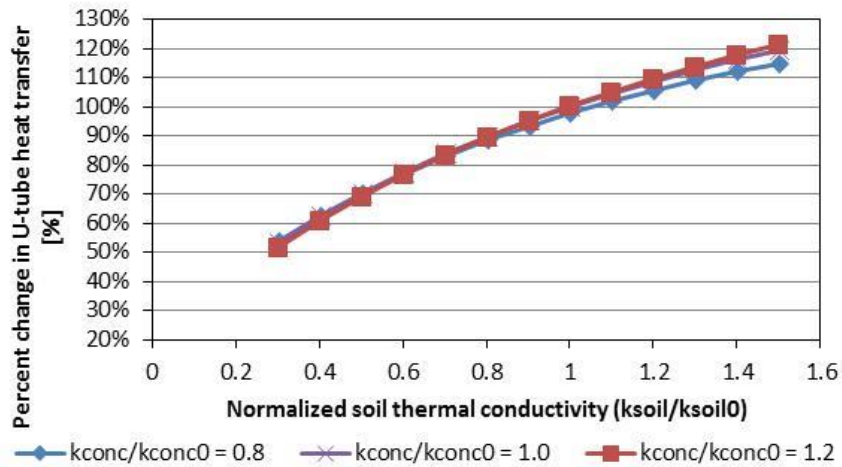


Figure 3-20: The impact of the thermal conductivity of ground for various thermal conductivity of concrete on the U-tube heat transfer

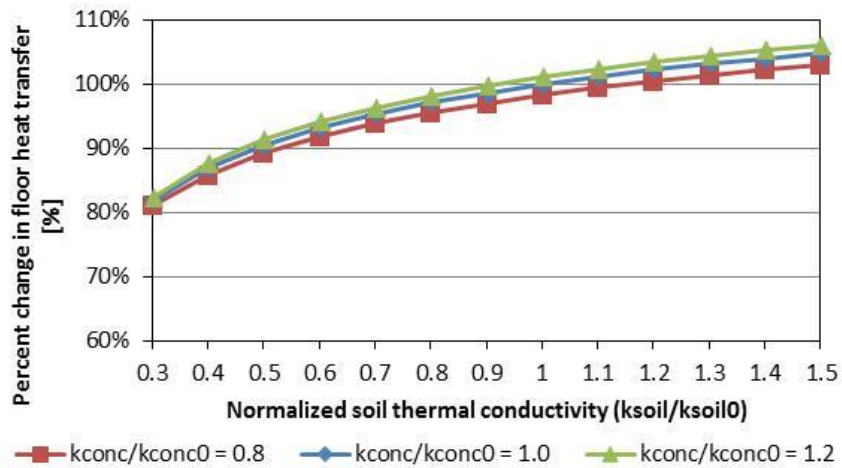


Figure 3-21: The impact of the thermal conductivity of ground for various thermal conductivity of concrete on the floor heat transfer

3.6.5. Impact of the thermal conductivity of concrete

To evaluate the effect of the thermal conductivity of concrete on thermal performance of a thermo-active foundation, a sensitivity analysis was performed as shown in Figure 3-22 and Figure 3-23. Concrete is a common material for a building foundation and a floor. As expected, like the case of the

thermal conductivity of ground, increasing the thermal conductivity of concrete increases the heat transfer between the U-tube pipes and the ground, and improves the thermal performance of a thermo-active foundation (Figure 3-22). Additionally, increasing the thermal conductivity of concrete causes the more heat transfer through a floor (Figure 3-23).

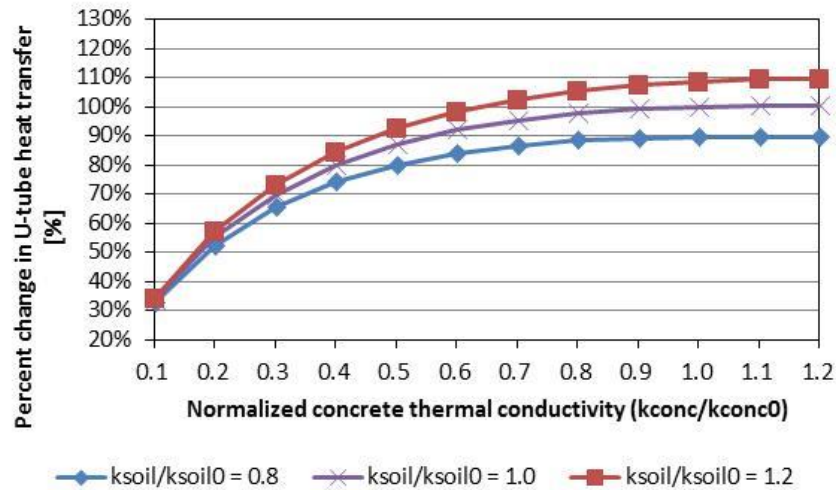


Figure 3-22: The impact of the thermal conductivity of concrete for various thermal conductivity of ground on the U-tube heat transfer

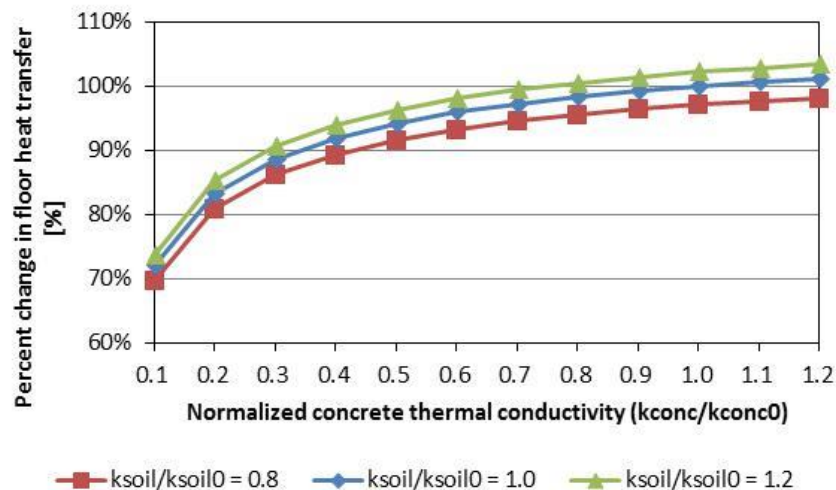


Figure 3-23: The impact of the thermal conductivity of concrete for various thermal conductivity of ground on the floor heat transfer

3.6.6. Impact of insulation level of slab-on floor

The insulation level of slab-on-grade floor is an important parameter for building foundation heat transfer (Krarti, 2010). In addition, since thermal piles are placed just below a building foundation, the effect of thermo-active foundation on ground-coupled heat transfer through a slab-on-grade floor can be significant and should be evaluated. Generally, slab-on-grade floors for commercial or residential buildings have an insulation layer with a specific R-value depending on the energy efficiency codes and climate conditions. In this analysis, it assumes that the floor has a uniform insulation that covers the entire floor area. Figure 3-24 summarizes the impact of the normalized thermal conductivity of the slab-on-grade floor insulation on the building foundation heat transfer. The thermal conductivity of the base case floor insulation (k_{insul_0}) is set to be 1.0 W/m-K, and Q_{floor_0} is the resulting foundation heat transfer. As shown in Figure 3-24, as the floor insulation thermal conductivity decreases (and thus the floor insulation R-value increases), the ground-coupled floor heat transfer increases.

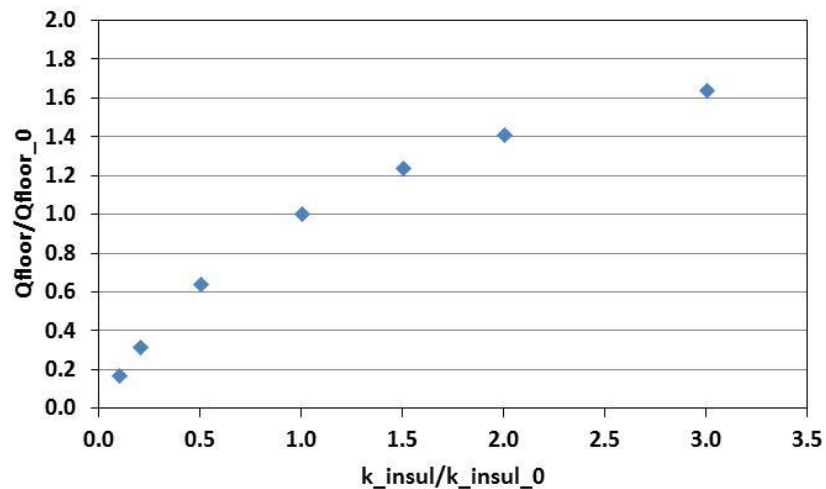


Figure 3-24: Effect of insulation level of above-grade floor on ground-coupled floor heat transfer

3.6.7. Thermal Interferences of neighboring thermal pile

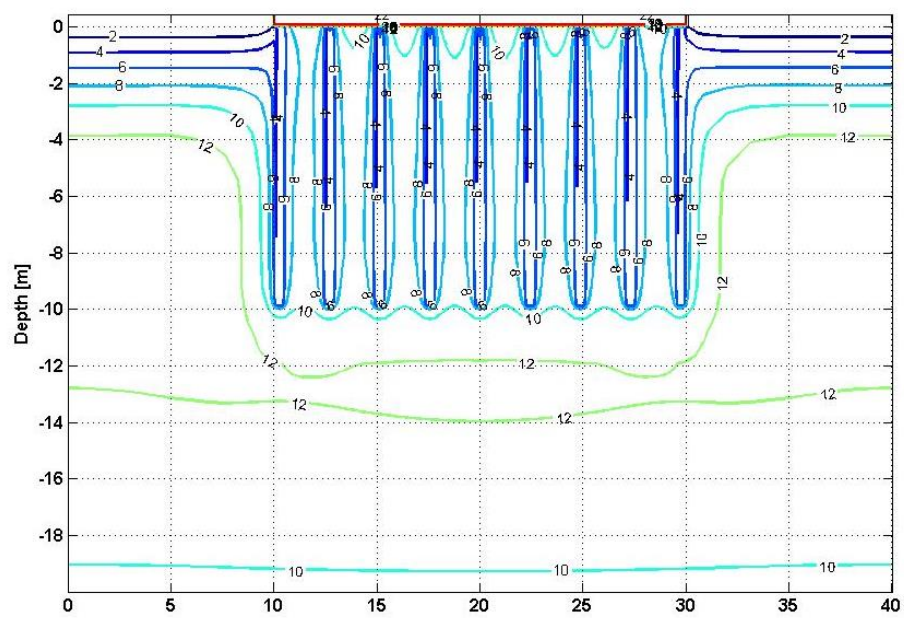
The analysis in the previous sections uses only a single foundation with one thermal pile located in the middle of the slab-on-grade floor and thus neglects any thermal interactions between multiple thermal piles. However, a foundation configuration with multiple thermal piles is more likely to be considered to meet heating and cooling requirements for buildings. In this section, the thermal interactions between several adjacent thermal piles are evaluated for several pile depths and distances between piles. Table 3-15 presents the boundary conditions and initial conditions of the three-dimensional numerical model used for this analysis assuming that the multi thermal piles are designed using a parallel configuration.

Table 3-15: Summary of boundary and initial conditions of the numerical model for a thermo-active foundation with multiple thermal piles

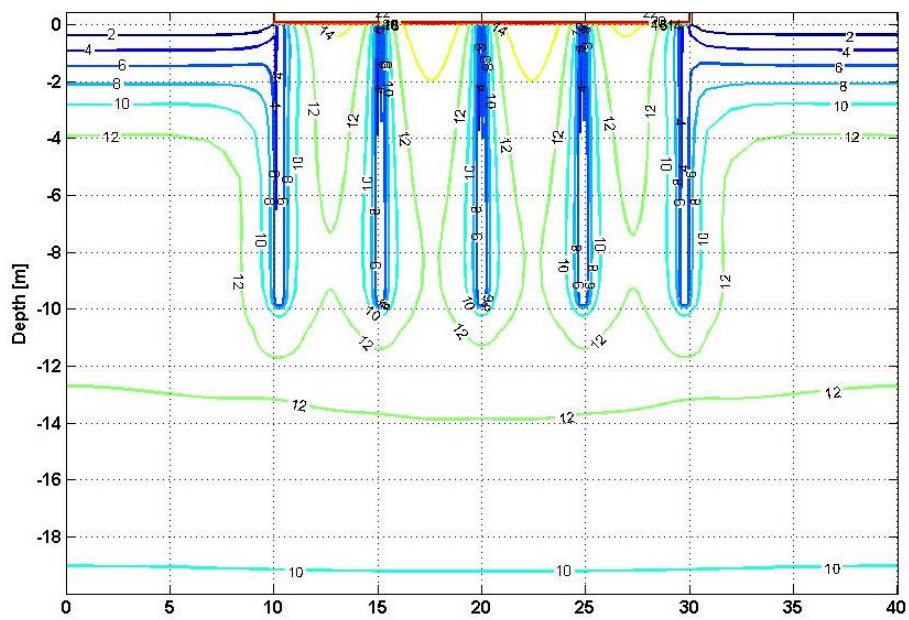
Model Size			
	Length(X)	Width(Y)	Depth(Z)
Domain Size	Length(X) = 50 (m)	Width (Y) = 36 (m)	Depth (Z) = 20 (m)
Foundation Size	Length(X) = 0.5 (m)	Width (Y) = 0.5 (m)	Depth (Z) = 10 (m)
Slab Size	Length(X) = 30 (m)	Width (Y) = 16 (m)	Depth (Z) = 0.25 (m)
Thermal Properties			
	Thermal Conductivity	Density	Specific Heat
Ground Thermal Properties	1.3 (W/m·K)	2240 (kg/m3)	837 (J/kg·K)
Concrete Thermal Properties (Foundation)	1.8 (W/m·K)	2400 (kg/m3)	880 (J/kg·K)
U-tube Pipe Information	Depth = 9.8 (m) Diameter = 0.025 (m) Thermal Conductivity = 0.3 (W/m·K)		
Circular Fluid Information	Thermal Conductivity = 0.580 (W/m·K) Density = 1000 (kg/m3) Specific Heat = 4181 (J/kg·K) Volumetric Flow Rate = 6.892E-5 (m3/seconds) Reynolds Number = 2772 (Turbulent Flow)		
Temperature-based Boundary & Initial Conditions			

Ambient Temperature	$T_{OA} = T_{OA,mean} - T_{OA,amp} \cdot \cos\left(\frac{w \cdot \text{time}}{2\pi}\right) [^{\circ}\text{C}]$ $w = \text{angular frequency} = \frac{2\pi}{(3600 \times 24 \times 365)}$ $T_{OA,mean} = \text{mean outside air temperature } [^{\circ}\text{C}] = 15[^{\circ}\text{C}]$ $T_{OA,amp} = \text{amplitude of outside air temperature fluctuation } [^{\circ}\text{C}] = 17[^{\circ}\text{C}]$
Inlet Temperature	$T_{\text{Inlet Fluid}} = T_{\text{Inlet Fluid},mean} - T_{\text{Inlet Fluid},amp} \cdot \cos\left(\frac{w \cdot \text{time}}{2\pi}\right) [^{\circ}\text{C}]$ $w = \text{angular frequency} = \frac{2\pi}{(3600 \times 24 \times 365)}$ $T_{\text{Inlet Fluid},mean} = \text{mean inflow fluid temperature } [^{\circ}\text{C}] = 15.5[^{\circ}\text{C}]$ $T_{\text{Inlet Fluid},amp} = \text{amplitude of inflow fluid temperature fluctuation } [^{\circ}\text{C}] = 13.5[^{\circ}\text{C}]$
Top & Bottom Boundary Conditions	$T_{\text{water}} = 9.7 (^{\circ}\text{C}) \text{ (Groundwater temperature as a bottom boundary condition)}$ $T_{\text{in}} = 22 (^{\circ}\text{C}) \text{ (Indoor space temperature as a top surface of a slab)}$
Outer Edge Boundary Condition	Adiabatic

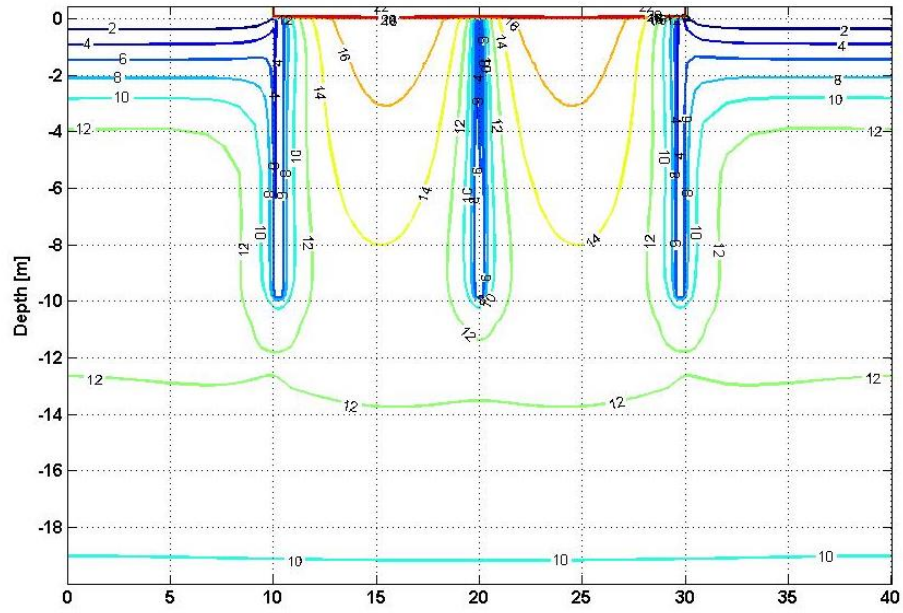
In this analysis, by changing number of thermal piles, the center-to-center distance between thermal piles can be varied. Figure 3-25 and Figure 3-26 illustrates the temperature distribution within the ground medium around thermal piles during, respectively winter and summer seasons. The center-to-center distances between thermal piles considered in Figure 3-25 and Figure 3-26 are (a) 3.3m, (b) 5m, (c) 10m, and (d) 20m. As shown in both Figure 3-25 and Figure 3-26, it is found that the thermal interference between thermal piles is decreased as the distance between the piles increases.



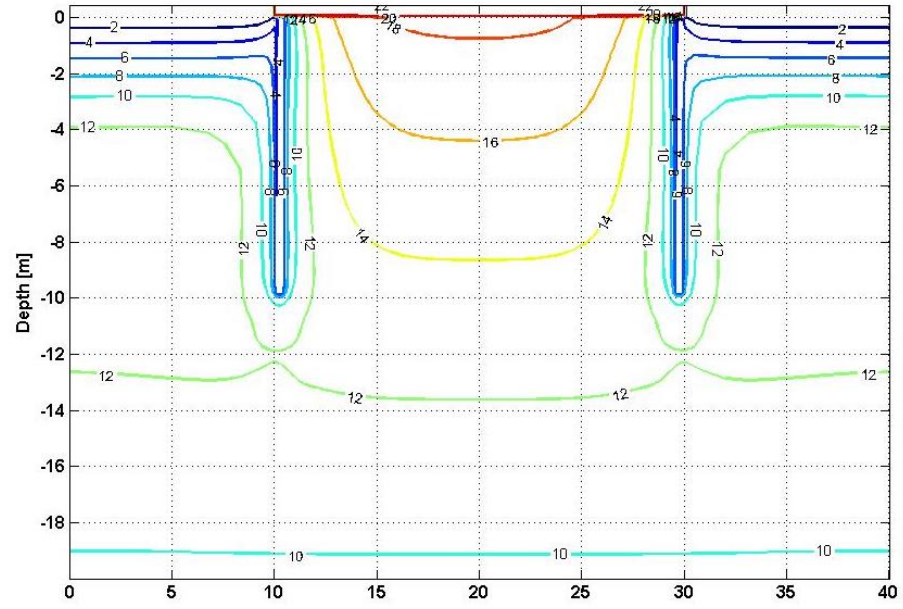
(a)



(b)

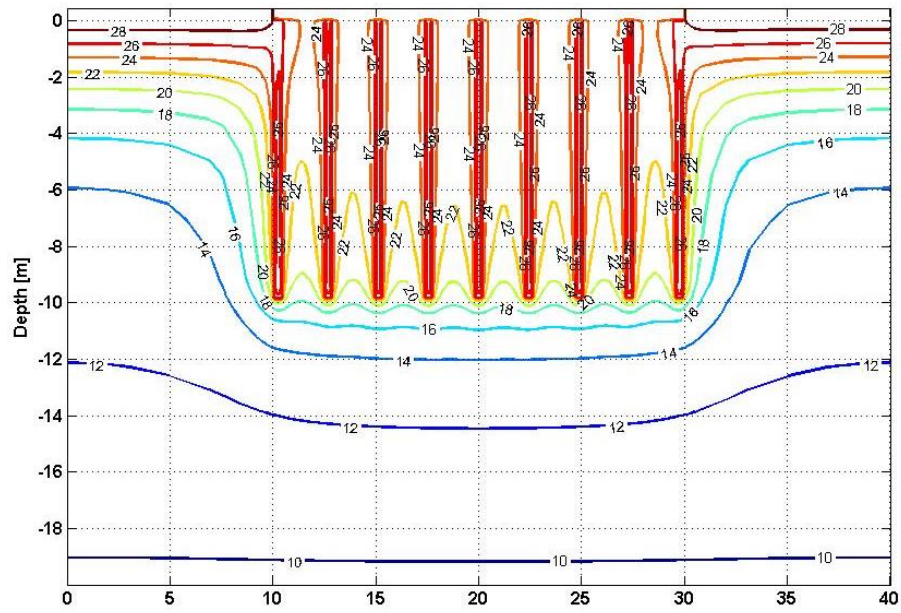


(c)

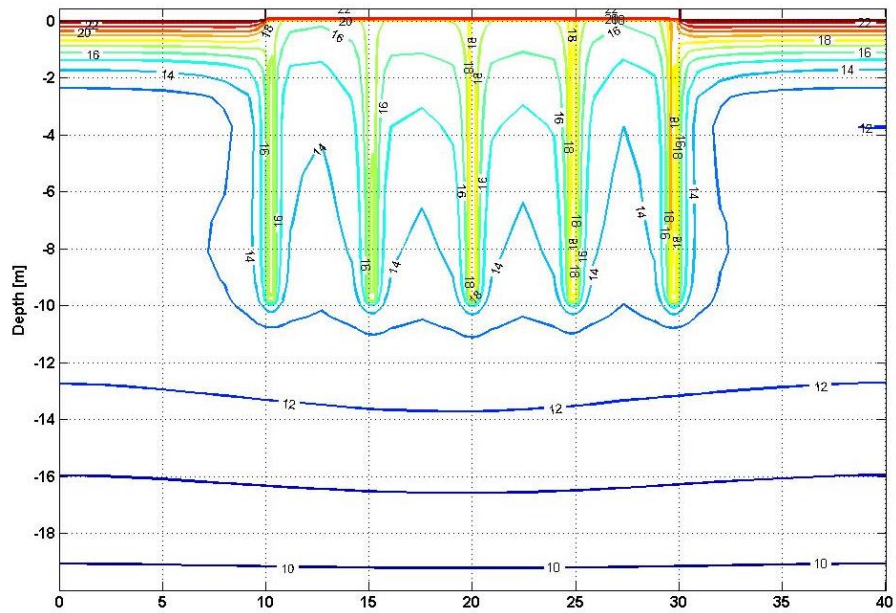


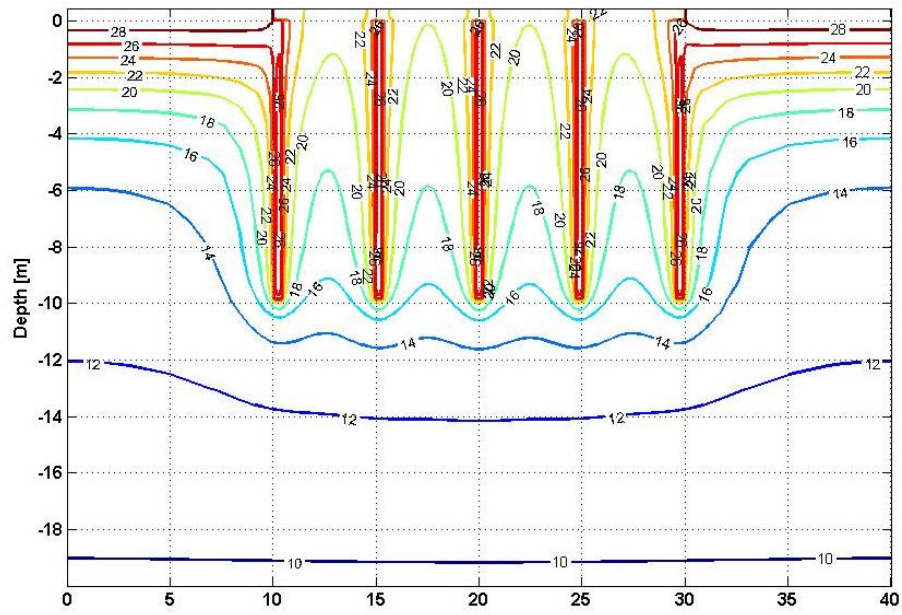
(d)

Figure 3-25: Temperature isotherms of different thermo-active foundations with variable number of thermal piles during the winter season; the center-to-center distance between piles is (a) 3.3m, (b) 5m, (c) 10m, and (d) 20m, $T_{out}=0.28^{\circ}\text{C}$, $T_{in}=22^{\circ}\text{C}$

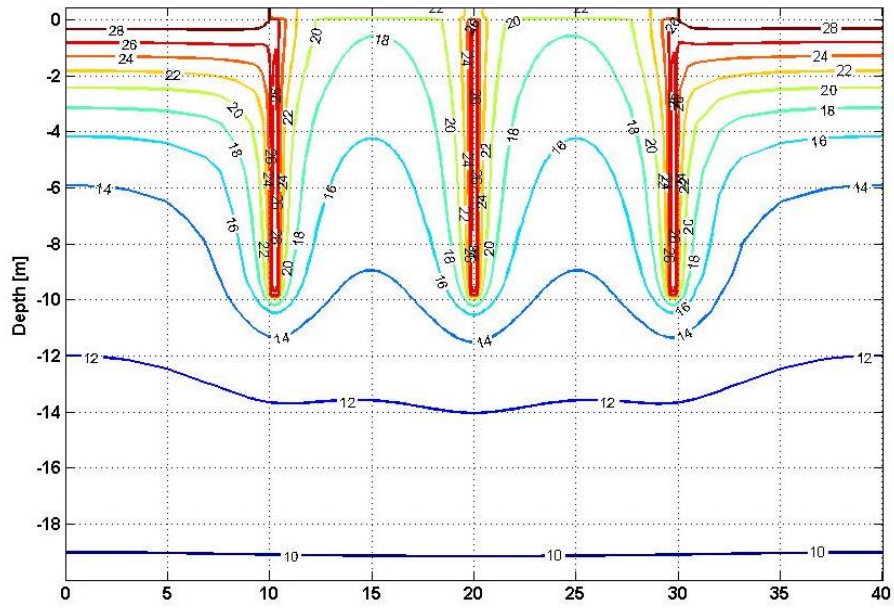


(a)





(b)



(c)

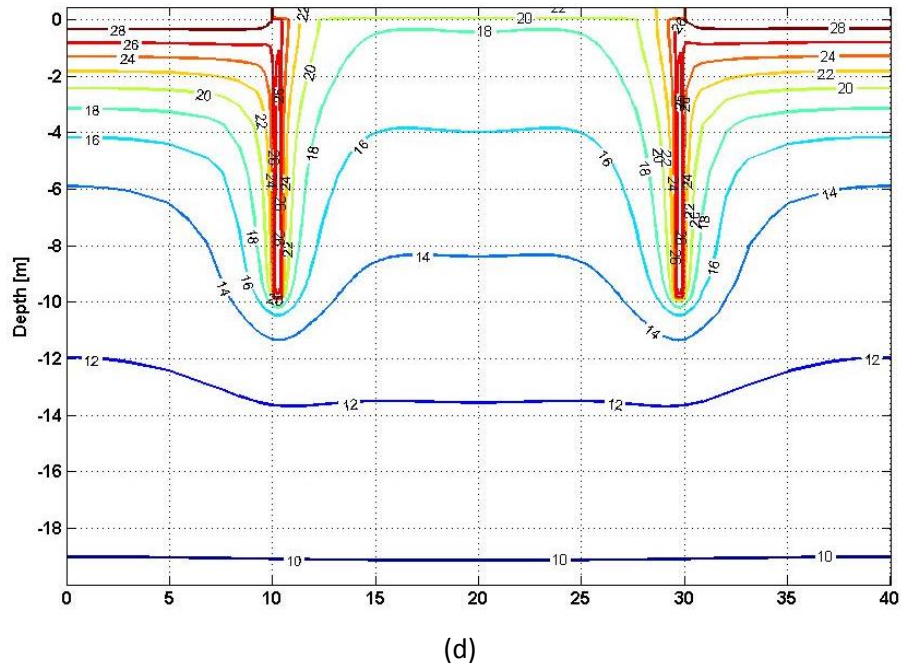


Figure 3-26: Temperature isotherms of different thermo-active foundations with variable number of thermal piles during the summer season; the center-to-center distance between piles is (a) 3.3m, (b) 5m, (c) 10m, and (d) 20m, $T_{out}=29.7^{\circ}\text{C}$, $T_{in}=22^{\circ}\text{C}$

Figure 3-27 shows the impact of the thermal pile aspect ratio on thermal performance of a thermal pile. The aspect ratio is defined as the ratio of the pile depth to the distance between two adjacent thermal piles. As shown in Figure 3-27, the thermal interactions between thermal piles decrease as the aspect ratio increases. No thermal impact of adjacent thermal piles is noted when the aspect ratio is higher than 0.5.

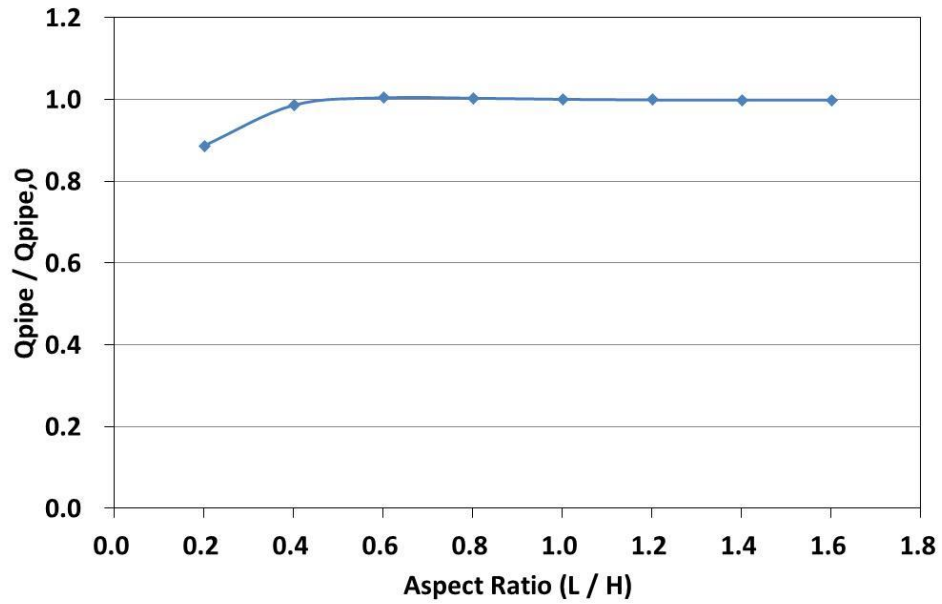


Figure 3-27: Thermal interactions between adjacent thermal piles for several pile aspect ratios

3.7. Summary

In this chapter, a three-dimensional transient numerical model for a thermo-active foundation has been developed in the Cartesian coordinate system. The numerical model is based on the implicit finite difference method. The numerical model considered in this study is representative of a concrete foundation and can be used to estimate the heat transfer exchanged between the thermal pile and the ground medium under various design and operating conditions. In addition, using the three-dimensional numerical model in the Cartesian coordinates, the effects of the indoor temperature of a building on the thermal performance of a thermo-active foundation can be analyzed.

Using a proper discretization scheme to optimize the accuracy and the computational efforts, the transient three-dimensional numerical model has been validated with the experimental data

obtained from a laboratory set-up in the Centrifuge Lab of the Geotechnical Engineering and Geomechanics, the University of Colorado at Boulder. The experimental set-up was specific for a small scale model thermo-active foundation with a concrete pile in a ground domain. As a result, using the given information from the experiment, the overall RMSE result was 2.32 °C, which was relatively high, even though the value was within the acceptable tolerance range of the typical type-k thermocouples. So, the additional series of sensitivity analyses was performed to analyze which parameter would have effects on the RMSE results. Then, based on the results, the numerical model was calibrated generating the lower RMSE. Using the validated numerical model, a comparative analysis was performed between two numerical models: one in the Cartesian coordinates and the other in the Cylindrical coordinates. As a result of the comparison analysis, the overall RMSE was 0.26°C.

Utilizing the 3D numerical model developed in this chapter, a series of sensitivity analyses has been carried out to evaluate the impact of selected design and operating parameters on the performance of thermo-active foundations. The parameters analyzed in this chapter were the thermal conductivities of ground and foundation material, the foundation depth, the circular fluid volumetric flow rate, the shank space, the location of a foundation, and the number of U-tube loops. From this sensitivity analyses, it was found that higher heat transfer exchanged between the thermo-active foundation and ground can be achieved by increasing the thermal conductivities of ground and foundation material, the foundation depth, the fluid velocity, or shank space of the U-tube loops within the same pile. In addition, it was also found that the foundation depth, the fluid velocity, and the shank space have the minor impacts on the heat transfer through an above-grade floor.

Using the three-dimensional numerical model, the effect of distance between thermal piles was investigated in this chapter. For the considered boundary and initial conditions, it was found that as the thermal pile aspect ratio ($\text{Aspect ratio} = \frac{\text{distance between piles}}{\text{pile depth}}$) increased, the thermal interactions

between thermal piles decreased. When the aspect ratio is higher than 0.5, it was found that thermal interactions can be neglected.

CHAPTER 4. ANALYSIS FOR THERMAL COUPLING

4.1. Introduction

As an energy source, geothermal energy is beneficial for building systems due to the fact that it is clean and sustainable energy. There have been several researches to investigate energy performances of ground source heat pump (GSHP) systems. Especially, Eskilson (Eskilson, 1987) and Yavuzturk (Yavuzturk, 1999) developed a good approach, G-function method, to estimate thermal performances of GSHP systems.

However, there have been few researches for thermo-active foundation (TAFs) systems. Some researches were actual field experimental studies, and other researches used numerical methods to investigate its thermal performances. In general, those approaches provide good results, but these methods require much computation times as well as much experiences to perform reliable and accurate analysis. So, using these approaches it is hard to consider correlations between several parameters that have impacts on thermal performances of TAFs systems. In other words, it needs a new simplified approach to investigate correlations between several variables and factors of TAFs systems, and to estimate thermal impact of TAFs systems on building heat transfer.

In this chapter, a simplified approach is proposed to estimate annual average heat transfer through ground heat exchanger pipes and through ground floor is developed. The new approach is built on the patterns of the results from a series of detailed numerical simulations. The design parameters used in this approach are foundation pile size, and number of foundations. In this analysis, an assumption is required that heat exchanger pipes are integrated into all foundations of a building.

4.2. Simulation Settings

4.2.1. Description of numerical model

A series of simulations is performed to estimate the impacts of design parameters on thermal performances of TAFs systems as well as on thermal interactions between indoor space and ground. In order for these analyses, a numerical finite difference model developed in Chapter 3 is utilized to investigate these design parameters, such as foundation size, foundation height, and number of foundations. Figure 4-1, Table 4-1 and Table 4-2 briefly describes the input data and settings for the numerical model.

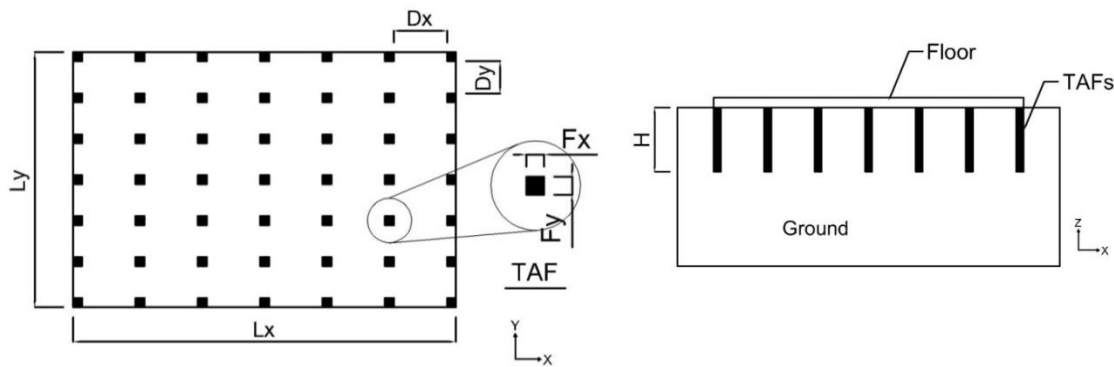


Figure 4-1: Schematic image of numerical model

Table 4-1: Description of sizes of the numerical model

	X [m]	Y [m]	Z [m]
Ground size	60m	60m	30m
Slab size	30m	20m	0.25m

Table 4-2: Description of inputs of numerical model

Thermal Conductivity	Ksoil = 1.3 W/m (Ground) Kconc = 1.8 W/m (Slab & Foundations)
Thermal Resistance	Rinsul = 4 m ² K/W

Outdoor Air Temperature (T _{out})	Temp _{out} = T _{mean} - T _{amplitude} * cos(ω* time); T _{mean} = 10.24236 °C T _{amplitude} = 12.30833 °C ω = 2 * pi / (3600 * 24 * 365)
Inlet Fluid Temperature (T _{inlet})	Temp _{out} = T _{F_mean} - T _{F_amplitude} * cos(ω* time); T _{F_mean} = 11.0 °C T _{F_amplitude} = 09.0 °C ω = 2 * pi / (3600 * 24 * 365)
Indoor Air Temperature (T _{in})	T _{in} = 20 °C
Ground Water Temperature (T _{water})	T _{water} = 20 °C

4.2.2. Grid sensitivity analysis

Because of limitations in computing capabilities, finer grids require more simulation time in a finite difference numerical model. So, a sensitivity analysis is performed to determine the adequate grid scheme for simulations in this chapter. The sensitivity analysis on the grid dependence is performed in terms of Root Mean Square Error (RMSE) and computing time. A very fine grid scheme is used as a reference case against which all the other discretization schemes are compared. Using RMSE method (Equation 4-1), the magnitude of the differences between the predictions using the reference and any other schemes are compared. The RMSE values are calculated based on heat transfer through ground heat exchanger pipes in Watts.

$$RMSE = \sqrt{\frac{\sum_{i=1}^n (W_{1,i} - W_{2,i})^2}{n}}$$

Equation 4-1

$W_1 = [W_{1,1}, W_{1,2}, W_{1,3}, \dots, W_{1,n}]$ and $W_2 = [W_{2,1}, W_{2,2}, W_{2,3}, \dots, W_{2,n}]$

The RMSE values are shown in Table 4-3 and Figure 4-2 for several grid schemes. The finer the grid is, the more accurate the numerical solution is characterized by lower RMSE values, but the more

computing time the numerical model consumes. Therefore, from this analysis it is determined that the adequate number of grid node is 481,032 which have RMSE value of 1.0W and CPU time of 7925.6seconds.

Table 4-3: The impact of grid node numbers on both CPU time and RMSE values for numerical simulations

	Node	RMSE [W]	Time [seconds]
1	47,700	203.0	92.7
2	69,384	114.4	204.2
3	96,720	55.8	358.7
4	120,700	27.2	609.5
5	162,108	16.0	1009.0
6	216,216	8.7	2127.2
7	278,100	5.0	2955.8
8	347,652	2.8	3958.3
9	347,760	3.0	4504.4
10	425,196	1.7	6224.2
11	481,032	1.0	7925.6
12	540,432	0.5	9752.5
13	636,012	0.0	12776.1

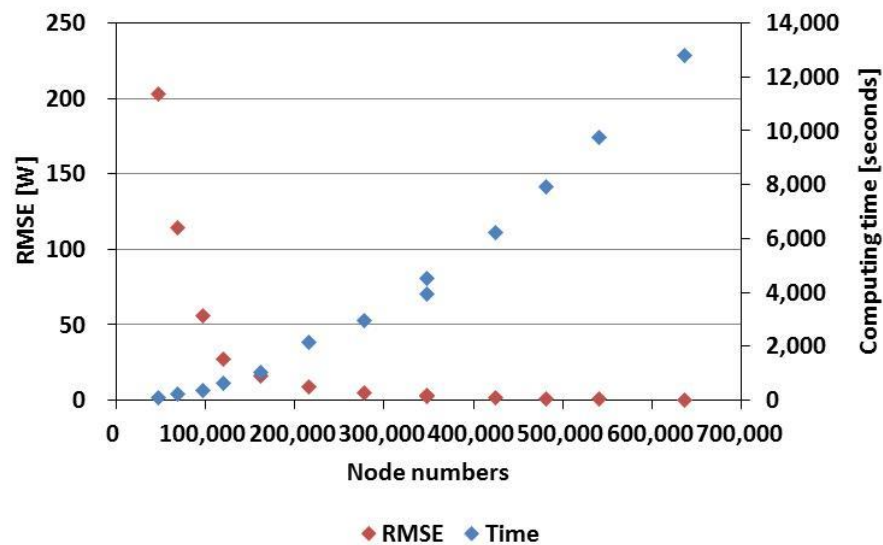


Figure 4-2: Variations of CPU time and RMSE values associated with the numerical solutions as functions of the number of the grid nodes

4.2.3. Sensitivity analysis

Sensitivity analyses are designed to estimate impacts of several parameters on thermal performances of TAFs systems and on thermal interactions between indoor temperature and ground temperature which is influenced by TAFs systems. The parameters researched in this chapter are number of foundations and foundation sizes (length, width, height), and then the correlations between parameters are investigated. Table 4-4 describes the numbers of foundations used in the sensitivity analysis. Figure 4-3 illustrates the different configurations of number of foundations used to estimate the impact of this parameter on heat transfer through heat exchanger pipes and ground floor. Table 4-5 describes different foundation pile sizes. The correlation between design parameters and thermal performances of thermal pile, and the correlation between design parameters and thermal interactions through ground floor is investigated. All cases of sensitivity analysis have the same slab size as shown in Table 4-1.

Table 4-4: Description of settings for sensitivity analysis

Number of Foundations, N		Nx					
		2	3	4	5	6	7
Ny	2	4	6	8	10	12	14
	3	6	9	12	15	18	21
	4	8	12	16	20	24	28
	6	12	18	24	30	36	42
	7	14	21	28	35	42	49

Table 4-5: Description of foundation sizes for sensitivity analysis

Height [m]	H[m] = 5, 10, 15, 20
Foundation Size [m]	Fx[m] = 0.5, 0.6, 0.7, 0.8, 1.0
	Fy[m] = 0.5, 0.6, 0.7, 0.8, 1.0

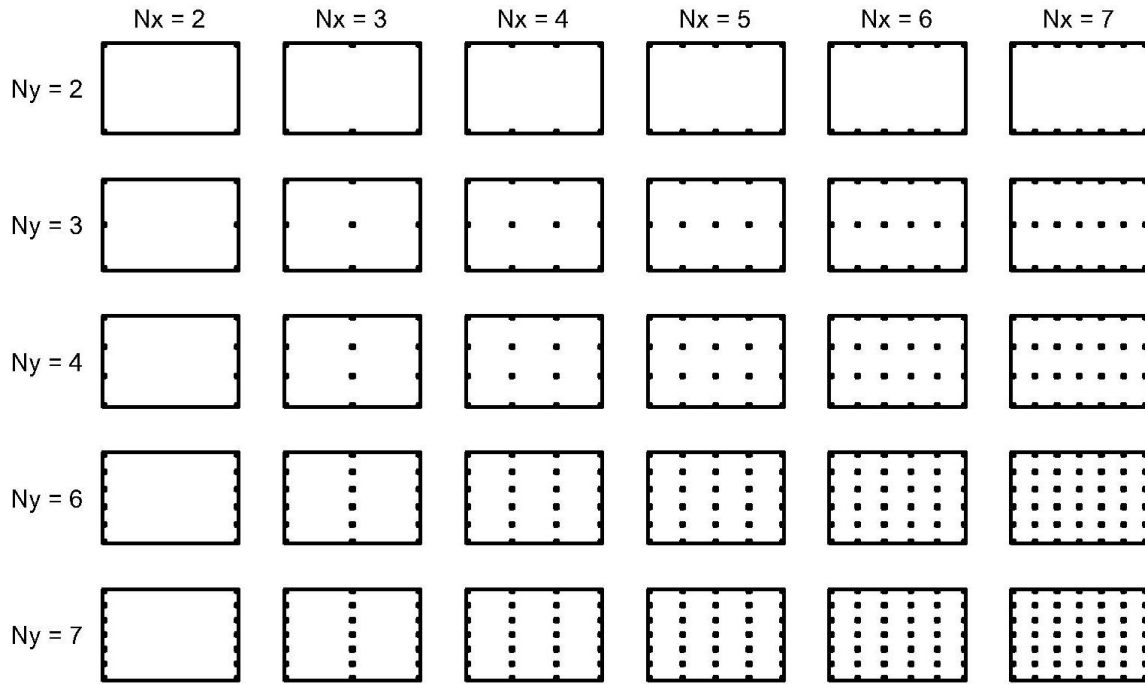


Figure 4-3: Configurations of number of foundations

4.3. Correlation between Design Parameters and Performance of TAFs Piles

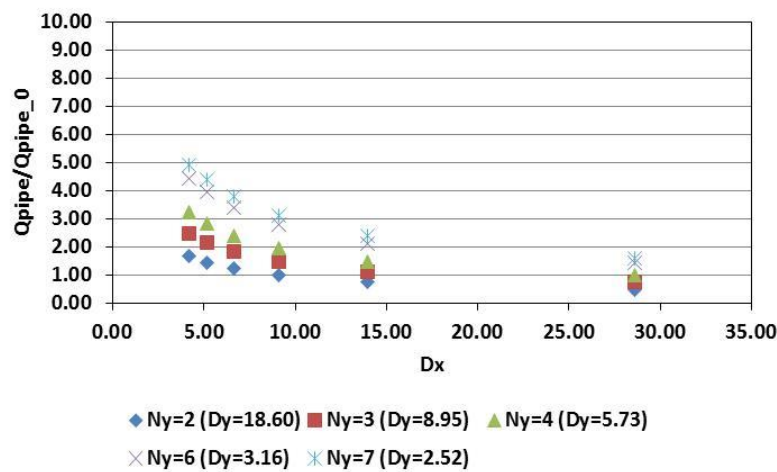
4.3.1. Formularization of the correlation between design parameters

This paper assumes that a building uses all foundation piles as thermo-active foundations. According to the results in Chapter 3, thermal performance of thermo-active foundation is affected by several design parameters, such as size of thermal pile, and numbers of TAF piles. So, considering the impacts of several parameters on pipe heat transfer rate, this chapter explore the correlation between parameters, and formularize the correlations.

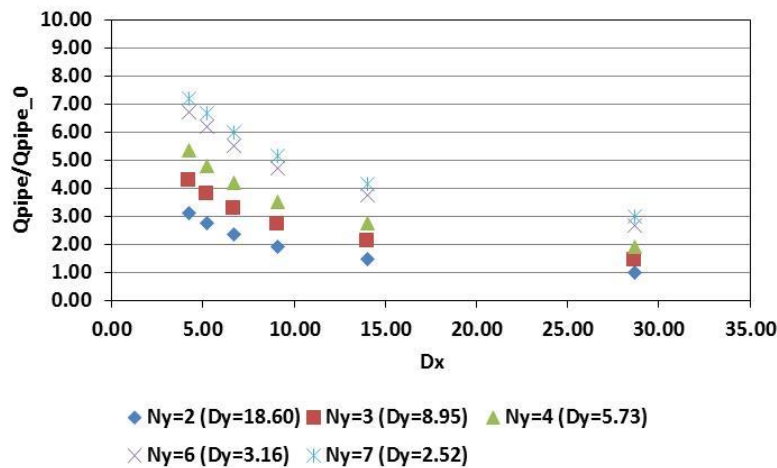
As presented in Chapter 3, for specific thermal properties of ground and foundation pile, the most impact on thermal performance of a thermal pile is caused by foundation size. Additionally, since it needs to explore the effect of multi-thermal piles on overall pipe heat exchanger rate, this analysis has

design parameters related to numbers of thermal piles and distances between thermal piles for a specific size of an above-grade floor. Figure 4-4 presents the variations of pipe heat transfer rate for several design parameters; different depths of thermal pile, and different numbers of thermal piles, and so different distances between thermal piles as shown in Figure 4-3. Q_{pipe_0} is the base heat transfer rate of heat exchanger pipe for the case of $N_x=2$ and $N_y=2$ with $H=0.5\text{m}$, and $F_x=0.7\text{m}$ and $F_y=0.7\text{m}$.

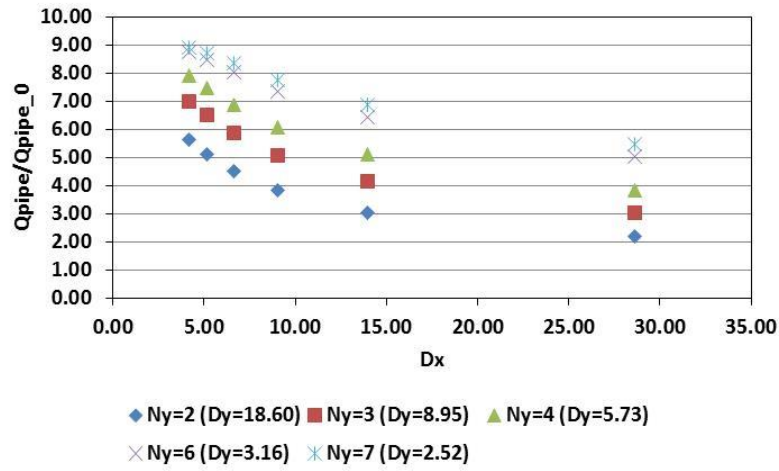
As shown in Figure 4-4, the more numbers of thermal piles, and so the shorter distances between thermal piles has higher heat transfer through heat exchanger piles. It is also found that for the same diameter of a thermal pile the higher depth of pile has higher pipe heat transfer.



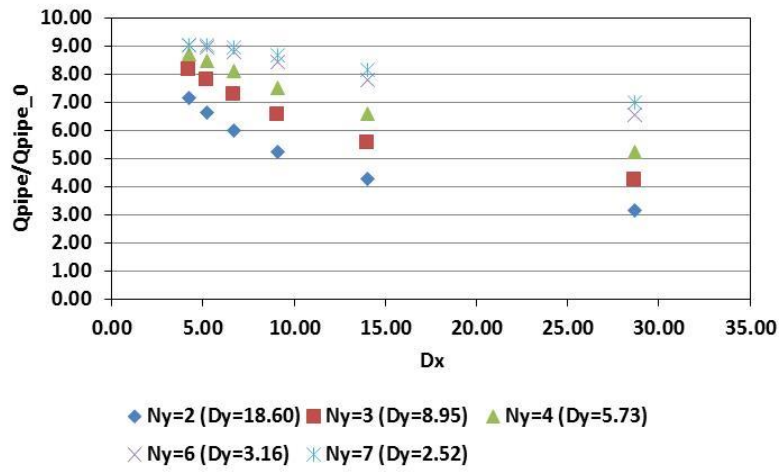
(a)



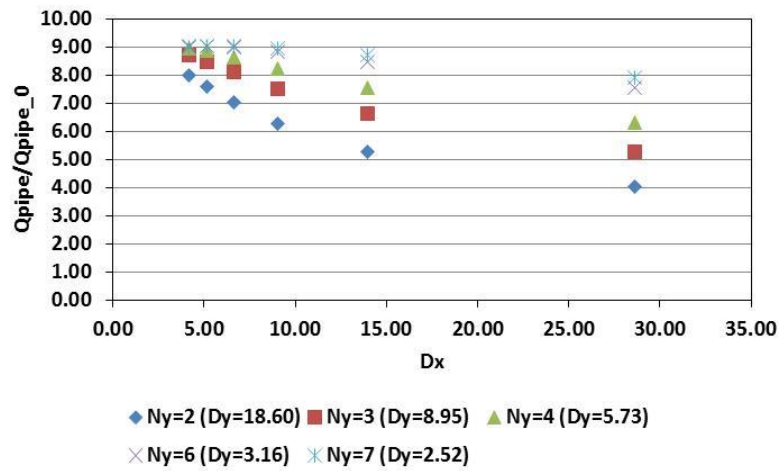
(b)



(c)



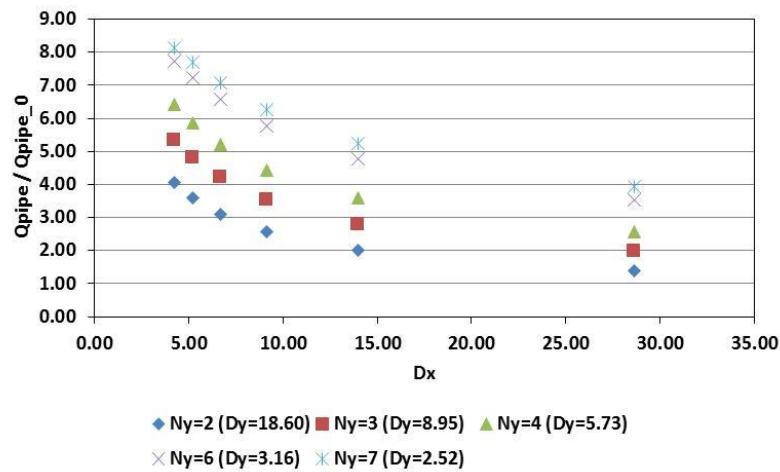
(d)



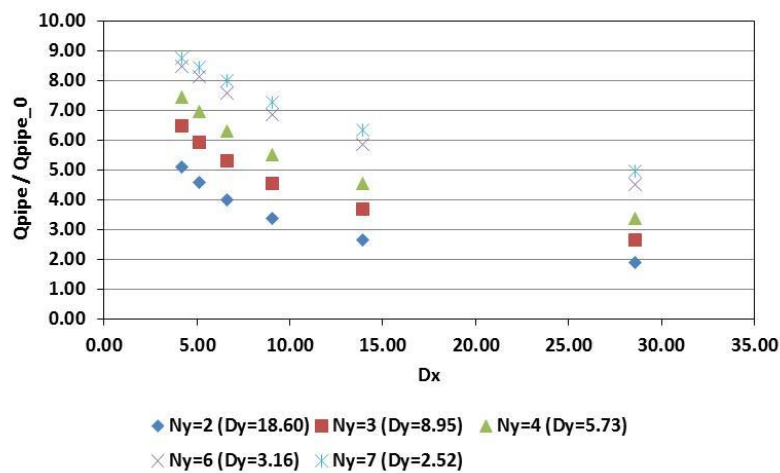
(e)

Figure 4-4: The variation of pipe heat transfer for different distance between piles for different pile depth: (a) depth=3m, (b) depth=5m, (c) depth=10m, (d) depth=15m, (e) depth=20m

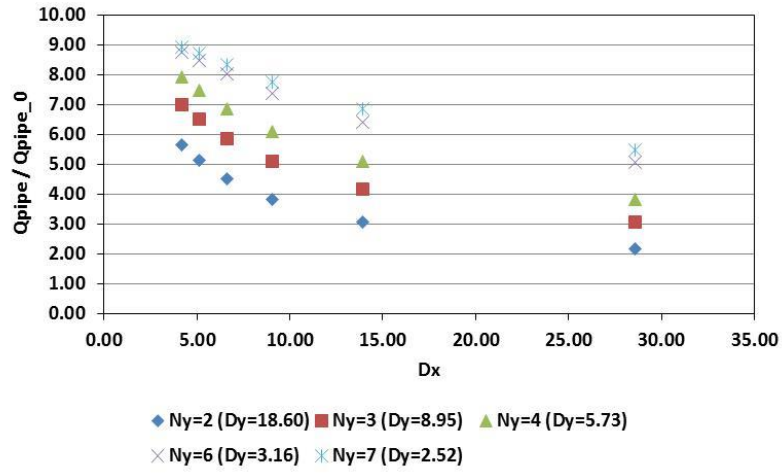
Figure 4-6 shows the variations of heat transfer through heat exchanger pipes for several parameters; different numbers of thermal piles (different distances between piles), and different length and width (Fx and Fy) of a thermal pile while the same depth of pile is considered. As presented in Figure 4-6, as length and width of a thermal pile increases for the same depth of thermal pile, the heat transfer through heat exchanger pipes increases for the same numbers of thermal piles.



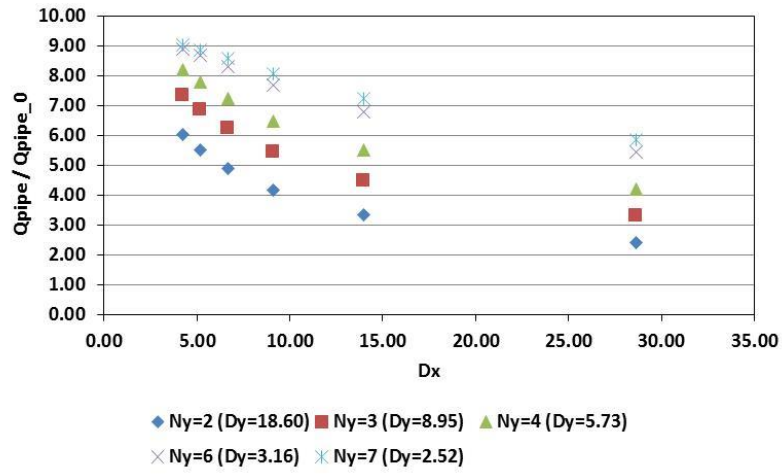
(a)



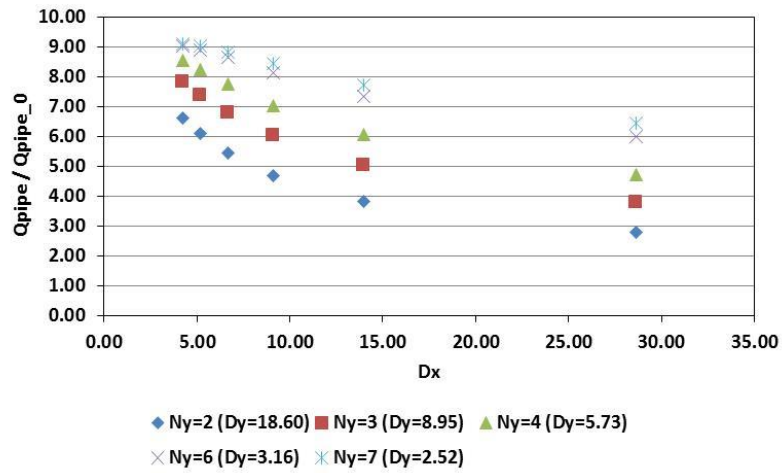
(b)



(c)



(d)



(e)

Figure 4-5: The variation of pipe heat transfer for different distance between piles, for different diameter of thermal pile: (a) $F_x, F_y=0.5m$, (b) $F_x, F_y=0.6m$, (c) $F_x, F_y=0.7m$, (d) $F_x, F_y=0.8m$, (e) $F_x, F_y=1.0m$

Based on these results presented in Figure 4-4 and Figure 4-5, in order to explore the correlation between several design parameters, this paper defines two variables of Z_n and Z_q as a function of hydraulic diameter D_h , number of piles, and sizes of a thermal pile as shown in Equation 4-2 and 4-3.

$$Z_n = \frac{16N_xN_yA}{D_xD_y} = \frac{4D_hN_xN_yP}{D_xD_y}$$

$$D_x = \left(\frac{L_x - F_xN_x}{(N_x - 1)} \right), D_y = \left(\frac{L_y - F_yN_y}{(N_y - 1)} \right)$$
Equation 4-2

$$Z_q = \ln \left(\frac{Q_{\text{pipe}}}{Q_{\text{pipe}_0}} * \frac{D_h}{H} + \frac{D_h}{N_xN_y} \right)$$
Equation 4-3

Where

D_x, D_y = The distance between foundations in X-axis and in Y-axis [m]

L_x, L_y = The size of the slab in X-axis and in Y-axis [m]

F_x, F_y = The size of a foundation in X-axis and in Y-axis [m]

N_x, N_y = The number of foundations in X-axis and in Y-axis

H = The height of a foundation [m]

D_h = The hydraulic diameter of a foundation [m] ($D_h = 4A/P$)

A = The area of a foundation [m^2]

P = The perimeter of a foundation [m]

Using the variable defined in Equation 4-2 and Equation 4-3, the pattern of heat transfer rate for different numbers of thermal piles and for different sizes of thermal pile can be illustrated as shown in

Figure 4-6. According to the Equation 4-2 and Equation 4-3, when N_x and/or N_y increases or when F_x and/or F_y increases, the value of Z_n increases. And, in Figure 4-6, it is found that as Z_n increases, Z_q increases. In other words, as Z_n increases, heat transfer rate through heat exchanger pipe increases. In the same way, when H and D_h increases, Z_n increases, and so the pipe heat transfer rate increases. As shown in Figure 4-6, the data from numerical simulations are well lined up on the regression model with very good R^2 value. The regression model which represents the actual data pattern is described in Equation 4-4. And by substituting Z_n in Equation 4-4 by Equation 4-2, Equation 4-4 can be converted into Equation 4-5.

$$Z_q = 29.311 \times (1 - 1.488 \times \exp(-0.473 \times Z_n^{0.03})) \quad \text{Equation 4-4}$$

with $R^2 = 0.999$

$$\frac{Q_{\text{pipe}}}{Q_{\text{pipe}_0}} = \frac{H}{D_h} \times \left[\exp \left(29.311 \times (1 - 1.488 \times \exp(-0.473 \times Z_n^{0.03})) \right) - \frac{D_h}{N_x N_y} \right] \quad \text{Equation 4-5}$$

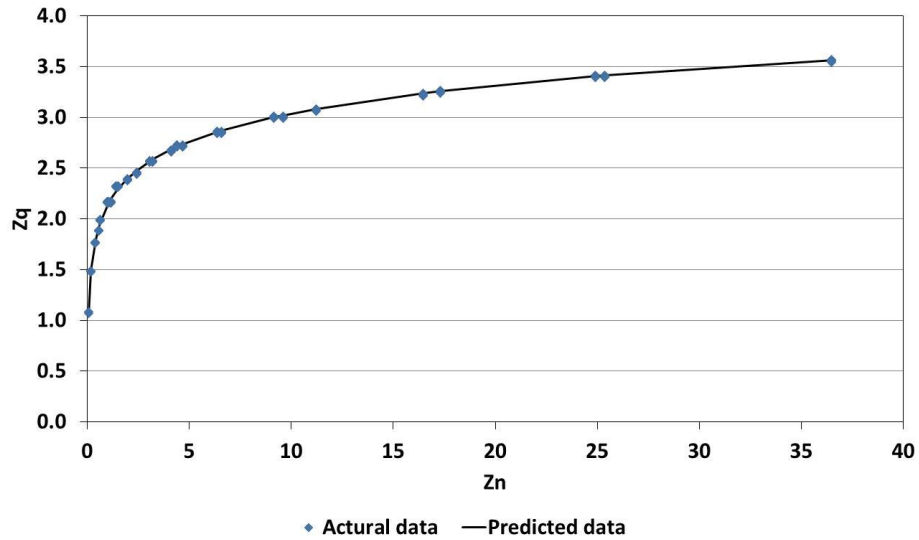


Figure 4-6: Comparison analysis between actual data from a numerical model and predicted data from a simplified model

4.3.2. Verification of the new formularization for heat transfer through thermal piles

In order to verify the new rule-of-thumb formulization of correlation between numbers and design parameters of a thermal pile and pipe heat transfer rate, it requires verification analysis using several cases with different design parameters. In Figure 4-7, it is illustrated that the results of the verification analysis with several new cases are well matched to the new expression of correlation of design parameters and pipe heat transfer rates.

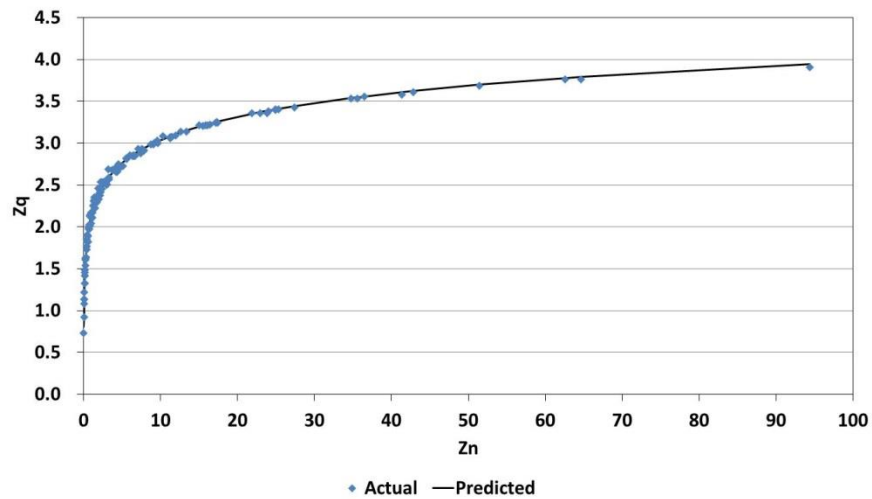


Figure 4-7: Verification analysis by comparing actual data from a numerical model and predicted data from a simplified model

Figure 4-8 shows the results of a comparative analysis between the actual data from a numerical model and the predicted data from a simplified model expressed by Equation 4-5 for the additional set of simulations. The R^2 and RMSE are 0.9966 and 0.0394, respectively, which indicate a good agreement.

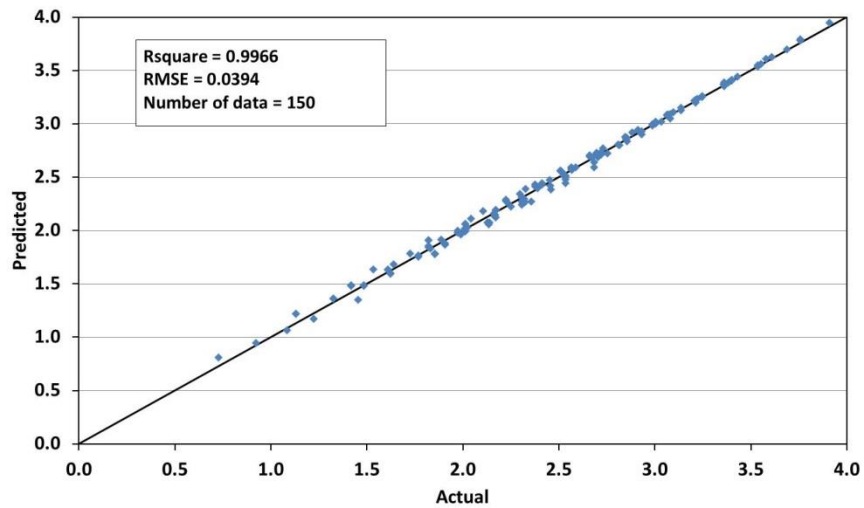


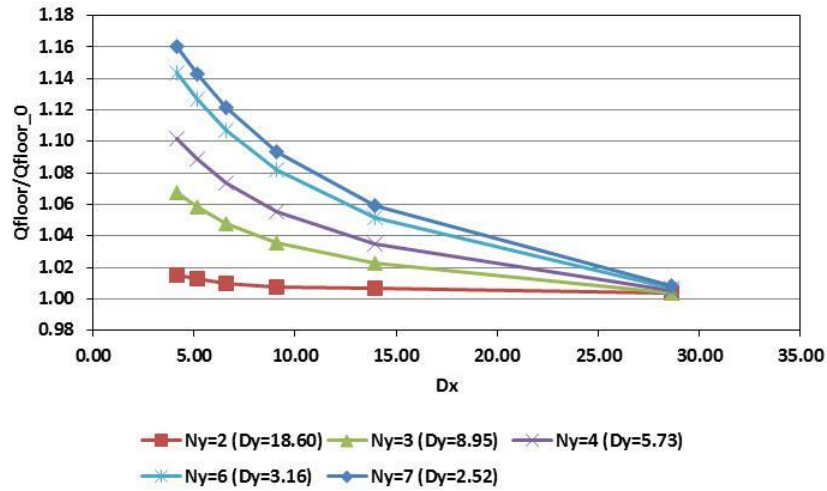
Figure 4-8: Scatter diagram to compare the predictions of the annual average heat transfer through heat exchanger pipes with the actual data from a numerical model

4.4. Ground-Coupled Heat Transfer Caused by TAFs System

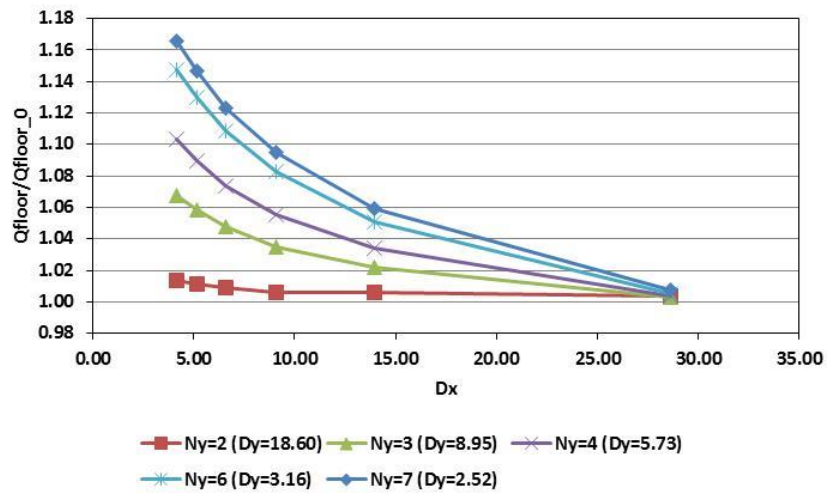
4.4.1. Formularization of the correlation between design parameters

Compared to the conventional vertical ground source heat pump system (GSHP), TAFs need to consider the impact of ground-coupled heat transfer through above-grade slab of a building. Generally, earth-contact heat transfer influences building energy loads regarding to cooling and/or heating indoor spaces (Energy Audit 2nd edition, Krarti). Since ground heat exchanger pipes are integrated into foundation piles beneath a building, ground surface temperature beneath a building would be affected by thermal piles, and so it would affect the heat transfer through an above-grade floor slab. Thus it is important to investigate thermal impacts of thermal piles on heat transfer through ground floor. In this section, based on several simulations using the 3D numerical model developed in this paper, the correlation among several design parameters of TAFs system is analyzed and formularized.

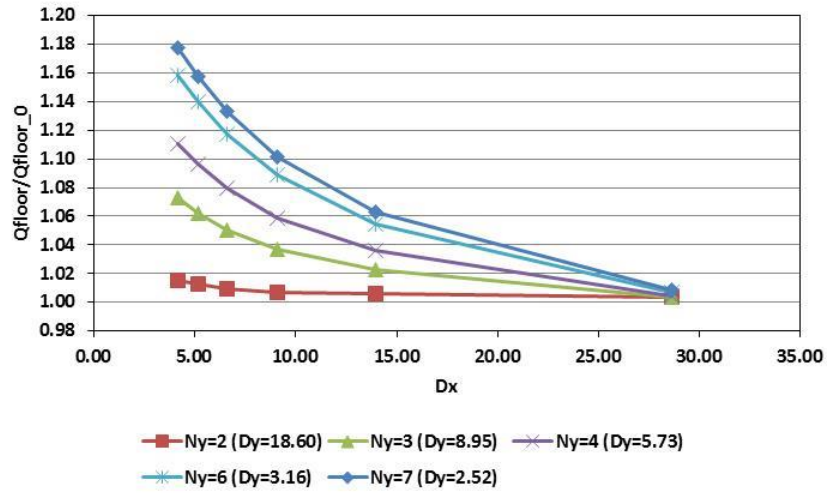
From a series of simulations for different numbers and different sizes of TAF piles, it is found that heat transfer through ground floor is influenced by several design parameters of TAFs system. Figure 4-9 shows the correlation between distances of foundation piles for several pile depths.



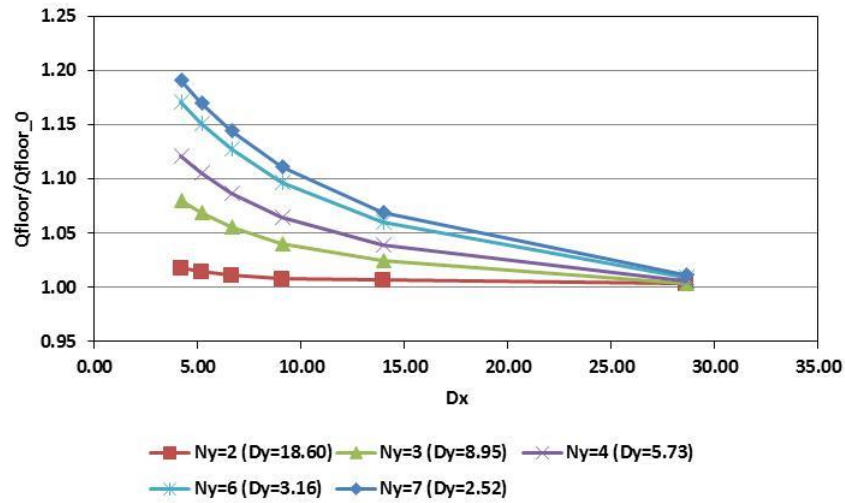
(a)



(b)



(c)



(d)

Figure 4-9: The variation of floor heat transfer for different distance between piles for different pile depths: (a) depth=5m, (b) depth=10m, (c) depth=15m, (d) depth=20m

Based on the results of sensitivity analysis in Figure 4-9, the correlation of the design parameters can be expressed by Equation 4-6 and by Equation 4-7. In Equation 4-7, Q_{floor_0} is the base case of ground floor heat transfer. The base case in this analysis has no thermal piles beneath a building, i.e. it is just ground floor heat transfer in normal conditions. Figure 4-10 presents the results of simulations for several depths of pile and for several numbers of thermal piles.

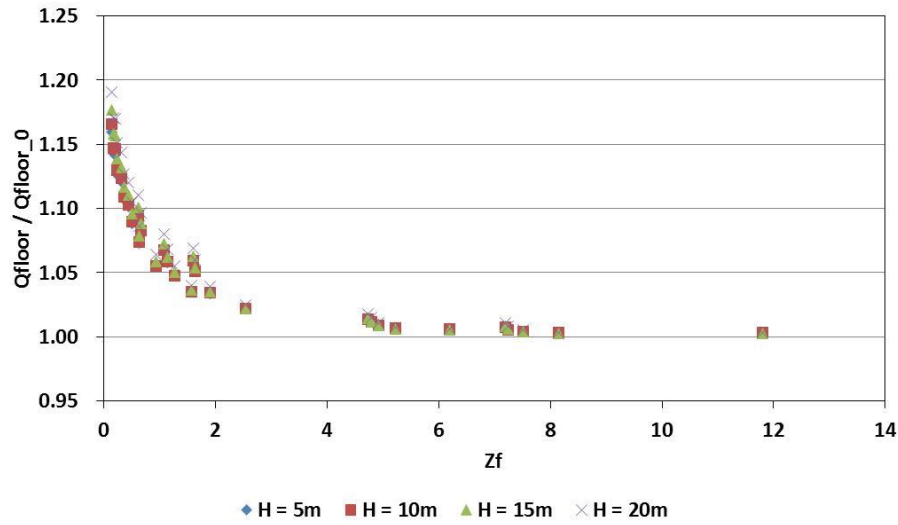


Figure 4-10: The effect of foundation depth for ground floor heat transfer

However, in Figure 4-10, it is found that the effect of depth of thermal pile on annual average heat transfer through ground floor is small, so that this effect can be neglected in Equation 4-6 and Equation 4-7. This result is consistent with the results of sensitivity analysis performed in Chapter 3 for single thermal pile. The possible reason for this result is that the longer foundation has more surface area facing ground medium with higher heat capacities.

According to the resulting Figure 4-11 and Equation 4-6 and Equation 4-7, when N_x and/or N_y increases or when F_x and/or F_y increases, the value of Z_f decreases, and thus the value of Z_g increases.

$$Z_f = \frac{D_x}{N_x^2} + \frac{D_y}{N_y^2}$$

$$D_x = \left(\frac{L_x - F_x N_x}{(N_x - 1)} \right), D_y = \left(\frac{L_y - F_y N_y}{(N_y - 1)} \right)$$

Equation 4-6

$$Z_g = \frac{Q_{\text{floor}}}{Q_{\text{floor}_0}} - \frac{1 - D_h}{(N_x N_y)^2}$$

Equation 4-7

Where

D_x, D_y = The distance between foundations in X-axis and in Y-axis [m]

L_x, L_y = The size of the slab in X-axis and in Y-axis [m]

F_x, F_y = The size of a foundation in X-axis and in Y-axis [m]

N_x, N_y = The number of foundations in X-axis and in Y-axis

D_h = The hydraulic diameter of a foundation [m] ($D_h = 4A/P$)

A = The area of a foundation [m^2]

P = The perimeter of a foundation [m]

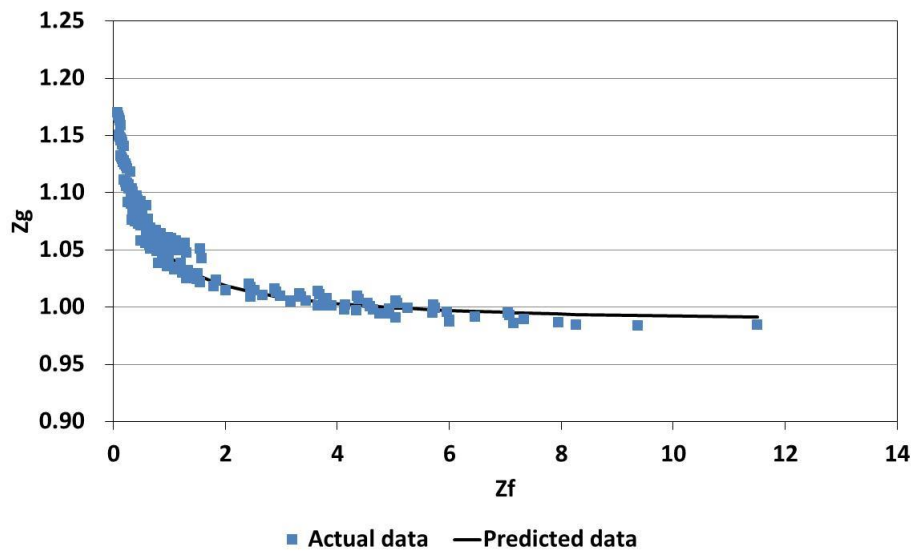


Figure 4-11: Comparison analysis between actual data from a numerical model and predicted data from a simplified model

As shown in Figure 4-11, the actual data from numerical simulations are well lined up on the predicted model with reasonable R-square value of 0.973. The regression model which represents the actual data pattern is described in Equation 4-8.

$$Z_g = 0.984 \times \text{EXP} \left(\frac{0.085}{Z_f - 0.438} \right) \quad \text{Equation 4-8}$$

with $R^2 = 0.973$

Therefore, the final expression to evaluate the rate of Q_{floor} against the base case can be defined in Equation 4-9:

$$\frac{Q_{\text{floor}}}{Q_{\text{floor}_0}} = 0.984 \times \text{EXP} \left(\frac{0.085}{Z_f - 0.438} \right) + \frac{1 - D_h}{(N_x N_y)^2} \quad \text{Equation 4-9}$$

4.4.2. Verification of the new formularization of heat transfer through ground floor

In order to verify the new expression of correlation between design parameters affecting heat transfer through ground floor, this paper performs a verification analysis with having additional simulations for different cases. Figure 4-12 and Figure 4-13 shows the results of a comparative analysis between the actual data from the numerical model and the predicted data from a simplified model expressed by Equation 4-6 and Equation 4-7 for the additional set of simulations. The R^2 and RMSE are 0.9683 and 0.0113, respectively, which indicate a good agreement.

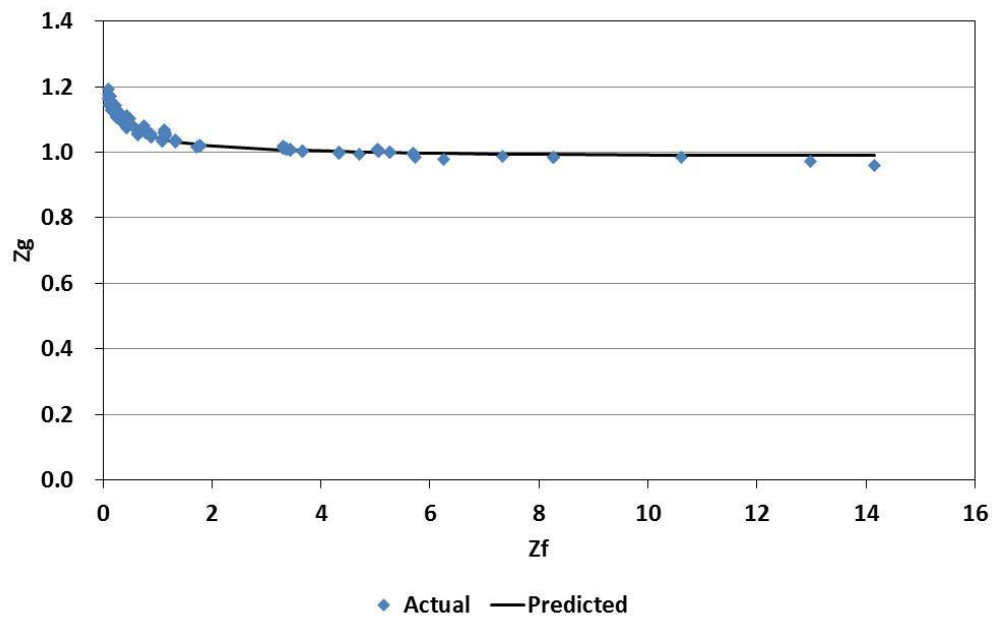


Figure 4-12: Verification analysis by comparing actual data from a numerical model and predicted data from a simplified model

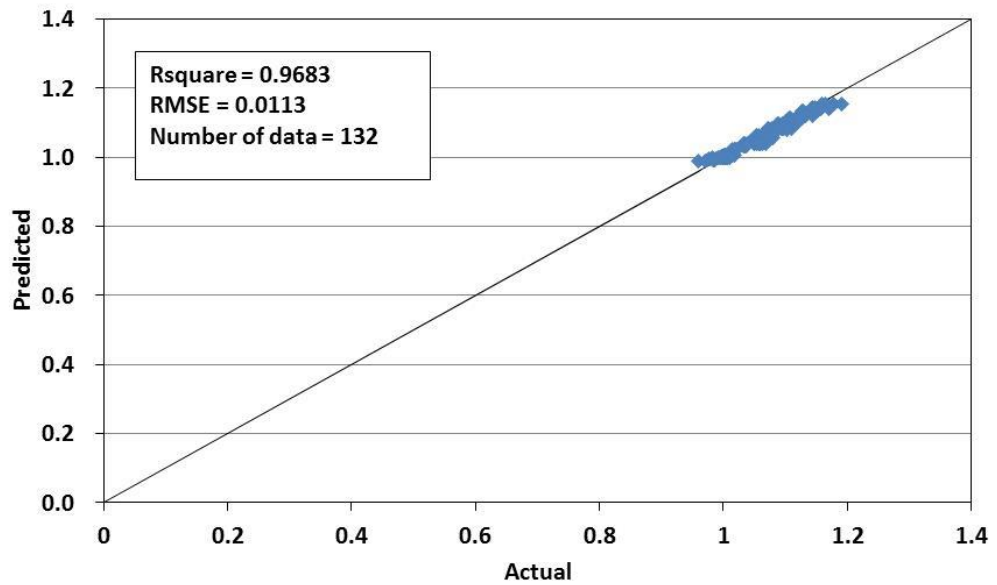


Figure 4-13: Scatter diagram to compare the predictions of the annual average heat transfer through ground floor with the actual data from a numerical model

4.5. Summary

In this chapter, a simplified approach was proposed to estimate annual average heat transfer through ground heat exchanger pipes and through ground floor is developed. The new approach was built on the patterns of the results from a series of detailed numerical simulations. The design parameters used in this approach are foundation size, number of foundations, and height of foundation. In this analysis, an assumption is required that heat exchanger pipes are integrated into all foundations of a building.

CHAPTER 5. THERMAL RESPONSE FACTOR MODEL

5.1. Introduction

The outlet fluid temperature of the heat exchanger U-tube loops is a key parameter for a ground source heat pump system. So, it is important to estimate outlet fluid temperature from ground heat exchanger pipes for simulating GSHP and TAF systems. Currently thermal response function method, which is also called G-functions, have been used to estimate the outlet fluid temperature of the heat exchanger pipes as well as to integrate GSHP model within detailed building energy simulation tools. As aforementioned in Chapter 2, Eskilson developed G-function method for long-time steps first (Eskilson, 1987), and then Yavuzturk improved this method to estimate short-time step G-functions (Yavuzturk, 1999). Both short-time and long-time step G-functions have to be generated to model properly the thermal performance of GSHPs. It should be noted that for the short-time step analysis, the time step is from 2.5 min to 200 hours. For long-time step analysis, the time step is over 200 hours. To determine the response of boreholes to a step function heat pulse, Eskilson utilized a superposition approach as illustrated in Figure 5-1.

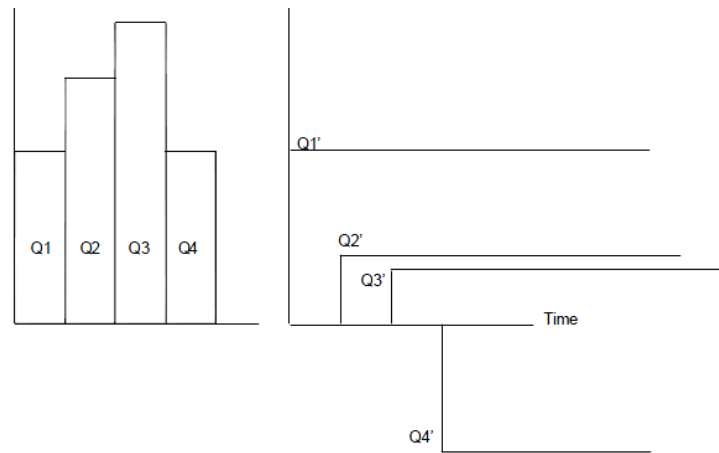


Figure 5-1: Superposition of piece-wise linear step heat inputs (Spitler, 2000)

Using G-functions, temperature change at the borehole wall is calculated in response to a unit time step heat input pulse. Once the temperature response of the borehole field to a single unit step heat pulse is determined, the response to ground coupled heat exchangers to any heat (rejection/extraction) rate can be determined by decomposing the heat rejection/extraction rate into a series of unit step pulses. Then, to obtain the overall response, the response to each unit step pulse is superimposed. Using the superposition principle, the borehole wall temperature at the end of the n^{th} time period is described in the following equation (Spitler, 2000):

$$T_{\text{borehole}} = T_{\text{ground}} + \sum_{i=1}^n \frac{(Q_i - Q_{i-1})}{2\pi k} g\left(\frac{t_n - t_{i-1}}{t_s}, \frac{r_b}{H}\right) \quad \text{Equation 5-1}$$

where

t	=	Time
t_s	=	Time scale = $H^2/9\alpha$
H	=	Borehole depth
k	=	Ground thermal conductivity
T_{borehole}	=	Average borehole temperature
T_{ground}	=	Undisturbed ground temperature
Q	=	Step heat rejection/extraction pulse
r_b	=	Borehole radius
i	=	Index to denote the end of a time step

5.2. Modification of the G-function Calculation for Several Configurations of a Pile Foundation

In Eskilson's G-function method, Eskilson (1987) considered the heat transfer in the ground medium as radial heat conduction, and a cylinder shaped deep borehole was targeted (Equation 5-2). For this reason, Eskilson developed the thermal resistance $R_q(t)$ using the heat conduction equation in cylindrical coordinates, and considering radial conductive heat transfer. To considering the circular

borehole model in the existing G-function calculation (Equation 5-3), the mathematical equation of G-function has the perimeter coefficient of 2π .

$$\frac{1}{\alpha} \frac{\partial T}{\partial t} = \frac{\partial^2 T}{\partial r^2} + \frac{1}{r} \frac{\partial T}{\partial r} + \frac{1}{r^2} \frac{\partial^2 T}{\partial \theta^2} + \frac{\partial^2 T}{\partial z^2} \quad \text{Equation 5-2}$$

$$g\left(\frac{t}{t_s}, \frac{r_b}{H}\right) = \frac{2\pi k(T_b - T_g)}{Q} \quad \text{Equation 5-3}$$

However, there is a very important fact that there are several different configurations of a building foundation pile based on building structural loads and ground mechanical conditions. In other words, without any consideration on the difference of sectional configuration of a foundation pile, using the existing G-function values may cause inaccurate results from analyzing thermal performances of a thermo-active foundation. Therefore, it needs to modify the G-function equation taking into account a cross-sectional design of a foundation.

5.2.1. Circular Sectional Foundation

Eskilson expressed the heat extraction rate $q(t)$ as presented in Equation 5-4. To complete the boundary condition, Eskilson used a prescribed heat flux $q(t)=q$. The main goal of Eskilson's approach was to get the borehole temperature $T_b(t)$, and so Eskilson used a prescribed heat flux over the borehole length ($H \cdot q(t)$, H =borehole length).

$$q(t) = \frac{1}{H} \int_D^{D+H} 2\pi r z k \left. \frac{\partial T}{\partial r} \right|_{r=r_b} dz \quad \text{Equation 5-4}$$

In Eskilson's approach borehole wall temperature can be calculated as shown in Equation 5-5. Eskilson assumed the ground temperature as zero ($T_g = 0$). In other word, in Equation 5-5, the term of $q \cdot R_q(t)$ may imply the temperature changes caused by a prescribed heat transfer rate q , and the solution can be denoted as T_q . Thus, by using T_q derived by a prescribed heat transfer rate, the temperature changes of borehole wall can be calculated. For this reason, Eskilson developed the thermal resistance $R_q(t)$ using the heat conduction equation in cylindrical coordinates, and considering radial conductive heat transfer. Eskilson identified the factor $R_q(t)$ as the time-dependent thermal resistance for the heat extraction step which is zero for $t < 0$.

$$T_b(t) = T_g - q \cdot R_q(t) \quad \text{Equation 5-5}$$

$$T_q(t) = -q \cdot R_q(t), \quad R_q(t) = 0 \text{ for } t < 0 \quad \text{Equation 5-6}$$

In Eskilson's approach, R_q is identified in two ways: one is the solution of a continuous line source theory, and the other is the solution of heat conduction equation used to express the boundary condition at the borehole wall. According to Eskilson's research and Carslaw and Jaeger (1959), the solution of a continuous line source is presented in Equation 5-7.

$$R_q(t) = \frac{1}{4\pi k} \left[\ln \left(\frac{4\alpha t}{r^2} \right) - \gamma \right] \quad \text{Equation 5-7}$$

$\left(5 \frac{r_b^2}{a} < t < \frac{t_s}{10} \right), \gamma = 0.5772 \text{ (Euler's constant)}, t_s = \frac{H^2}{9\alpha}$

Based on the fundamental heat conduction theory, the mathematical formulation of the heat extraction rate q for a circular sectional model (Figure 5-2) is given by Eskilson, 1987. Using a prescribed heat extraction rate, the temperature of borehole/foundation wall can be calculated.

$$q = \frac{1}{H} \int_D^{D+H} 2\pi r z k \left. \frac{\partial T_q}{\partial r} \right|_{r=r_b} dz \quad \text{Equation 5-8}$$

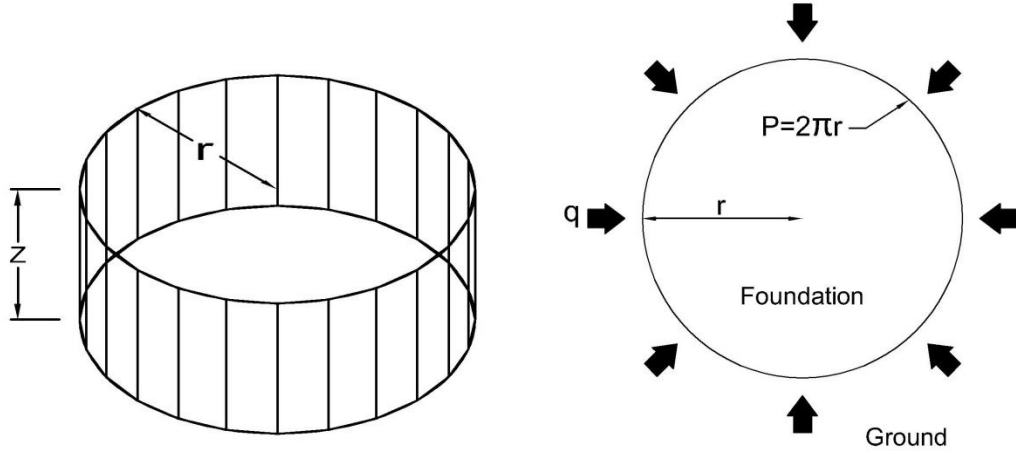


Figure 5-2: Configurations of a circular sectional foundation

In the dimensional analysis, if let the dimensionless variables $z = 1$, $r' = \frac{r}{H}$, $z' = \frac{z}{H}$, and $T' = \frac{2\pi k}{q} T_q$, then Equation 5-8 becomes:

$$1 = \int_{D/H}^{1+D/H} \left(\frac{r_b}{H} \right) \left. \frac{\partial T'}{\partial r'} \right|_{r'=r_b/H} dz' \quad \text{Equation 5-9}$$

$$1 = \int_{D/H}^{1+D/H} r' \left. \frac{\partial T'}{\partial r'} \right|_{r'=r_b/H} dz' \quad \text{Equation 5-10}$$

$$1 = r' \left. \frac{\partial T'}{\partial r'} \right|_{r'=r_b/H} \quad \text{Equation 5-11}$$

$$\frac{1}{r'} \partial r' = \partial T' \quad \text{Equation 5-12}$$

$$\text{Ln}(r') + c = T' \quad \text{Equation 5-13}$$

$$\ln\left(\frac{r_b}{H}\right) + c = \frac{2\pi k}{q} T_q \quad \text{Equation 5-14}$$

$$T_q = \frac{q}{2\pi k} \left(\ln\left(\frac{r_b}{H}\right) + c \right) \quad \text{Equation 5-15}$$

According to Equation 5-6, Equation 5-7 and Equation 5-15, it is found that R_q is a function of time and r_b/H . So, the thermal resistance R_q is expressed by:

$$R_q(t) = \frac{1}{2\pi k} \cdot g\left(\frac{t}{t_s}, \frac{r_b}{H}\right) \quad \text{Equation 5-16}$$

5.2.2. Rectangular Sectional Foundation

Employing the Eskilson's approach which is for the case of a circular sectional pile foundation, and using the fundamental heat conduction theory, the mathematic formulation for a rectangular sectional model (Figure 5-3) with a prescribed heat extraction (q) can be derived in the following steps.

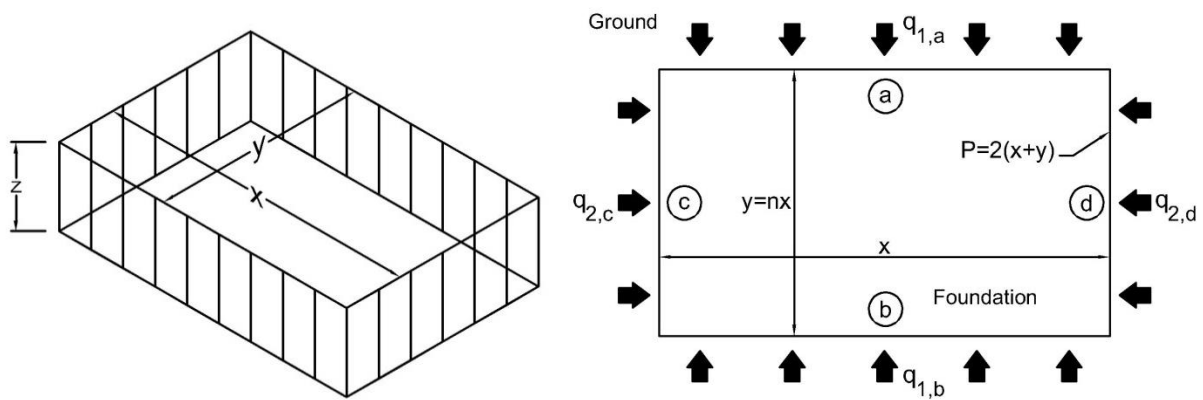


Figure 5-3: Configurations of a rectangular sectional foundation

Unlike the case of a circular shape and the other equilateral polygon, a rectangular shape is complex due to the issues caused by two variables (x and y) to be considered. In addition, the average temperatures on the length side and the width side can be different when constant heat flux is implemented around a rectangular perimeter. So, for a rectangular sectional foundation, more attention will be required. Because of the different dimensions of length and width of a rectangle, the average temperature on the perimeter can be calculated in a weighted average method (Dharaiya et al. 2012).

$$T_q = T_1 \left(\frac{x}{x+y} \right) + T_2 \left(\frac{y}{x+y} \right)$$

$$T_1 = \frac{T_a + T_b}{2}, \quad T_2 = \frac{T_c + T_d}{2}$$

Equation 5-17

The overall heat extraction q on a rectangular perimeter is the sum of the heat extractions on each side of a rectangle.

$$q = q_1 + q_2, \quad q_{1,a} = q_{1,b}, \quad q_{2,c} = q_{2,d}$$

$$q_1 = q \left(\frac{x}{x+y} \right), \quad q_2 = q \left(\frac{y}{x+y} \right)$$

Equation 5-18

If the dimensionless variables are defined as $z = 1$, $x' = \frac{x}{H}$, $y' = \frac{y}{H}$, $z' = \frac{z}{H}$, and $n = \frac{y}{x} = \frac{y'}{x'}$, then the heat extractions q_1 and q_2 can be expressed by:

$$q_1 = \frac{1}{H} \int_D^{D+H} 2xz k \frac{\partial T_1}{\partial y} dz = 2x' k \frac{\partial T_1}{\partial y'} = \frac{2y' k}{n} \frac{\partial T_1}{\partial y'}$$

Equation 5-19

$$q_2 = \frac{1}{H} \int_D^{D+H} 2yz k \frac{\partial T_2}{\partial x} dz = 2y' k \frac{\partial T_2}{\partial x'} = 2nx' k \frac{\partial T_2}{\partial x'}$$

Equation 5-20

$$q_1 = 2x' k \frac{\partial T_1}{\partial y'}, \quad q_2 = 2y' k \frac{\partial T_2}{\partial x'}$$

Equation 5-21

$$q_1 = \frac{2y'k}{n} \frac{\partial T_1}{\partial y'}, \quad q_2 = 2nx'k \frac{\partial T_2}{\partial x'} \quad \text{Equation 5-22}$$

$$\frac{1}{y'} \partial y' = \frac{2k}{nq_1} \partial T_1, \quad \frac{1}{x'} \partial x' = \frac{2nk}{q_2} \partial T_2 \quad \text{Equation 5-23}$$

$$\ln(y') + c_1 = \frac{2k}{nq_1} T_1, \quad \ln(x') + c_2 = \frac{2nk}{q_2} T_2 \quad \text{Equation 5-24}$$

$$T_1 = \frac{nq_1}{2k} [\ln(y') + c_1], \quad T_2 = \frac{q_2}{2nk} [\ln(x') + c_2] \quad \text{Equation 5-25}$$

$$T_q = T_1 \left(\frac{x'}{x' + y'} \right) + T_2 \left(\frac{y'}{x' + y'} \right) \quad \text{Equation 5-26}$$

$$T_q = \left(\frac{x'}{x' + y'} \right) \frac{nq_1}{2k} [\ln(y') + c_1] + \left(\frac{y'}{x' + y'} \right) \frac{q_2}{2nk} [\ln(x') + c_2] \quad \text{Equation 5-27}$$

$$T_q = \frac{y'q_1}{2(x' + y')k} [\ln(y') + c_1] + \frac{x'q_2}{2(x' + y')k} [\ln(x') + c_2] \quad \text{Equation 5-28}$$

$$T_q = \frac{y'q \left(\frac{x'}{x' + y'} \right)}{2(x' + y')k} [\ln(y') + c_1] + \frac{x'q \left(\frac{y'}{x' + y'} \right)}{2(x' + y')k} [\ln(x') + c_2] \quad \text{Equation 5-29}$$

$$T_q = \frac{x'y'q}{2(x' + y')^2k} [\ln(y') + c_1] + \frac{x'y'q}{2(x' + y')^2k} [\ln(x') + c_2] \quad \text{Equation 5-30}$$

$$T_q = \frac{x'y'q}{2(x' + y')^2k} [\ln(y') + \ln(x') + c_3] \quad \text{Equation 5-31}$$

$$T_q = \frac{xyq}{2(x + y)^2k} \left[\ln \left(\frac{xy}{H^2} \right) + c_3 \right] \quad \text{Equation 5-32}$$

Finally, after deriving the equations with combining a weighted average temperature and the overall heat extraction, the resulting thermal resistance R_q can be computed:

$$R_q(t) = \frac{1}{\frac{2(x + y)^2k}{xy}} \cdot g\left(\frac{t}{t_s}, \frac{xy}{H^2}\right) \quad \text{Equation 5-33}$$

5.2.3. Equilateral Triangular Sectional Foundation

This configuration is an ideal case to generalize this approach. For an equilateral triangular section (Figure 5-4), the point of center of mass (G) of a triangle is introduced to derive the mathematical formulation with only one variable (i.e. $y = \frac{1}{3}h = \frac{\sqrt{3}}{3}x$, and $h = \sqrt{3}x$).

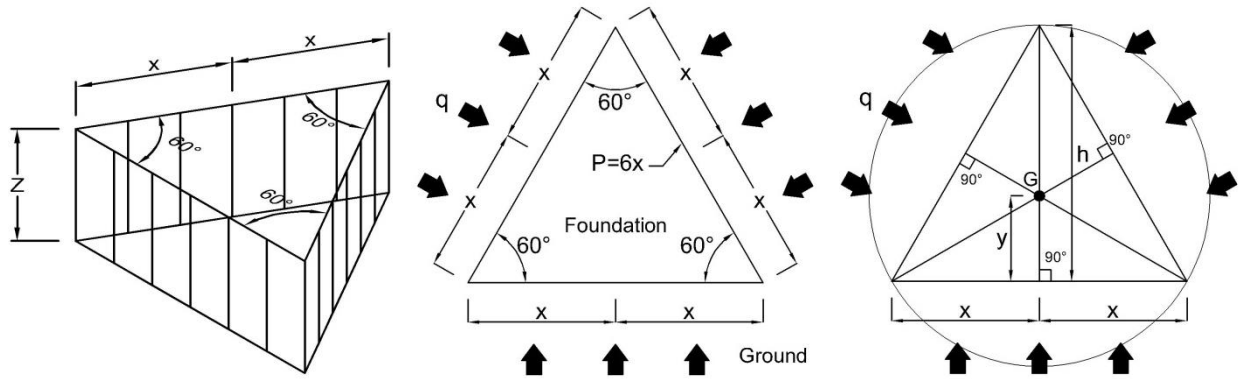


Figure 5-4: Configurations of an equilateral triangular sectional foundation

Since the model is an equilateral triangle, the modeling can be simplified by using symmetry, and so the heat extraction can be expressed by:

$$q = \frac{1}{H} \int_D^{D+H} 3 \cdot 2xz k \frac{\partial T}{\partial y} dz \quad \text{Equation 5-34}$$

In the dimensional analysis, if let the dimensionless variables are $z = 1$, $x' = \frac{x}{H}$, $z' = \frac{z}{H}$, and $T' = \frac{6\sqrt{3}k}{q} T_q$ as well as let $\partial y = \frac{1}{\sqrt{3}} \partial x$ because of $y = \frac{1}{3}h = \frac{\sqrt{3}}{3}x = \frac{1}{\sqrt{3}}x$, then the overall heat extractions q around the perimeter become:

$$1 = \int_{D/H}^{1+D/H} x' \cdot \frac{\partial T'}{\partial x'} dz' \quad \text{Equation 5-35}$$

$$1 = x' \frac{\partial T'}{\partial x'} \quad \text{Equation 5-36}$$

$$\frac{1}{x'} \partial x' = \partial T' \quad \text{Equation 5-37}$$

$$\text{Ln}(x') + c = T' \quad \text{Equation 5-38}$$

$$\text{Ln}\left(\frac{x}{H}\right) + c = \frac{6\sqrt{3}k}{q} T_q \quad \text{Equation 5-39}$$

$$T_q = \frac{q}{6\sqrt{3}k} (\text{Ln}\left(\frac{x}{H}\right) + c) \quad \text{Equation 5-40}$$

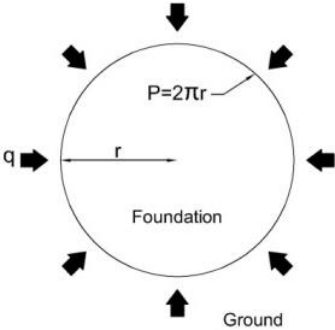
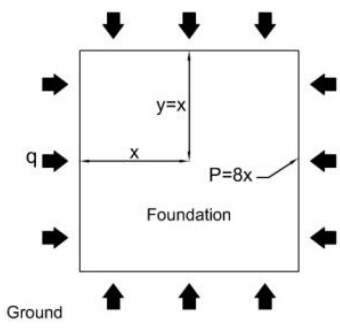
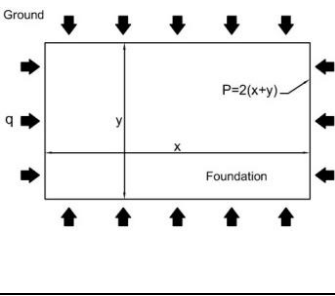
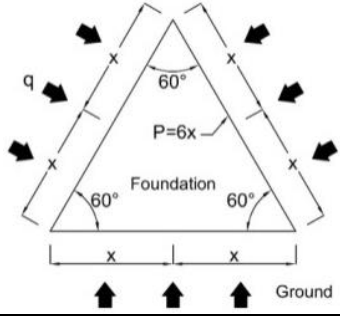
And the resulting thermal resistance R_q for an equilateral triangular sectional foundation is:

$$R_q(t) = \frac{1}{6\sqrt{3}k} \cdot g\left(\frac{t}{t_s}, \frac{x}{H}\right) \quad \text{Equation 5-41}$$

5.2.4. The Modified G-function Equations

Based on the mathematically derived heat conduction equations for different configurations of a thermo-active foundation in the previous sections, the modified G-function equations could be achieved. Table 5-1 describes the resulting modified G-function equations for a circular section, a square section, a rectangular section and an equilateral triangular section. As shown in Table 5-1, when the length and width has the same value in the case of a rectangular section, the modified G-function becomes that for a square sectional foundation case. Each case has a different coefficient in the equation: 2π for a circular section, 8 for a square section, $\frac{2(x+y)^2}{xy}$ for a rectangular section, and $6\sqrt{3}$ for an equilateral triangular section.

Table 5-1: The modified G-function equations for different cross-sectional configurations of thermo-active foundation

<p>Circular section</p> 	$g\left(\frac{t}{t_s}, \frac{r_b}{H}\right) = \frac{2\pi k(T_b - T_g)}{q}$	<p>Square section</p> 	$g\left(\frac{t}{t_s}, \frac{x}{H}\right) = \frac{8k(T_b - T_g)}{q}$
<p>Rectangular section</p> 	$g\left(\frac{t}{t_s}, \frac{xy}{H^2}\right) = \frac{2(x+y)^2 k(T_b - T_g)}{xy q}$	<p>Equilateral triangular Section</p> 	$g\left(\frac{t}{t_s}, \frac{x}{H}\right) = \frac{6\sqrt{3}k(T_b - T_g)}{q}$

5.2.5. The Fractional Shape Factor for the Modified Thermal Response Factor

In Section 4.2, the existing thermal response factor (G-function) equation was modified to take into account the different cross-sectional configurations of a thermo-active foundation. Aforementioned, it was found that each case had a different coefficient in the equation: 2π for a circular section, 8 for a square section, $\frac{2(x+y)^2}{xy}$ for a rectangular section, and $6\sqrt{3}$ for an equilateral triangular section.

This paper proposes the generalized term to represent these coefficients which are related to the perimeter of a cross-sectional configuration of a foundation. By employing the hydraulic diameter

(D_H) and the perimeter of a foundation section (P), the generalized term can be expressed. The hydraulic diameter used in this paper is the term commonly used to analyze noncircular tubes and channels as well as to a round tube.

$$D_H = \frac{4A}{P} \quad \text{Equation 5-42}$$

D_H = the hydraulic diameter

A = the cross sectional area of a foundation

P = the perimeter of the foundation

The coefficients derived in the previous sections are expressed by the fractional shape factor, which is dimensionless and consists of the hydraulic diameter and the perimeter of a foundation (Equation 4-43). Therefore, Equation 4-44 is the modified G-function equation with the new expression. The fractional shape factors (F_s) of different configurations of a thermo-active foundation are described in Table 5-2.

$$F_s = \left(\frac{2P}{D_H} \right) \quad \text{Equation 5-43}$$

$$g\left(\frac{t}{t_s}, \frac{P}{D_H}\right) = F_s \frac{k(T_b - T_g)}{q} = \left(\frac{2P}{D_H} \right) \frac{k(T_b - T_g)}{q} \quad \text{Equation 5-44}$$

The resulting values of $F_s = \left(\frac{2P}{D_H} \right)$ are well matched with the coefficients derived in the previous sections. In other words, the modified G-function equation can be validated by comparing the F_s values and the coefficients mathematically derived in the previous sections.

Table 5-2: The hydraulic diameters for different configurations of foundation section

Configuration	Image	Hydraulic diameter
Circular section		$A = \pi r^2$ $P = 2\pi r$ $D_H = \frac{4A}{P} = \frac{4\pi r^2}{2\pi r} = 2r$ $F_s = \frac{2P}{D_H} = \frac{2 \cdot 2\pi r}{2r} = 2\pi$
Square section		$A = (2x)(2y) = 4xy = 4x^2$ $P = 2(2x + 2y) = 4(x + y) = 8x$ $D_H = \frac{4A}{P} = \frac{4 \cdot 4x^2}{8x} = 2x$ $n = \frac{y}{x} = 1$ $F_s = \frac{2P}{D_H} = \frac{2 \cdot 8x}{2x} = 8$
Rectangular section		$A = xy$ $P = 2(x + y)$ $D_H = \frac{4A}{P} = \frac{4 \cdot xy}{2(x + y)}$ $F_s = \frac{2P}{D_H} = \frac{2(2(x + y))^2}{4xy} = \frac{2(x + y)^2}{xy}$
Equilateral Triangular section		$A = \sqrt{3}x^2$ $P = 3 \cdot 2x = 6x$ $D_H = \frac{4A}{P} = \frac{4\sqrt{3}x^2}{6x} = \frac{2\sqrt{3}}{3}x$ $F_s = \frac{2P}{D_H} = \frac{2 \cdot 6x}{\frac{2\sqrt{3}}{3}x} = 6\sqrt{3}$

5.2.6. Verification Analysis of the Modified Thermal Response Factor Model

The three dimensional numerical model for a thermo-active foundation was developed and validated in Chapter 3. Using the 3D numerical model, the average foundation wall temperature is calculated. Due to the fact that this paper mainly uses the Cartesian coordinate system in the numerical model, the configuration of a thermo-active foundation should have a square or a rectangular cross section, and so a square cross section is used in this paper. Then, the appropriate coefficient for a square section and the appropriate modified G-function should be used from Table 5-1 and Table 5-2.

$$g\left(\frac{t}{t_s}, \frac{x}{H}\right) = \frac{8k(T_b - T_g)}{q}, \quad F_s = 8 \text{ (square)} \quad \text{Equation 5-45}$$

From the numerical solution, the average temperature of the foundation wall is calculated, and then G-functions are calculated by using Equation 4-31 for both long-time and short time step models to be consistent with Eskilson's method and Yavuzturk's method.

$$g\left(\frac{t}{t_s}, \frac{x}{H}\right) = \begin{cases} (a) \text{ Long - time step: } \frac{8k(T_b - T_g)}{q} \\ (b) \text{ Short - time step: } \frac{8k(T_b - R_{total} \cdot q - T_g)}{q} \end{cases} \quad \text{Equation 5-46}$$

For short-time step G-function calculation, an overall thermal resistance (R_{total}) of the thermo-active foundation should be defined. This resistance should include convective resistance for the circulating fluid, the conductive thermal resistance of the U-tube pipes, and the conductive thermal resistance of the borehole/foundation material (Yavuzturk, 1999).

$$R_{\text{total}} = R_{\text{fluid}} + R_{\text{pipe}} + R_{\text{foundation}} \quad \text{Equation 5-47}$$

here

R_{total} = total thermal resistance of a thermo-active foundation [$^{\circ}\text{C}\cdot\text{m}/\text{W}$]

R_{fluid} = convective thermal resistance of a circular fluid [$^{\circ}\text{C}\cdot\text{m}/\text{W}$]

R_{pipe} = conductive thermal resistance of a pipe [$^{\circ}\text{C}\cdot\text{m}/\text{W}$]

To verify the calculation procedure for the thermal response factors of a thermo-active foundation developed in this chapter, the thermal response factors of a TAF system is compared with the reference data which is calculated by Eskilson's method and Yavuzturk's method for conventional GSHP system for the same boundary conditions. In this verification analysis, the borehole/foundation model's aspect ratio (a ratio of radius to depth, r_b/H) is 0.0005. According to the comparative analysis in Chapter 3, the square cross sectional foundation has a similar thermal performance to a circular cross sectional foundation for the same boundary conditions as well as for the same aspect ratio. This result implies that the predicted G-functions should be expected to be similar to the reference data.

Comparison analysis of long time-step thermal response factors

Figure 5-5 illustrates the results of the comparative analysis between the predicted model using the modified G-functions, and the reference data for the same boundary conditions. As shown in Figure 5-5, the modified G-functions using the Equation 4-29 (a) generate the well matched results to the reference data as expected.

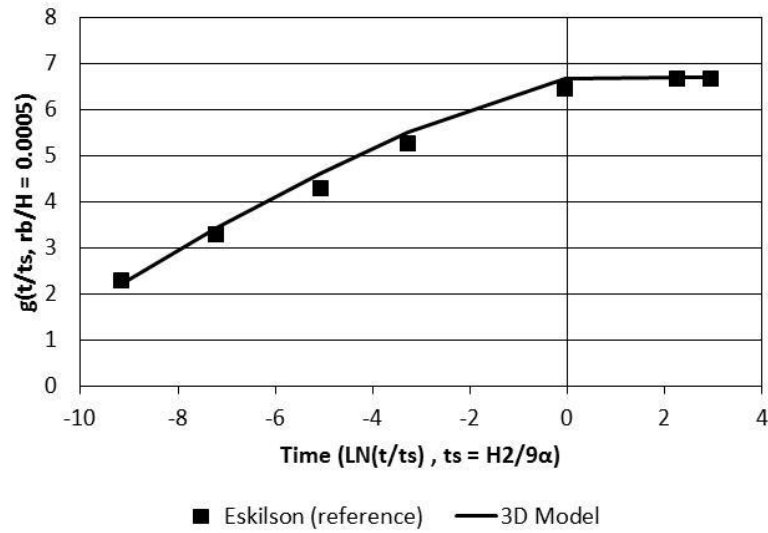


Figure 5-5: Long-time step G-function variation (with $t_s = H^2/9\alpha$)

As an application of the long-time step model, the average fluid temperature can be calculated:

$$T_{\text{fluid}} = T_{\text{foundation}} + R_{\text{total}} \times Q \quad \text{Equation 5-48}$$

Where,

- T_{fluid} = The average fluid temperature (°C)
- $T_{\text{foundation}}$ = The average foundation wall temperature (°C)
- Q = Unit heat extraction/rejection rate (W/m)
- R_{total} = Total thermal resistance of foundation (m/W)

Comparison analysis of short time-step thermal response factors

In the result of the comparison analysis for short-time steps, it is found that the predicted G-functions using the modified G-function equation matches well with the reference data as presented in Figure 5-6.

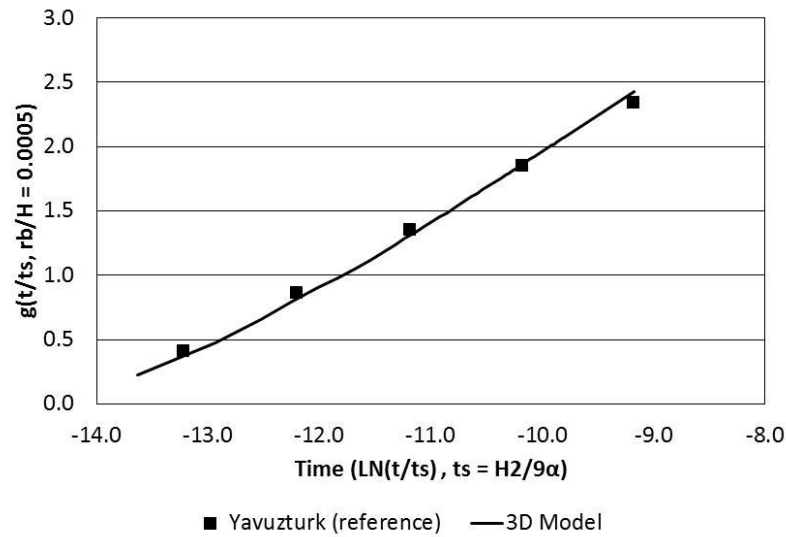


Figure 5-6: Short-time step G-function variation

Figure 5-7 illustrates the resulting G-function curves for both short-time steps and long-time steps from the reference data and from the predicted model using the modified G-function equation developed in this paper. As shown in Figure 5-7, the short-time step G-functions developed in this paper is well lined up with the long-time step G-functions using the modified G-function equation.

In addition, Figure 5-7 also highlights that the existing G-function equation doesn't produce reasonable result. In Figure 5-7, the modified G-function equation produces the reasonable G-function values, while the G-function values using the existing G-function equation are much lower than the reference data.

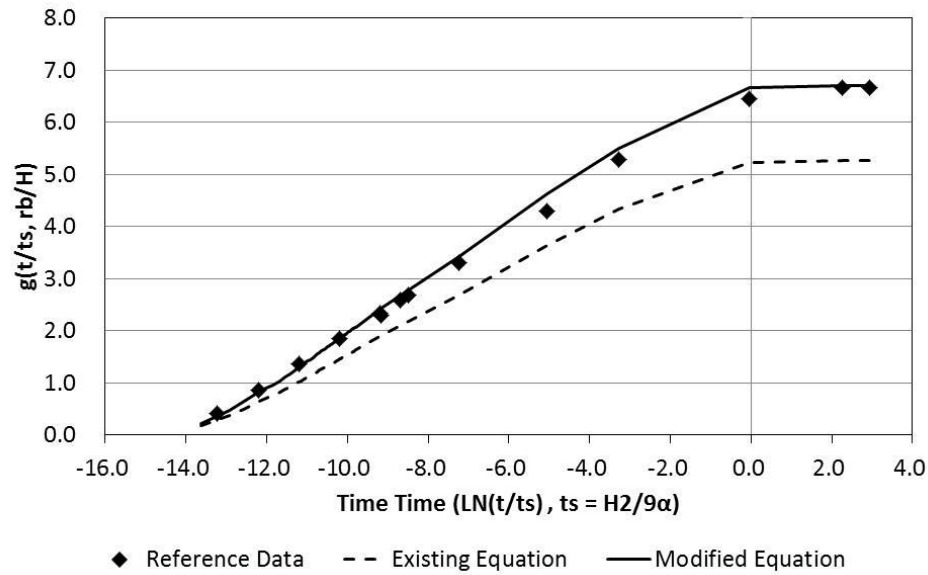


Figure 5-7: Long-time step and short-time step G-function obtained from the 3-D numerical model

5.3. The Effect of Indoor Air Temperature on the G-function

5.3.1. Develop of the G-function Calculation for the Effect of Indoor Air Temperature

Compared to GSHP systems, TAF systems have additional boundary condition on the top surface of the ground domain caused by an above-grade slab floor. So in order to account for the additional boundary condition, the scheme of G-function calculation specific to TAF systems needs to be modified from the approach of G-function calculation of GSHP systems. The modified approach for TAF system is to superpose ground heat exchanger model with a prescribed heat flux and an above-grad floor slab model as illustrated in Figure 5-8.

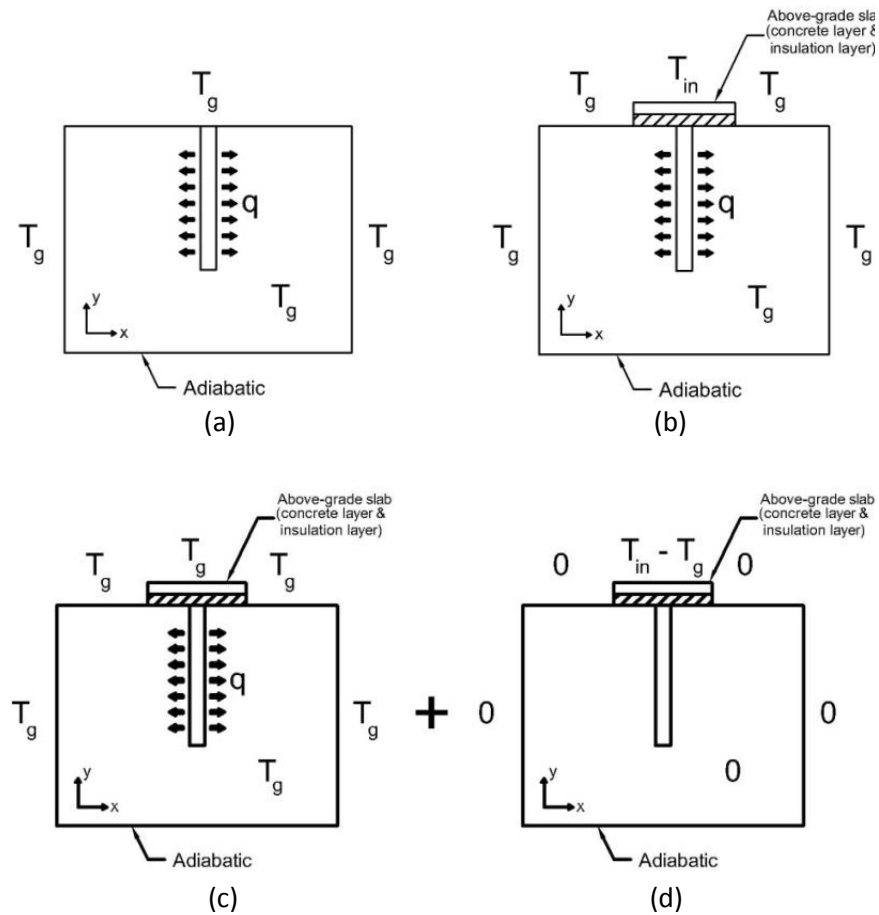


Figure 5-8: The scheme of thermal response factor model for TAF systems

Figure 5-8 (a) represents the existing G-function model developed by Eskilson, and Figure 5-8 (b) is for TAF pile with additional boundary conditions including above-grade slab floor and indoor air temperature. Figure 5-8 (c) and Figure 5-8 (d) represents the breakdown of Figure 5-8 (b). This breakdown of the numerical model takes account of the impact of indoor air temperature on TAF systems installed below an above-grade floor of a building. The numerical model calculates the foundation wall temperature, and then the temperature profiles of two models are combined, and used to calculate G-function values utilizing an appropriate equation described in Table 5-2.

The G-function calculation is carried out for TAF systems that have 1 thermal pile. In the 3D numerical modeling, the indoor air temperature is assumed to be 20 °C, and the ground temperature is set as 8 °C. Figure 5-9 shows the foundation wall temperature variations and G-function curves of the cases with and without thermal effect of indoor air temperature, respectively, which aspect ratio is 5.0. In Figure 5-9, it is found that for short time steps the imposed-constant heat flux in the numerical model caused similar drops of foundation wall temperature in both cases, and so the G-function curves of the two cases for the short time steps are similar to each other. This result indicates that the thermal effect of indoor air temperature on foundation wall temperature is small enough to be neglected for short time steps.

However, for the long time steps there are different results between the two cases depending on existence of indoor air temperature. As described in Figure 5-9, the foundation wall temperature variation of the case with thermal effect of indoor air temperature goes to be reversed around at $\ln(t/t_s) = -0.148$ while the case without thermal effect of indoor air temperature doesn't reverse the pattern. Therefore, this results in the different G-function curves (Figure 5-9). This result represents that indoor air temperature affects foundation wall temperature and its G-function values for long time steps. Consequently, this result implies that the existing G-function calculation model for conventional GSHP system, which doesn't consider the thermal effect of indoor air temperature on borehole wall temperature, may not be appropriate to simulate TAF system, and so using the inappropriate G-functions may cause over- or under-estimate the thermal performances of TAF systems.

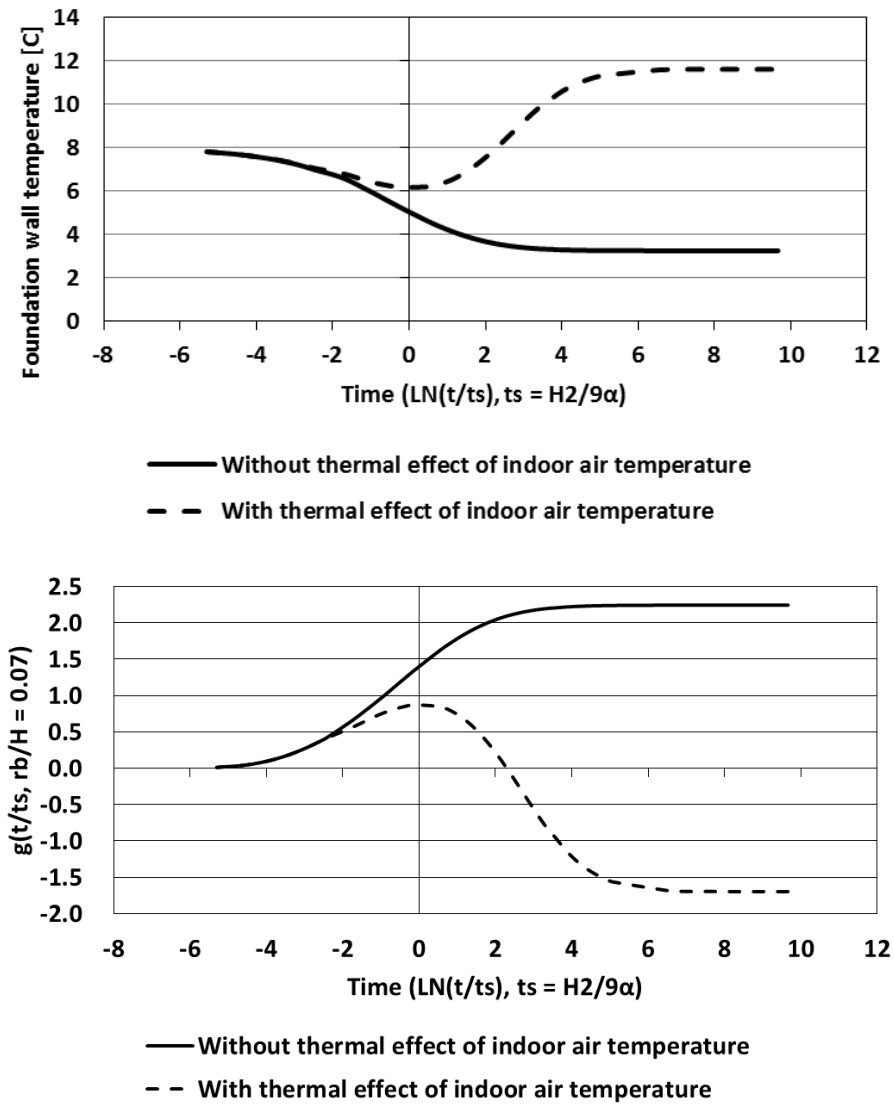


Figure 5-9: Foundation wall temperature variations and G-function curves of the cases with/without thermal effect of indoor air temperature, AR=5.0

5.3.2. Comparative Analysis of Modified G-functions

In this analysis, this section uses the actual field test data performed by Murphy et al. in Denver, CO. (Murphy et al., 2014). The field test was a 2 year-long study involving an assessment of the thermal and thermo-mechanical responses of two energy foundations. The actual energy foundations were installed beneath an eight story building in Denver. The energy foundation was installed under an

interior column, and it has a depth of 14.8m and a diameter of 0.91m. Table 5-3 presents the summary of specifications of the energy foundation used in the actual field test.

Table 5-3: Summary of specifications of the energy foundation

Foundation pile size [m]	Depth – 14.8m Diameter – 0.91m
Total length of heat exchanger pipes [m]	89
Ground type	Fill (0 – 3m) Sand and gravel (3 – 4.6m) Claystone (below 4.6m)
Fluid type	10/90 Methanol/water
Fluid flow rate [m ³ /s]	0.00033
Pipe inside diameter [m]	0.044
Fluid viscosity [Pa-s]	0.00115
Reynold's number	8201.65
Fluid mass density [kg/m ³]	987.2
Specific heat of fluid [J/kg-C]	4018.4

Using the EnergyPlus source code (PlantGroundHeatExchanger), this analysis predicts outlet fluid temperature against the inlet fluid temperature given by the actual field test. For calculating outlet fluid temperature, the inlet fluid temperature data as well as thermal properties of a model used in the actual field test are required, and Table 5-3 presents the summary of inputs in the model. Since the actual field test does not provide all necessary information required for modeling, this paper has to make some assumptions in order to calculate G-functions and to predict outlet fluid temperature as presented in Table 5-4.

Table 5-4: Summary of assumptions in thermal properties of the model

Ground	
Thermal conductivity [W/m-K]	1.3
Thermal heat capacity [J/m ³ -K]	1874880
Grout (Concrete)	
Thermal conductivity [W/m-K]	1.8
Polyethylene pipe	
Thermal conductivity [W/m-K]	0.36

According to Murphy et al. who performed the actual field test, variable speed pumps were used in the actual experiment to circulate fluid through the energy foundations and the borehole field (Murphy et al., 2014). So, the flow rate through the energy foundations might be changed during the test as the demand for cooling/heating from the building changed. However, Murphy et al. did not monitor the fluid flow rate during the test. They found that there were relatively steady heat exchanges between the ground and heat exchanger during the summer and winter seasons, but there were significant fluctuations during the spring and fall seasons. According to Murphy et al. these result may indicate that during the spring and fall seasons the thermal demand might be lower than the summer and winter seasons, so that the flow rate might be lower during the swing seasons. In other words, the experimental data of Murphy et al.'s actual test had the significant uncertainty of the flow rate for the swing seasons rather than the summer and winter seasons. For this reason, this analysis is mainly focused on the summer and winter seasons to compare the predicted data and the actual experimental data from Murphy et al with the assumption of the constant flow rate in the outlet fluid temperature calculations.

Figure 5-10 and Figure 5-11 illustrates the inlet and outlet fluid temperatures for typical week in the summer season and for typical week in the winter season, respectively. As shown in Figure 5-10 and

Figure 5-11, using the constant flow rate in the calculation, the predicted outlet temperatures have the similar pattern of the inlet fluid temperatures during the summer and winter seasons.

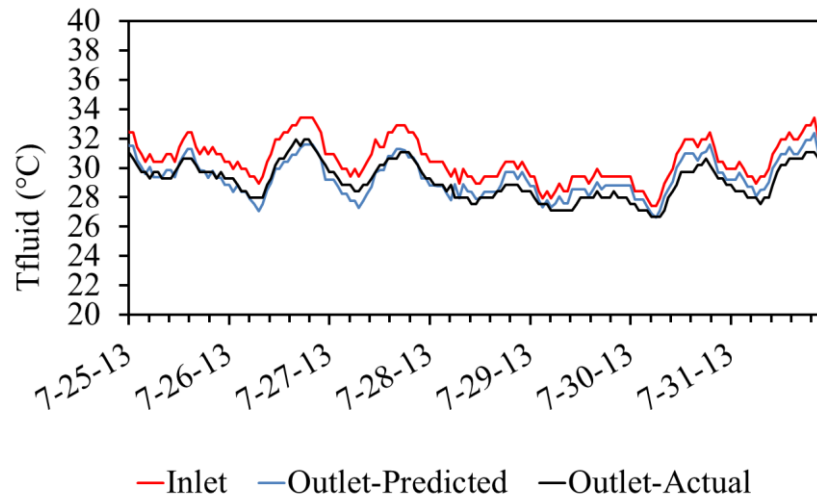


Figure 5-10: The inlet fluid temperatures, and outlet fluid temperatures of actual data, and of predicted data for typical week in the summer season

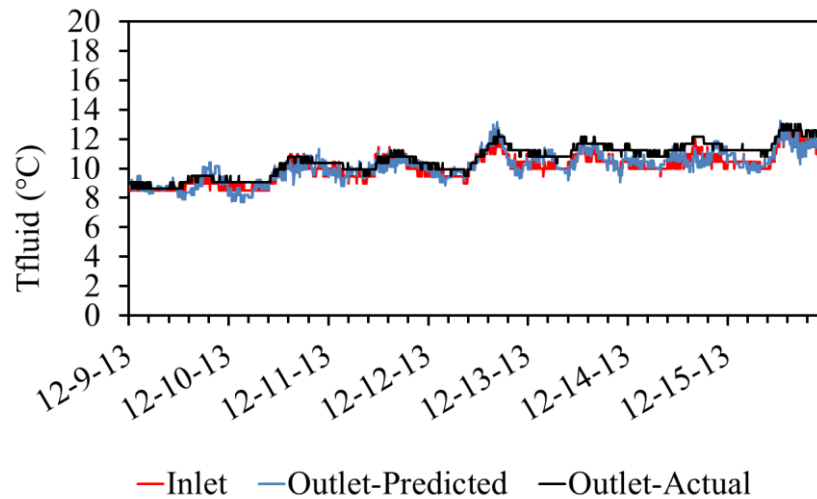


Figure 5-11: The inlet fluid temperatures, and outlet fluid temperatures of actual data, and of predicted data for typical week in the winter season

Figure 5-12 and Figure 5-13 presents that the predicted data is similar to the actual experimental data in histograms, and Mean Bias Error (MBE). Based on the results presented in Figure 5-12 and Figure 5-13, using the new G-functions for TAF system the predicted outlet temperatures well

agree to the actual experimental data for summer and winter seasons without extreme differences. This analysis implies that ignoring the uncertainty during the spring and fall seasons, the new G-function method for TAF system developed in this chapter is capable to generate reasonable outlet fluid temperature for energy modeling which is needed in several whole-building energy simulation programs, like EnergyPlus and eQUEST.

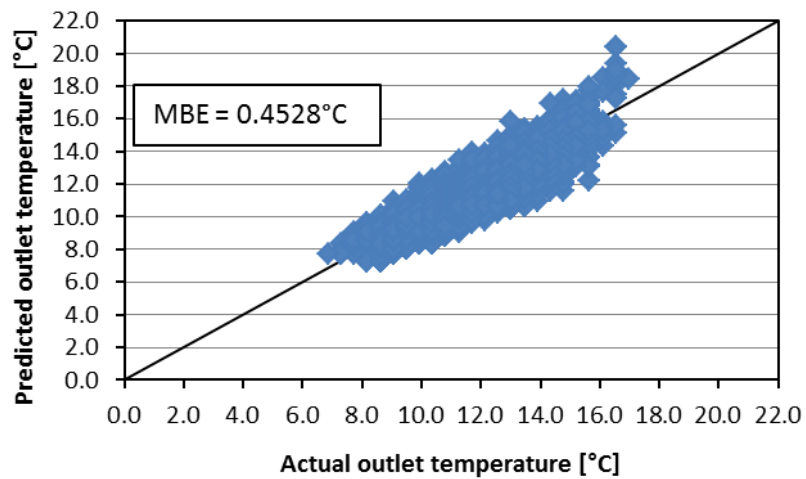


Figure 5-12: Scatter diagram to compare the predictions of the outlet fluid temperature and actual outlet fluid temperature for winter season

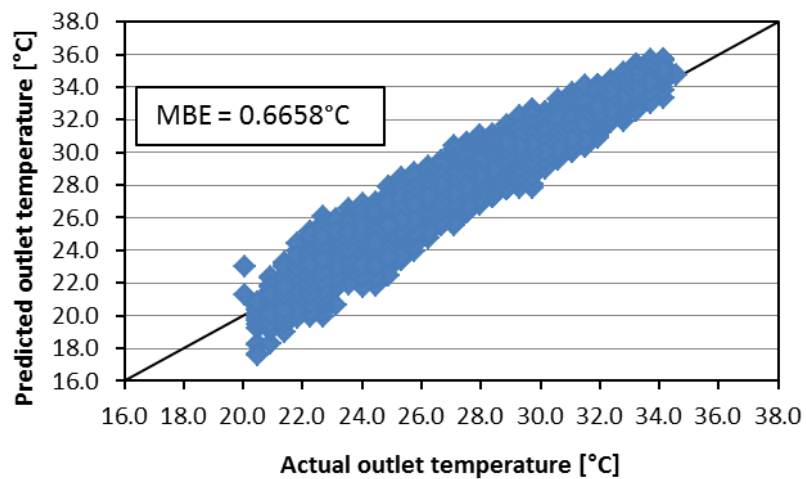


Figure 5-13: Scatter diagram to compare the predictions of the outlet fluid temperature and actual outlet fluid temperature for summer season

5.3.3. Sensitivity Analysis of the G-function Calculation

Using the developed new G-function approach for TAF system, this chapter performs a series of sensitivity analysis to look at the effects of several design parameters on G-functions. The design parameters studied in this section are depth of thermal pile, indoor air temperature, and soil thermal conductivity.

Effect of Depth of Thermal Pile

According to Loveridge et al. (2012b), the aspect ratio (length to diameter) of thermal pile ranges generally 10 through 50, while the aspect ratio of conventional borehole is 500 through 1000. So, this chapter explores the thermal piles which aspect ratio is 3.5, 5.0, 10.0, 15.0, and 20.0. In Figure 5-14 and Figure 5-15, the foundation wall temperature variations and the G-function curves for different aspect ratios are presented, respectively. Since foundation height is used to calculate t_s which is used to compute the normalized time, in Figure 5-14 and Figure 5-15, the temperature profiles and G-function curves of different aspect ratios are on the different normalized times.

In Figure 5-14, it is found that the lower aspect ratio thermal piles can be easily affected by indoor air temperature more than the higher aspect ratio thermal piles. This result implies that the foundation wall temperature of the shorter depth thermal pile or of the larger diameter thermal pile can be affected by the thermal effect of indoor air temperature. These different temperature variations result in the different fluctuations of G-function curves as shown in Figure 5-15. As the aspect ratio increases, the fluctuation of G-function curve pattern decreases and the G-function curve pattern is similar to that of the cases without thermal effect of indoor air temperature.

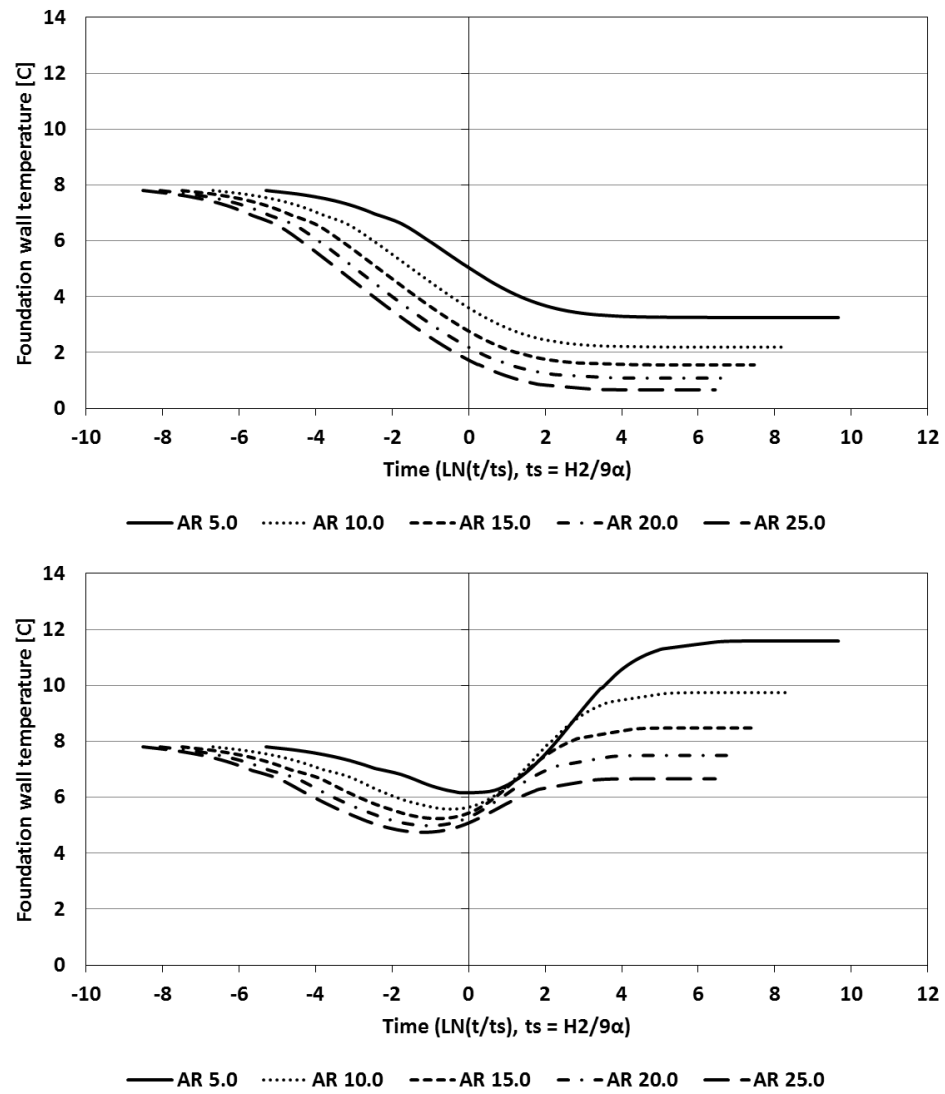


Figure 5-14: Foundation wall temperature variations of single TAF pile for different aspect ratios (ARs) without consideration of indoor air temperature (above) and with consideration of indoor air temperature (down)

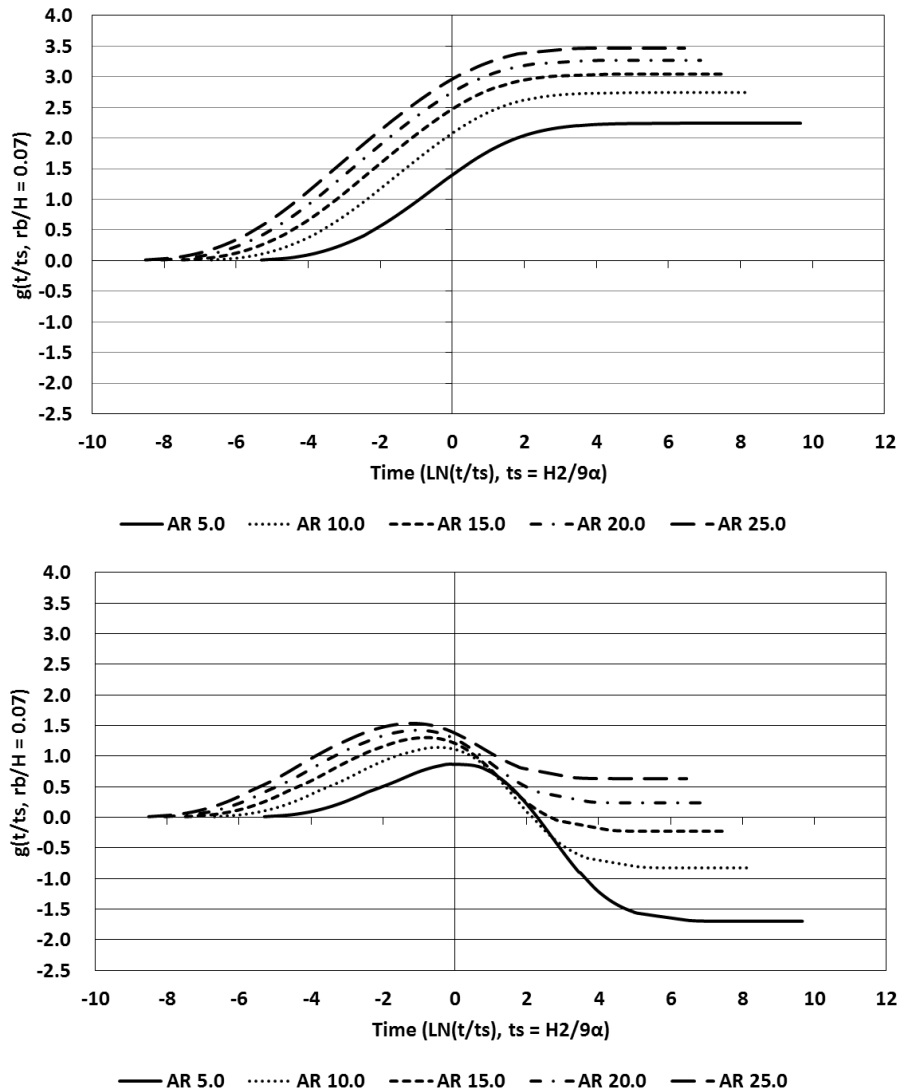


Figure 5-15: G-function curves of single TAF pile for different aspect ratios (ARs) without consideration of indoor air temperature (above) and with consideration of indoor air temperature (down)

Effect of Indoor Air Temperature

Since TAFs has an additional boundary condition representing indoor air temperature when calculating G-functions, it is important to study the effect of indoor air temperature on G-function values. So, this paper also performs a sensitivity analysis with several different indoor air temperature settings in Figure 5-8. The indoor air temperature settings are 16°C, 19°C, 22°C, 24°C, and 29°C with the

assumed annual average ground temperature of 9.7°C. In Figure 5-16, the resulting G-function curves developed in this paper are presented. As shown in Figure 5-16, as the indoor air temperature is lower, the thermal impact of it on the thermal pile decreases, and so the G-function curves has less changes for long-time steps compared to higher indoor air temperatures.

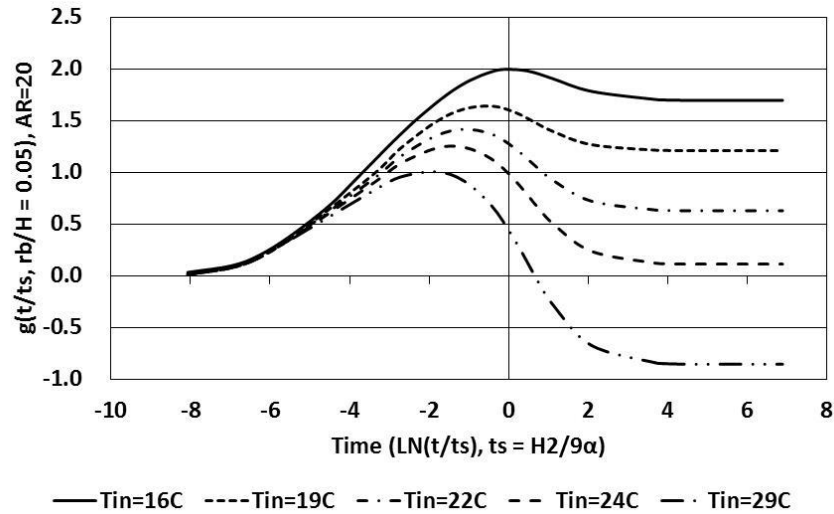


Figure 5-16: G-function curves of single TAF pile for different indoor air temperature settings for the aspect ratio of a thermal pile AR=20 with annual average ground temperature of 9.7°C

Effect of Soil Thermal Properties

Soil thermal properties are important factors for ground source heat pump systems including thermo-active foundation systems because soil is the main medium to transfer heat between thermal pile and ground. So, it is important to consider the impact of soil thermal properties on thermal performance of TAF systems. However, in reality it is difficult to evaluate specific soil thermal properties and determine the relevant input data for energy simulation modeling due to several influential mechanisms in soil such as decomposition of soil materials, migration of moisture, phase change due to freezing and thawing cycles as illustrated in Figure 5-17 and Table 5-5 (ASHRAE Fundamental, 2009). As shown in Figure 5-17, the impact of moisture content can be accounted for using the concept of

apparent soil thermal conductivity, because typically soil thermal conductivity increases with moisture content.

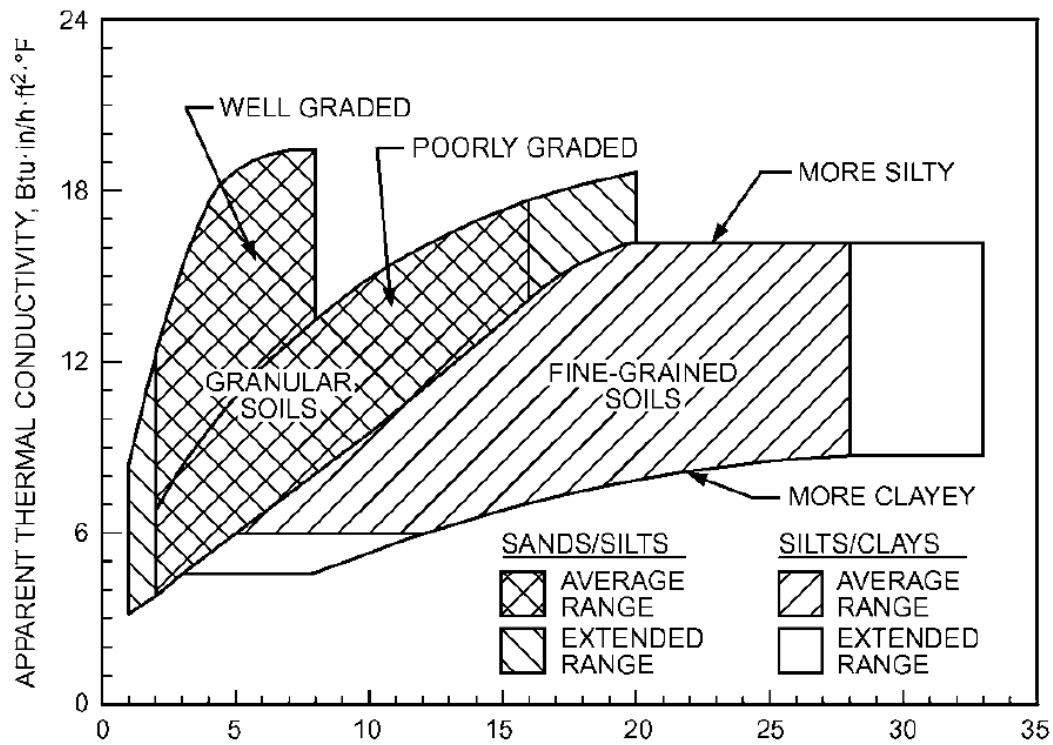


Figure 5-17: Apparent thermal conductivity for moist soils (Source: ASHRAE Fundamental, 2009)

Table 5-5: Typical soil thermal conductivity values (ASHRAE Fundamental, SI & IP, 2009)

Soil types	Normal range [W/(m·K)]	Recommended values [W/(m·K)]		Normal range [Btu·in/h·ft²·F]	Recommended values [Btu·in/h·ft²·F]	
		Low	High		Low	High
Sands	0.6 to 2.5	0.78	2.25	4.2 to 17.4	5.4	15.6
Silts	0.9 to 2.5	1.64	2.25	6 to 17.4	11.4	15.6
Clays	0.9 to 1.6	1.12	1.56	6 to 11.4	7.8	10.8
Loams	0.9 to 2.5	0.95	2.25	6 to 17.4	6.6	15.6

For the same aspect ratio of a thermal pile (AR=20), as presented in Figure 5-18, the lower thermal conductivity of soil has higher value of G-functions for the long time steps, and has the similar trend of the curve to the conventional G-function curve. This result implies that for the same aspect ratio of a thermal pile the lower soil thermal conductivity has less impact of indoor air temperature on the heat transfer between thermal pile and ground medium for the long time steps.

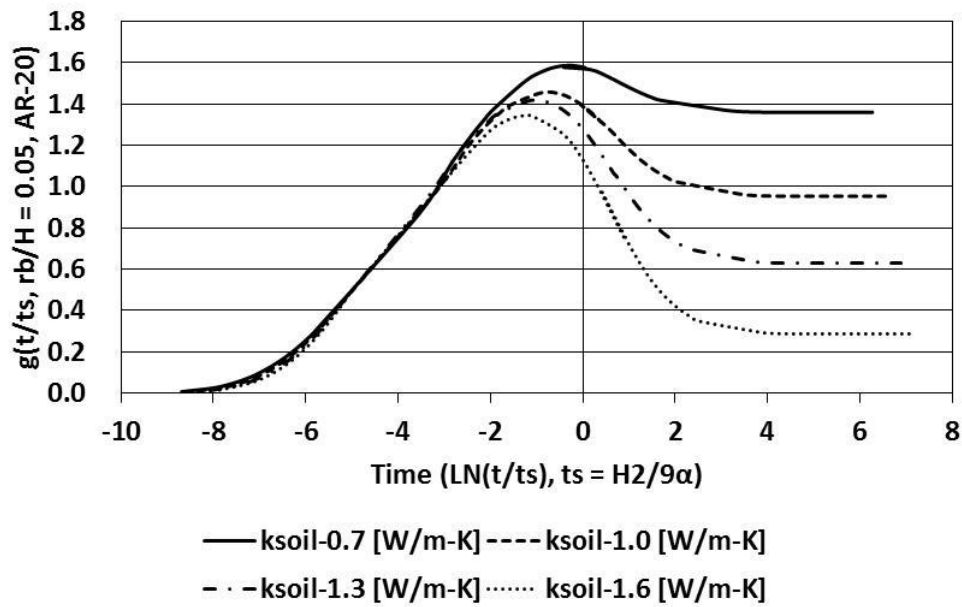


Figure 5-18: G-function curves for different soil thermal conductivities (ksoil)

5.4. Summary

The main purpose of this chapter was development of G-functions specific to a thermal foundation, and for this purpose this chapter considered two effects on G-functions: (i) the effect of different cross-sectional configuration of a foundation, and (ii) the effect of indoor air temperature.

Employing the fundamental heat conduction theory, the thermal response functions for three different types of cross-sectional configurations of a thermo-active foundation were derived

mathematically. Based on the derived heat conduction equations for the three different prototypical shapes, the modified G-function equations were developed, and then expressed by the perimeter and the hydraulic diameter of each configuration. The new expression term, which was called as the fractional shape factor, made the modified G-function equation simple and understandable.

Using the modified G-function equation and the validated three-dimensional numerical model for a square thermo-active foundation, the modified G-function equation was verified by comparing with the reference data by Eskilson's model (1987) and Yavuzturk's model (1999). As a result, using the same boundary conditions, the modified G-function equation was able to generate the very similar result to the reference data. In addition, the boundary conditions of a TAF system are different from those of a GSHP system because a TAF system is located below a building. So, this chapter considered the thermal effect of indoor air temperature on the foundation wall temperature variations and on G-function curves by superposing ground heat exchanger model with a prescribed constant heat flux and an above-grade floor slab model with constant indoor air temperature.

Using the actual field experiment data, this chapter validated the new G-function method. As a result of the validation analysis, the new G-function method generated the outlet fluid temperature close to the actual experiment data with the MBE of 0.45°C and 0.67°C for summer season and for winter season, respectively. In the sensitivity analysis, it was found that the pattern of G-function curve was similar to the trend of the conventional G-function curve as the aspect ratio of a thermal foundation was higher. This result means that longer depth thermal foundation was less affected by the indoor air temperature.

A series of sensitivity analysis presented in this chapter showed the effects of several design parameters on G-function calculations. The parameters studied were depth of thermal pile, indoor air temperature, and soil thermal conductivity. The findings of the sensitivity analysis are presented below:

- As depth of thermal pile increased, G-function was less affected by indoor air temperature.
- As indoor air temperature was closer to ground temperature, the impact of indoor air temperature on G-function of thermal pile decreased.
- When soil thermal conductivity was higher, the impact of indoor air temperature on G-function was higher.

CHAPTER 6. INTEGRATION OF THERMO-ACTIVE FOUNDATION MODELING IN ENERGYPLUS

6.1. Introduction

The thermal response factor (g-function) of a thermo-active foundation (TAF) is useful to model the thermal performance of TAF systems in detailed building energy simulation tools, such as EnergyPlus and DOE-2. As a first step, the average foundation wall temperature is estimated using Equation 6-1. Then, the average circulating fluid temperature is calculated from Equation 6-2. Finally, the average circulating fluid temperature is used to compute the outlet TAF fluid temperature. This outlet TAF temperature is the entering fluid temperature into a heat pump. Based on the efficiency of a heat pump system, climate conditions, and building thermal loads, the energy consumption of a building is computed using hourly or sub-hourly building energy simulation tools.

$$T_{\text{foundation}} = T_{\text{ground}} + \sum_{i=1}^n \frac{(Q_i - Q_{i-1})}{2pk} g\left(\frac{t_n - t_{i-1}}{t_s}, \frac{r_b}{H}\right) \quad \text{Equation 6-1}$$

$$T_{\text{fluid}} = T_{\text{foundation}} + R_{\text{total}} \times Q \quad \text{Equation 6-2}$$

where

t = Time

t_s = Time scale = $H^2/9\alpha$

H = Foundation depth

k = Ground thermal conductivity

$T_{\text{foundation}}$ = Average foundation wall temperature

T_{ground} = Undisturbed ground temperature

T_{fluid} = Average fluid temperature

Q = Step heat rejection/extraction pulse

r_b = Borehole radius

i = Index to denote the end of a time step

R_{total} = Total thermal resistance of a foundation

In this chapter, thermal response factor calculation approach for TAF systems are integrated into EnergyPlus to estimate the effectiveness of TAF systems in meeting heating and cooling loads for a typical office building in selected US locations. Furthermore, to evaluate the effect of design and operating parameters of TAF system performance, a series sensitivity analyses is carried out. The parameters considered include aspect ratio of foundation pile, and soil and concrete thermal conductivity. The analysis is performed using EnergyPlus tool to estimate the energy use for a prototypical office building located in selected US climates.

6.2. Application to Medium Sized Office Building

In this analysis, in order to assess the effectiveness of TAF systems, the G-functions for TAF systems are integrated into EnergyPlus program. This study utilizes the 3-D solution for TAF model to generate G-functions outlined in Chapter 5. The generated G-functions are integrated in EnergyPlus, a whole-building energy simulation program to evaluate the energy performances of TAF system providing heating and cooling to a building (EERE, 2010). In this analysis, a prototypical medium sized office building is considered to evaluate TAF system. This analysis compares energy performances and cost-effectiveness of TAF system against conventional ground source heat pump (GSHP) system with vertical boreholes. This analysis is carried out for three different U.S. climate conditions including Chicago, IL, New York, NY, Boulder, CO.

6.2.1. Building Description

As illustrated in Figure 6-1, the prototypical medium sized office building has three floors with 5 conditioned thermal zones per floor (EERE, 2013). The total building floor area is 4,982.67m² (53,633.04ft²), and all zones are assumed as conditioned area. Table 6-1 provides the detail information on the building sizes as modeled in EnergyPlus.

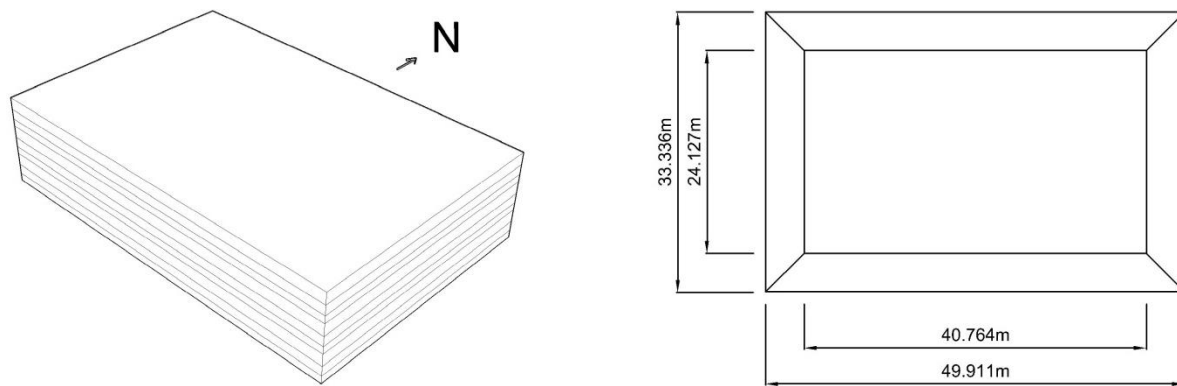


Figure 6-1: Example medium-sized office building modeled in EnergyPlus

Table 6-1: The description of the base prototypical multi-family residential building

Building Sizes Summary	
Building Size	(x) 49.911m (119.872ft) (y) 33.336m (65.089ft) (z) 11.887m (38.999ft)
Number of Floor	3 stories
Number of Units per Floor	5 units per floor (4 perimeter zones / 1 core zone)
Concrete Foundation Pile	(x) 0.5m (1.64ft) (y) 0.5m (1.64ft) (z) 10.0m (32.8ft)

The monthly average dry-bulb outdoor air temperature of all three US climate conditions is presented in Figure 6-2. As indicated in Figure 6-2, compared to Boulder, Chicago is colder in winter and warmer in summer, while New York is warmer in winter, and in summer seasons.

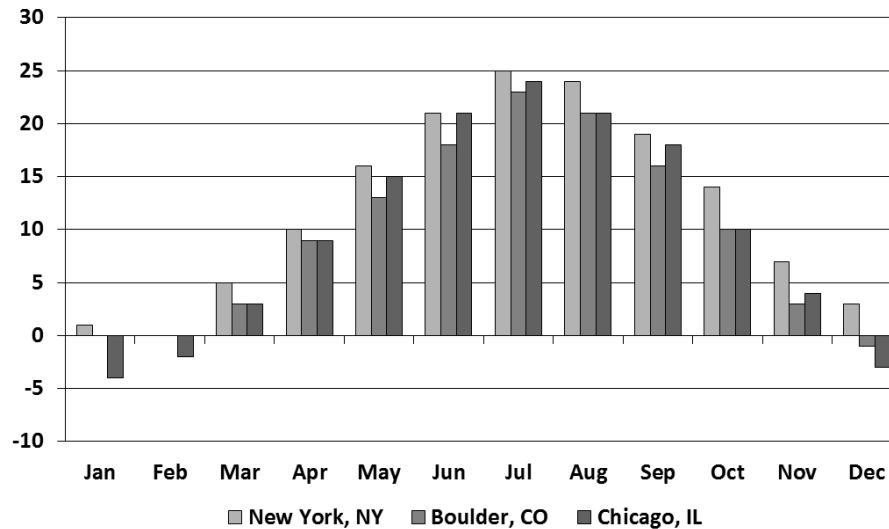


Figure 6-2: Monthly average outdoor air dry-bulb temperature of Boulder, CO., Chicago, IL, and New York, NY. (Sources: Boulder TMY2 724699, Chicago TMY3 725300, New York TMY3 744860)

The baseline building in EnergyPlus has a central chiller and central boiler for cooling and for heating, respectively. Table 6-2 presents the peak cooling/heating loads of the baseline building energy model for the three US climates considered in this analysis. In addition to the baseline HVAC systems, this analysis considers both GSHP and TAF systems as alternatives to provide cooling/heating to the prototypical building.

Table 6-2: The peak demand of the baseline for different U.S. climate conditions

Climate Condition	Electricity: Cooling	Gas: Heating
Chicago, IL	77.954[kW] / 265.99[kBtu/hr]	201.223[kW] / 686.60[kBtu/hr]
New York, NY	56.484[kW] / 192.73[kBtu/hr]	185.754[kW] / 633.82[kBtu/hr]
Boulder, CO	57.193[kW] / 195.15[kBtu/hr]	151.535[kW] / 517.06[kBtu/hr]

6.2.2. Modeling Approach

Figure 6-3 illustrates the schematic cooling/heating system model considered in EnergyPlus for both GSHP and TAF systems including ground coupled heat exchangers connected to ground coupled water-to-water heat pump. In particular, the GSHP and TAF system is modeled with the central cooling/heating system of the baseline model.

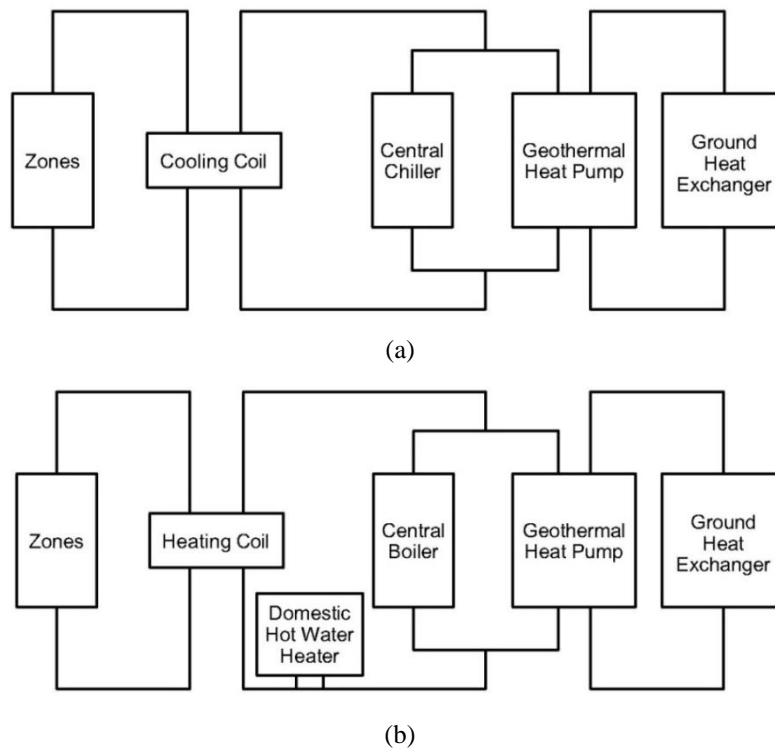


Figure 6-3: Schematic drawings for (a) cooling system loop, and (b) heating system loop coupled with water-to-water heat pump and ground coupled heat exchangers modeled in EnergyPlus

For the TAF system, it is assumed that the prototypical building has 77 pre-cast concrete foundation piles as shown in Figure 6-4. All the TAF piles are assumed to have heat exchanger piping loops. In general, for the conventional GSHP system uses 110 m per ton to determine the length of heat exchanger loops installed in vertical boreholes (OEE, 2004).

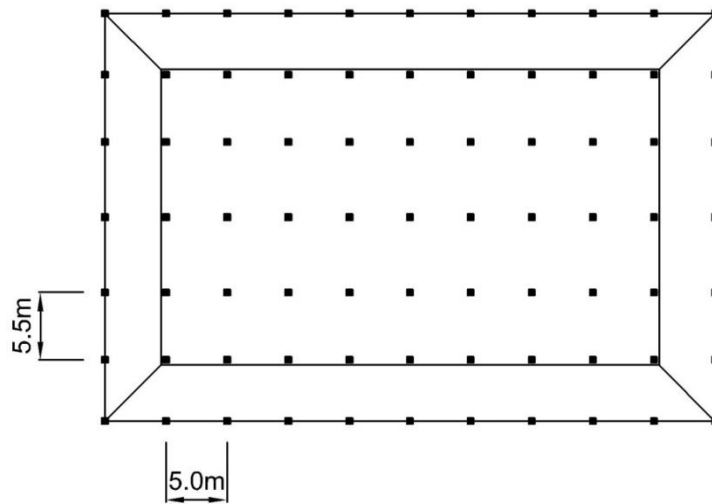


Figure 6-4: Foundation locations of the prototypical multi-family residential building

6.2.3. Discussion of Selected Results

Using the EnergyPlus, the analysis on energy consumption of the baseline is carried out to determine the heat pump sizes for the prototypical buildings in three different US climates illustrated in Figure 6-2. Then, the simulation analysis for both GSHP and TAF is performed, and compared with the baseline models to evaluate the energy savings due to the GSHP and TAF. As shown in Table 6-3, it is found that 20 ton heat pump is needed for both GSHP and TAF systems for Chicago, while 17.5 ton heat pump is needed for other climates. In Table 6-3, it is also found that the percent energy savings relative to the baseline model are presented in electricity and natural gas consumption for both GSHP and TAF systems. Since water-to-water ground coupled heat pumps consume electricity, site electricity consumptions include the electricity consumptions by the central chiller as well as by the heat pump for cooling/heating modes for both GSHP and TAF systems. However, the site natural gas consumption indicates only the consumption by the central boiler. For the overall comparison of energy performances of both GSHP and TAF systems, primary energy end-use savings relative to the baseline are presented in Table 6-3.

Table 6-3: Cooling/heating energy savings associated with plants

Climate	System Type	Heat Pump Size	Pipe Length [m]	Site energy savings		Primary energy savings
				Electricity	Gas	
Chicago, IL	GSHP	20.0 Ton	660	38.6%	97.9%	62.9%
	TAF	20.0 Ton	3080	43.1%	97.8%	65.5%
New York, NY	GSHP	17.5 Ton	660	43.3%	98.4%	57.0%
	TAF	17.5 Ton	3080	49.5%	98.3%	61.6%
Boulder, CO	GSHP	17.5 Ton	440	43.7%	98.0%	56.6%
	TAF	17.5 Ton	2310	50.3%	97.6%	61.6%

For the economic analysis to determine the cost-effectiveness of both GSHP and TAF systems, annual energy costs for heating/cooling are estimated using the average utility rates for electricity and natural gas provided by EIA for the three US climates as shown in Table 6-4 (EIA, 2014). Based on these utility data, the annual energy costs of GSHP and TAF systems are determined for the three US climates, and then compared to the annual energy cost of the baseline models (Table 6-5).

Table 6-4: Average utility rate of different states of U.S. (U.S. Energy Information Administration, 10/2014)

Energy Consumption	Electricity [cent/kWh]	GAS [\$ /MJ]
Illinois	13.14	0.00936
New York	19.42	0.01509
Colorado	11.74	0.00945

Table 6-5: Energy costs and percent energy cost savings

Climate	Chicago, IL		New York, NY		Boulder, CO	
System	Energy Costs	Percent Savings	Energy Costs	Percent Savings	Energy Costs	Percent Savings
Baseline	\$ 16,657.97	-	\$ 27,871.56	-	\$ 14,596.05	-
GSHP	\$ 9,670.36	41.9%	\$ 15,345.18	44.9%	\$ 7,988.38	45.3%
TAF	\$ 8,973.21	46.1%	\$ 13,669.90	51.0%	\$ 7,053.48	51.7%

Table 6-6 presents the initial costs and annual energy costs associated to both GSHP and TAF systems. According to the Department of Energy (2011), the average cost of a geothermal heat pump system is about \$2500 per ton of capacity in US. As aforementioned, the main purpose of TAF system is to reduce the need to excavate deep vertical boreholes of GSHP system by placing ground heat exchanger piping loops within the foundation piles. Generally, the drilling cost for boreholes is estimated \$29/m through \$39/m for different ground conditions, and so the average drilling cost is \$34/m (Rad et al. 2009). As shown in Table 6-6, it is found that the initial cost for TAF systems is almost 75% through 82% of the initial costs for GSHP systems in all three climates, while annual energy cost savings by TAF system relative to the baseline is higher than GSHP system. Then, this analysis estimates the simple payback periods (SPPs) relative to the baseline HVAC system for both GSHP and TAF for all three US climates. The SPP for TAF system ranges from 3.6 years (New York) to 7.4 years (Chicago), while the SPP for GSHP system varies between from 5.4 years (New York) to 10.6 years (Chicago). Thus, these results imply that TAF system is potential to be the cost effective alternatives to GSHP systems for all three US climates considered in this analysis.

Table 6-6: Overview of initial costs of cooling/heating systems

	Chicago, IL		New York, NY		Boulder, CO	
	GSHP	TAF	GSHP	TAF	GSHP	TAF
Heat Pump (\$2500/ton)	\$ 50,000.00	\$ 50,000.00	\$ 43,750.00	\$ 43,750.00	\$ 43,750.00	\$ 43,750.00
Piping (PE Pipe, \$69.99/100ft)	\$ 1,515.53	\$ 7,072.48	\$ 1,515.53	\$ 7,072.48	\$ 1,010.35	\$ 5,304.36
Drilling (\$34/m)	\$ 22,440.00 (6 x 110-m boreholes)	\$ 0.00	\$ 22,440.00 (6 x 110-m boreholes)	\$ 0.00	\$ 14,960.00 (4 x 110-m boreholes)	\$ 0.00
Initial Cost	\$ 73,955.53	\$ 57,072.48	\$ 67,705.53	\$ 50,822.48	\$ 59,720.35	\$ 49,054.36
Energy Cost Savings	\$ 6,987.61	\$ 7,684.76	\$ 12,526.38	\$ 14,201.65	\$ 6,607.68	\$ 7,542.58
Simple Payback Period	10.58	7.43	5.41	3.58	9.04	6.50

6.3. Application to Residential Building

The 3-D solution for TAF model of Figure 6-5 is used to generate G-functions using the procedure outlined in Chapter 5. These G-functions are then integrated in EnergyPlus, a whole-building simulation program that is then used to evaluate the energy performance for TAFs as heating and cooling systems for buildings (EERE, 2010). In the analysis carried out in this study, a prototypical multi-family building is considered to evaluate TAFs and compare its energy consumption and its cost-effectiveness against those obtained by conventional ground-source heat pump (GSHP) systems with vertical boreholes. The analysis is conducted for three climates including Boulder, CO, New York, NY, and Chicago, IL.

6.3.1. Building Description

As illustrated in Figure 6-5, the prototypical residential multi-family building has three floors with 6 apartment units per floor (EERE, 2013). The total building floor area is 2899m^2 (31210ft^2) including both conditioned and unconditioned spaces. The net conditioned floor area of the building is 2007.63m^2 (21609.96ft^2). Table 6-7 provides specific details on the size of each apartment unit as well as corridor spaces and construction details as modeled using EnergyPlus.

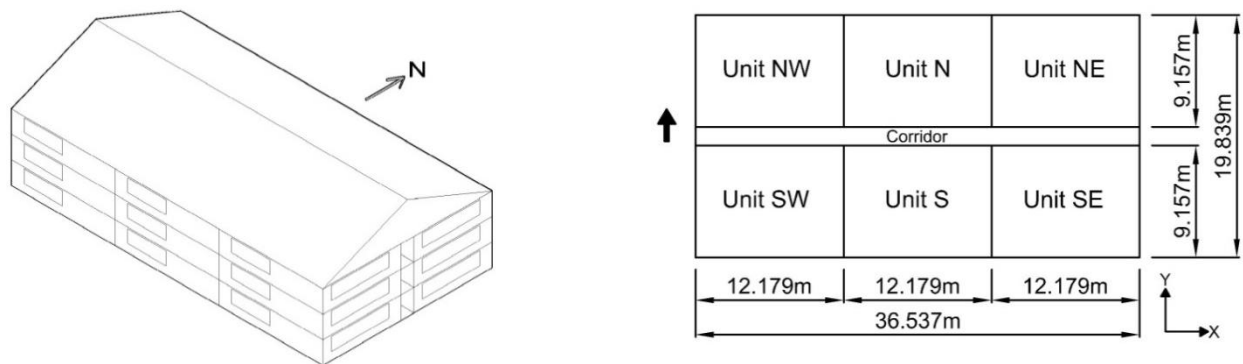


Figure 6-5: Example multi-family residential building modeled in EnergyPlus

Table 6-7: The description of the base prototypical multi-family residential building

Building Sizes Summary			
Unit Size	(x) 12.179m (39.957ft) (y) 9.157m (30.043ft) (z) 2.59m (8.50ft)		
Corridor Size	(x) 36.537m (119.872ft) (y) 1.525m (5.003ft) (z) 2.59m (8.50ft)		
Building Size	(x) 36.537m (119.872ft) (y) 19.839m (65.089ft) (z) 07.77m (25.49ft) (11.9m/39.0ft with attic)		
Number of Floor	3 stories		
Number of Units per Floor	6 units per floor		
Concrete Foundation Pile	(x) 0.5m (1.64ft) (y) 0.5m (1.64ft) (z) 10m (32.8ft)		
Building Envelope Summary			
	U-factor		
Construction	Boulder, CO	Chicago, CO	New York, NY
Exterior Roof	5.358 [W/K · m ²] 0.943 [Btu/h · ft ²]	5.358 [W/K · m ²] 0.943 [Btu/h · ft ²]	5.358 [W/K · m ²] 0.943 [Btu/h · ft ²]
Ceiling	0.136 [W/K · m ²] 0.024 [Btu/h · ft ²]	0.136 [W/K · m ²] 0.024 [Btu/h · ft ²]	0.136 [W/K · m ²] 0.024 [Btu/h · ft ²]
Exterior Wall	0.367 [W/K · m ²] 0.065 [Btu/h · ft ²]	0.367 [W/K · m ²] 0.065 [Btu/h · ft ²]	0.367 [W/K · m ²] 0.065 [Btu/h · ft ²]
Exterior Floor	0.184 [W/K · m ²] 0.032 [Btu/h · ft ²]	0.184 [W/K · m ²] 0.032 [Btu/h · ft ²]	0.288 [W/K · m ²] 0.051 [Btu/h · ft ²]

Figure 6-6 presents the monthly average dry-bulb outdoor air temperature of three climate conditions. As shown in Figure 6-6, compared to Boulder, Chicago has colder winter and warmer summer, while New York is warmer than Boulder during winter and summer months.

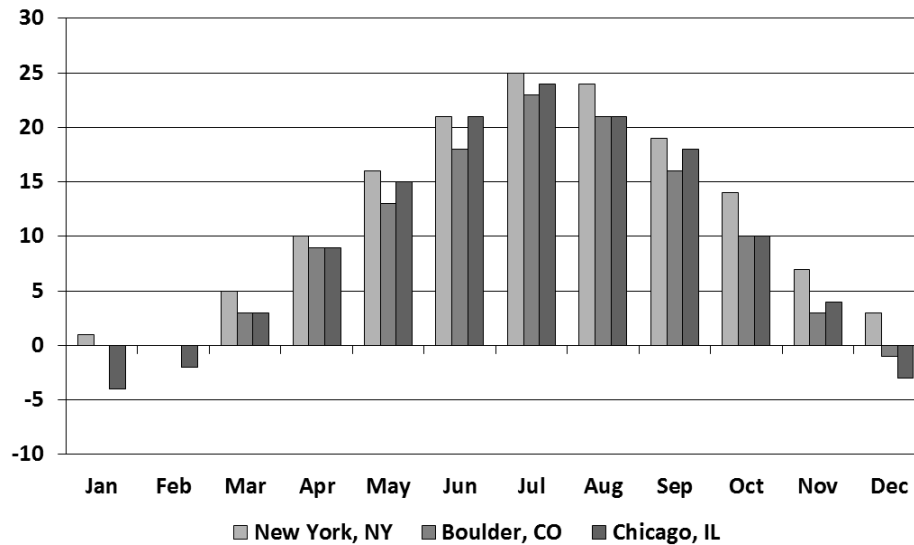


Figure 6-6: Monthly average outdoor air dry-bulb temperature of Boulder, CO., Chicago, IL, and New York, NY.

The baseline building energy model has a central chiller for cooling and boiler for heating. Table 6-8 presents the peak loads of the baseline building model found for the three US climates considered in the analysis. In addition to the baseline heating and cooling system, both GSHP and TAF systems are considered as alternatives to meet air conditioning needs for the prototypical residential multi-family building.

Table 6-8: The peak demand of the baseline for different U.S. climate conditions

Climate Condition	Electricity: Cooling	Gas: Heating
Chicago, IL	16.319[kW] / 85.03[kBtu/hr]	81.165[kW] / 277.38[kBtu/hr]
New York, NY	16.325[kW] / 82.45[kBtu/hr]	62.379[kW] / 213.11[kBtu/hr]
Boulder, CO	16.283[kW] / 78.13[kBtu/hr]	68.157[kW] / 232.72[kBtu/hr]

6.3.2. Modeling Approach

Figure 6-7 illustrates the schematic model considered in EnergyPlus for both GSHP and TAF systems which include general ground coupled heat exchangers. In particular, the TAF system is

modeled with the central cooling/heating system of the baseline model. The chiller and boiler may be needed for the three different climate conditions the water-to-water heat pump is sized of 8-ton based on the peak cooling loads.

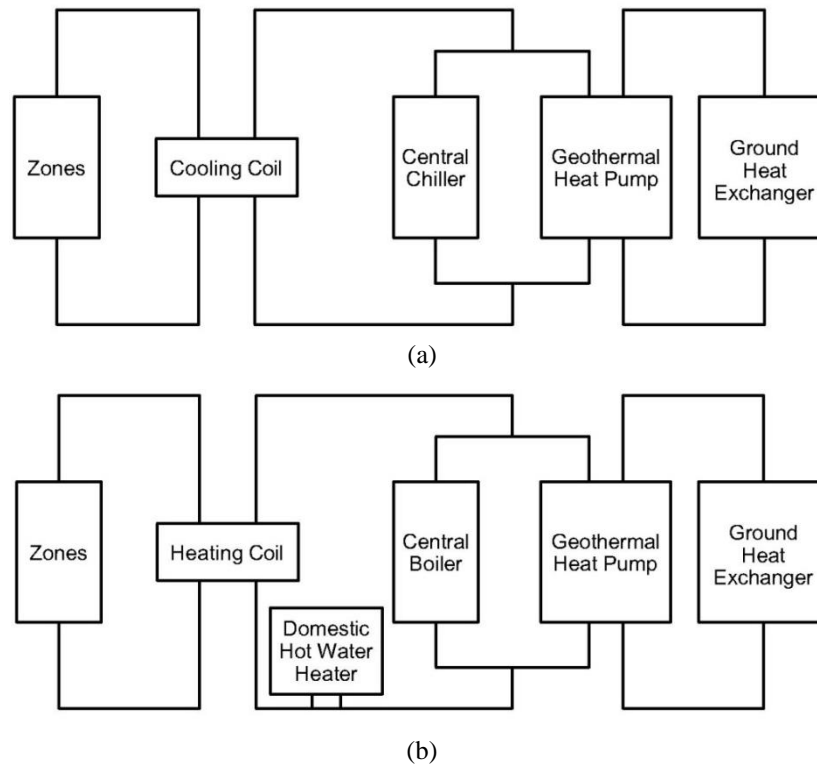


Figure 6-7: Schematic drawings for (a) cooling system loop, and (b) heating system loop coupled with water-to-water heat pump and ground coupled heat exchangers modeled in EnergyPlus

For the TAF system, the prototypical building is assumed to have 28 pre-cast concrete foundation piles as shown in Figure 6-8. Heat exchanger piping loops are installed in all the TAF piles. For the conventional GSHP system, 110 m per ton is used to determine the length of heat exchanger loops installed in vertical boreholes (OEE, 2004).

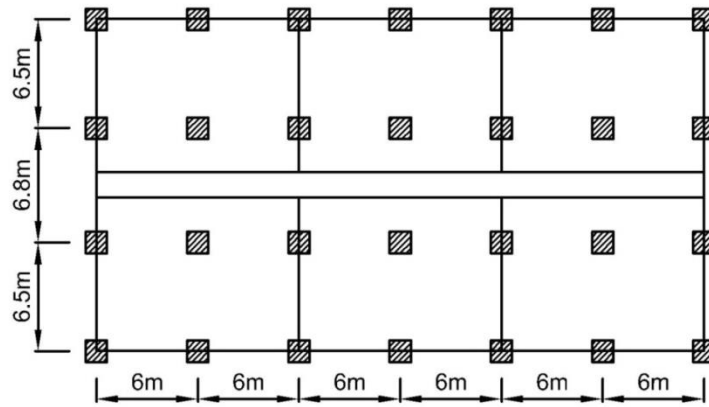


Figure 6-8: Foundation locations of the prototypical multi-family residential building

6.3.3. Discussion of Selected Results

The simulation analysis using EnergyPlus is then carried to first determine the heat pump size required as well as the annual heating and cooling energy end-use consumption for both GSHP and TAF when the residential buildings are located in the three US climates illustrated in Figure 6-6. As indicated in Table 6-9, it is found that 8-ton heat pump is needed for both GSHP and TAF systems for all three climates. Moreover, Table 6-9 indicates the percent reduction relative to the baseline HVAC system in electricity and natural gas consumption for both GSHP and TAF. Since ground coupled water-to-water heat pump consumes electricity, site electricity consumption provided in Table 6-9 for both GSHP and TAF systems includes the consumption by the central chiller as well as by the heat pump for cooling/heating modes. However, site natural gas only includes the consumption by the central boiler. To compare the overall energy performance of both GSHP and TAF systems, primary heating and cooling energy end-use savings relative to the baseline HVAC system are provided in Table 6-9. As shown in Table 6-9, while both ground-coupled systems provide significant energy use savings for heating and cooling the prototypical residential buildings, TAF results in slightly better performance in all three US climates considered in the analysis.

Table 6-9: Cooling/heating energy savings associated with plants

Climate	System Type	Heat Pump Size	Loop Length	Site Energy Savings		Primary Energy Savings
				Electricity	Gas	
Chicago, IL	GSHP	8 ton	660	6.4%	90.2%	76.6%
	TAF	8 ton	2800	10.4%	91.3%	78.2%
New York, NY	GSHP	8 ton	660	23.0%	97.7%	80.0%
	TAF	8 ton	2520	27.6%	97.9%	81.2%
Boulder, CO	GSHP	8 ton	440	68.1%	13.3%	25.1%
	TAF	8 ton	1680	70.4%	13.3%	25.6%

To assess the cost-effectiveness of both GSHP and TAF systems, annual heating and cooling energy costs are estimated using average utility rates for electricity and natural gas reported by EIA for the three US locations as summarized in Table 6-10 (EIA, 2014). Using these utility rates, the annual heating and cooling energy costs associated with the three HVAC systems including the baseline (chiller and boiler), GSHP, and TAF are determined for the three US climates considered in the analysis as summarized in Table 6-11.

Table 6-10: Average utility rate of different states of U.S. (U.S. Energy Information Administration, 10/2014)

Energy Consumption	Electricity [cent/kWh]	GAS [\$ /MJ]
Illinois	13.14	0.00936
New York	19.42	0.01509
Colorado	11.74	0.00945

Table 6-11: Energy costs and percent energy cost savings

Climate	Chicago, IL		New York, NY		Boulder, CO	
System	Energy Costs	Percent Savings	Energy Costs	Percent Savings	Energy Costs	Percent Savings
Baseline	\$ 11,088.82	-	\$ 16,966.31	-	\$ 9,194.15	-
GSHP	\$ 7,523.28	32.2%	\$ 10,130.18	40.3%	\$ 4,241.95	53.9%
TAF	\$ 7,181.89	35.2%	\$ 9,522.90	43.9%	\$ 4,087.21	55.5%

Table 6-12 shows the initial costs estimated to install GSHP and TAF systems. According to the Department of Energy (2011), in US the average cost of a geothermal heat pump system is \$2500 per ton of capacity. So, it costs \$20,000 for 8-ton heat pump for both GSHP and TAF systems. As noted earlier, the main benefit of TAF relative to GSHP is the elimination of the need to excavate deep vertical boreholes to install ground heat exchanger piping loops since these are placed within the foundation piles. The excavation cost for boreholes is estimated at \$34/m (Rad et al. 2009). Thus, the excavation varies with the depth and length of ground heat exchanger loops and thus the location as shown in Table 6-12. The initial cost for TAF systems is determined to be almost 50% of the installation costs for GSHP systems in all three climates. As shown in Table 6-12, the simple payback periods (SPPs) relative to the baseline HVAC system for both GSHP and TAF are estimated for all three US climates. The SPP for TAF ranges from 3.5 years (New York) to 6.8 years (Chicago), while SPP for GSHP varies between from 6.4 to 12.5 years. These results indicate that TAF systems offer cost effective alternatives to GSHPs for all three US climates considered in the analysis.

Table 6-12: Overview of initial costs of cooling/heating systems

	Chicago, IL		New York, NY		Boulder, CO	
	GSHP	TAF	GSHP	TAF	GSHP	TAF
Heat Pump (\$2500/ton)	\$20,000.0	\$20,000.0	\$20,000.0	\$20,000.0	\$20,000.0	\$20,000.0
Piping (PE Pipe, \$69.99/100ft)	\$1,010.4	\$6,429.5	\$1,515.5	\$5,786.6	\$1,010.4	\$3,857.7
Drilling (\$34/m)	\$14,960.0 (4 x 110-m boreholes)	\$0.0	\$22,440.0 (6 x 110-m boreholes)	\$0.0	\$14,960.0 (4 x 110-m boreholes)	\$0.0
Initial Cost	\$35,970.4	\$26,429.5	\$43,955.5	\$25,786.6	\$35,970.4	\$23,857.7
Energy Cost Savings	\$2,885.3	\$3,906.9	\$6,836.1	\$7,443.4	\$4,952.2	\$5,106.9
Simple Payback Period	12.5	6.76	6.4	3.5	7.3	4.7

6.4. Summary

In this chapter, the thermal response factors developed in Chapter 5 are integrated within EnergyPlus to perform a series of sensitivity analyses to assess the contribution of a thermo-active foundation system to saving cooling and heating loads of central chiller and boiler for a prototypical building. In this chapter, two example applications are presented to show the effectiveness of TAF systems compared to the conventional central chiller and boiler systems, and to the conventional GSHP systems for different three climate conditions; Chicago, New York, and Boulder. As a result, it is found that TAF system can save cooling and heating energy consumptions similar to GSHP systems with lower initial cost due to the elimination of drilling cost required for deep boreholes of GSHP systems.

In summary, the thermal response factors of a thermo-active foundation developed in this thesis can be integrated seamlessly in any detailed building energy simulation program. The simulation analysis can then be used to optimize the design and operation of TAF systems. Some design guidelines for TAF systems are presented in the following chapters.

CHAPTER 7. DESIGN GUIDELINES FOR THERMO-ACTIVE FOUNDATIONS

7.1. Background

Geothermal energy is considered as an attractive renewable energy source especially for cooling and heating buildings. Indeed, earth is typically cooler than ambient air during cooling seasons, and is warmer than ambient air during heating seasons in most US climates. There have been several studies to assess the thermal performance of ground-source heat pump systems (GSHPs), and to develop design strategies for these systems to meet building thermal loads. No design guidelines are available for thermo-active foundations.

One of the common problems with GSHP systems is under-sized ground heat exchanger loop (Fisher et al. 2005). Using simulation analysis, Fisher et al. (2005) presented the impact of sizing issue of ground heat exchanger loop on the fluid temperature variations. Shonder et al. (1998) reported that the ground loop capacity is the most important factor that determines the outlet loop fluid temperature which is the entering temperature to the heat pump. In their study, they found that the recommended maximum outlet fluid temperature for cooling-dominated climates was 95°F (35°C), and that the efficiency of the heat pump began to decrease when the outlet temperature is above this recommended threshold. For heating dominated climates or periods, it was also observed that the efficiency of the heat pump decreases when the outlet fluid temperature is below 30°F (-1.0°C). Chiasson et al. (2010) discussed the possible problems related to improper sizing of heat exchanger loops for GSHP systems. In particular, they indicated that when ground-coupled heat exchanger loop size is undersized, the fluid outlet temperatures are affected by the imbalances in the thermal loads. This means that for heating-dominated regions the fluid outlet temperature progressively drops to the freezing point, and for

cooling-dominated regions, the fluid outlet temperatures can increase significantly. Moreover, Kavanaugh (2010) noted that short ground loops can cause lower efficiencies of the heat pump systems.

Under-sizing of ground-coupled heat exchanger loops can lead to more severe problems for a thermo-active foundation system than those for GSHPs. Indeed, thermo-active foundation systems have additional design constraints due to the structural considerations associated to the building foundations. These constraints include foundation pile depth, foundation radius, and total number of foundation piles.

In this chapter, the thermal response factors integrated within detailed building energy simulation tool are utilized to develop design guidelines for thermo-active foundation systems. In particular, the proper number of foundation piles suitable for specific heat pump capacities is determined for selected US climate zones.

7.2. Description of the Case Model Simulated in EnergyPlus

A prototypical medium sized office building is considered to perform the required analysis to develop design guidelines for TAF systems. The prototypical medium-sized office building provided by Department of Energy (DOE) has three-stories with five thermal zones for each floor as shown in Figure 7-1. The building floor area is $4,982.67 \text{ m}^2$ ($53,633.04 \text{ ft}^2$).

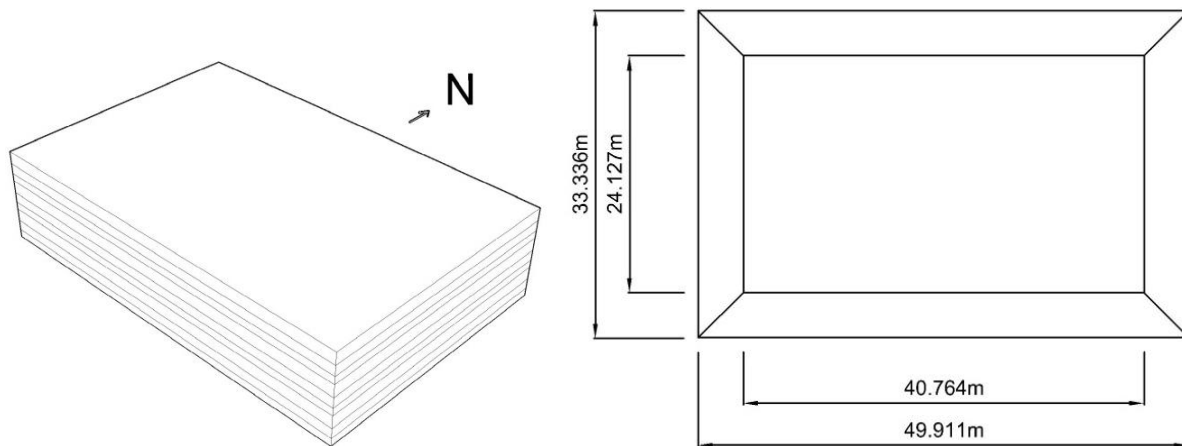


Figure 7-1: Schematic 3D image and floor plan of the medium sized office building

In EnergyPlus, a thermo-active foundation system is modeled with an auxiliary heating/cooling system. A schematic HVAC system with the conventional ground source heat pump system as modeled in EnergyPlus is illustrated in Figure 7-2. The baseline building energy model has a central chiller for cooling and a central boiler for heating.

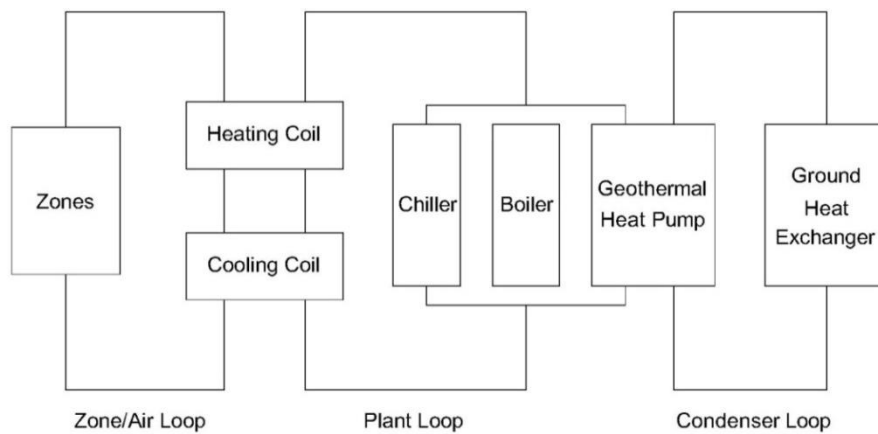


Figure 7-2: Schematic HVAC system with ground heat exchangers and a geothermal heat pump as modeled in EnergyPlus

For this analysis, some assumptions are employed including:

- In each thermal foundation pile, at least one U-tube heat exchanger is installed,
- There are no thermal interactions between adjacent foundation piles.

- Thermal influence between heat exchanger pipes in a thermal pile is neglected.

The input data used to model TAF systems in EnergyPlus are provided in Table 7-1. Table 7-2 lists the specifications of the geothermal water-to-water heat pumps considered in the building energy simulation analysis.

Table 7-1: The input data used for modeling TAF system in EnergyPlus

Ground thermal diffusivity [m²/sec]	9.41 X 10 ⁻⁷
Ground thermal conductivity [W/m·K]	1.30
Concrete thermal conductivity [W/m·K]	1.80
Pipe thermal conductivity [W/m·K]	0.36
Foundation radius [m]	0.25
Aspect Ratio (Height / Foundation diameter)	AR = 5, 10, 15, 20, 25, 30

Table 7-2: Specifications of geothermal heat pump systems (Manufacturer of NSW model – WaterFurnace, and Manufacturer of RWXW model – Johnson Controls)

Model	Nominal Tons	Mode*	Capacity		Efficiency
			Btu/h	W	
NSW-050	4	Cooling (25°C/77°F)	51,500	15,094	EER = 16.4 Btu/h·W
		Heating (0°C/32°F)	44,200	12,954	COP = 3.1
NSW-060	5	Cooling (25°C/77°F)	58,000	16,999	EER = 15.7 Btu/h·W
		Heating (0°C/32°F)	50,100	14,683	COP = 3.0
RWXW-140	12	Cooling (25°C/77°F)	155,000	45,428	EER = 17.0 Btu/h·W
		Heating (0°C/32°F)	127,000	37,222	COP = 3.1
RWXW-180	15	Cooling (25°C/77°F)	177,000	51,876	EER = 15.8 Btu/h·W
		Heating (0°C/32°F)	153,000	44,842	COP = 2.8
RWXW-210	18	Cooling (25°C/77°F)	212,000	62,134	EER = 17.0 Btu/h·W
		Heating (0°C/32°F)	173,000	50,703	COP = 3.1
RWXW-240	20	Cooling (25°C/77°F)	242,000	70,926	EER = 15.5 Btu/h·W
		Heating (0°C/32°F)	193,000	55,565	COP = 2.8
RWXW-360	30	Cooling (25°C/77°F)	351,000	102,872	EER = 16.2 Btu/h·W
		Heating (0°C/32°F)	296,500	86,899	COP = 3.2

7.3. Description of the Climate Conditions

In this chapter, seven sites are considered in the simulation analysis to cover seven different US climate zones. The sites and associated ASHRAE climate zones are described in Table 7-3 and Figure 7-3. In the simulation analysis performed with EnergyPlus, the same soil and concrete thermal properties are assumed for all sites. However, site-specific variations of the ground temperatures (Table 7-3) are considered for both developing the thermal response factors and performing a comprehensive energy simulation using EnergyPlus for each climate zone. For all climate zones, weather data in the form of Typical Meteorological Years (TMY) is utilized.

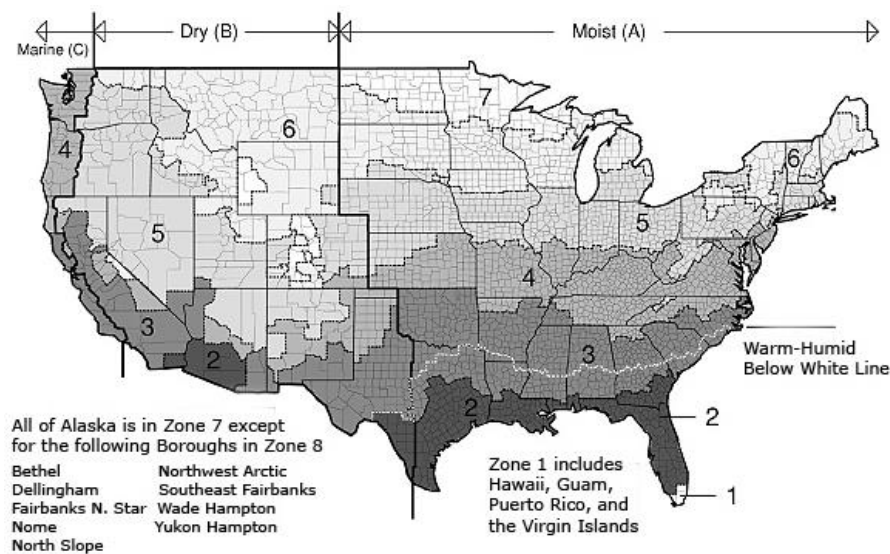


Figure 7-3: US ASHRAE Climate zones (ASHRAE Standard 90-1-2004)

Table 7-3: Summary of selected US sites and associated ASHRAE climate zones used in the energy analysis (ASHRAE Standard 90.1-2004)

Region	ASHRAE Climate Zone	Outdoor mean air temperature		Climate conditions	Annual average ground temperature (T_{ground})*
		Summer	Winter		
Dallas, TX	Zone 3A	27.7°C (81.9°F)	8.8°C (47.8°F)	Warm / Humid	17.9°C (64.2°F)
New York, NY	Zone 4A	23.3°C (74.0°F)	2.8°C (37.0°F)	Mixed / Humid	12.4°C (54.3°F)

Boulder, CO	Zone 5B	20.7°C (69.2°F)	0.5°C (32.9°F)	Cool / Dry	9.7°C (49.5°F)
Cheyenne, WY	Zone 6B	18.0°C (69.4°F)	-0.8°C (30.7°F)	Cold / Dry	7.3°C (45.1°F)
Anchorage, AK	Zone 7	13.3°C (56.0°F)	-5.8°C (21.6°F)	Very Cold	2.8°C (37.0°F)

*The reference of the annual average ground temperature is TMY data.

7.4. Design Guide Chart for Thermo-Active Foundations

7.4.1. Evaluation of Heat Exchanger Pipe Length per Heat Pump Capacity

In order to determine the proper design specifications for TAF systems, consistent design criteria are established for all the selected climate zones. For TAF systems, the design criteria are based on fluid outlet temperatures (which are also the entering fluid temperatures to the water-to-water heat pump systems). After reviewing several references and manufacturers' product information for heat pumps used in this chapter, it is found that the maximum recommended exiting water temperature (EWT) range is 25°C to 35°C, and the minimum EWT is around 0°C (Shonder et al. 1998). So, the main objective of the initial analysis is to find the required number of thermal foundation piles that can make the maximum EWT within the range from 30°C to 45°C, and then the number of thermal piles would be converted into the heat exchanger pipe length per heat capacity [m/ton].

Figure 7-4 through Figure 7-6 presents the average heat transfer rate of thermal pile per heat exchanger pipe length in [W/m] for three different annual average ground temperature conditions. As illustrated in Figure 7-4 through Figure 7-6, it is found that when the target is to ensure specific threshold of entering water temperature (EWT) to a heat pump, the average heat transfer rates per heat exchanger pipe length of different water-to-water heat pump capacities are similar with small ranges of deficiency. From Figure 7-4 through Figure 7-6, it is also found that the higher the annual average

ground temperature, the lower heat transfer rate per heat exchanger pipe length is required. In other words, the higher the annual average ground temperature, the more heat exchanger length per ton is required

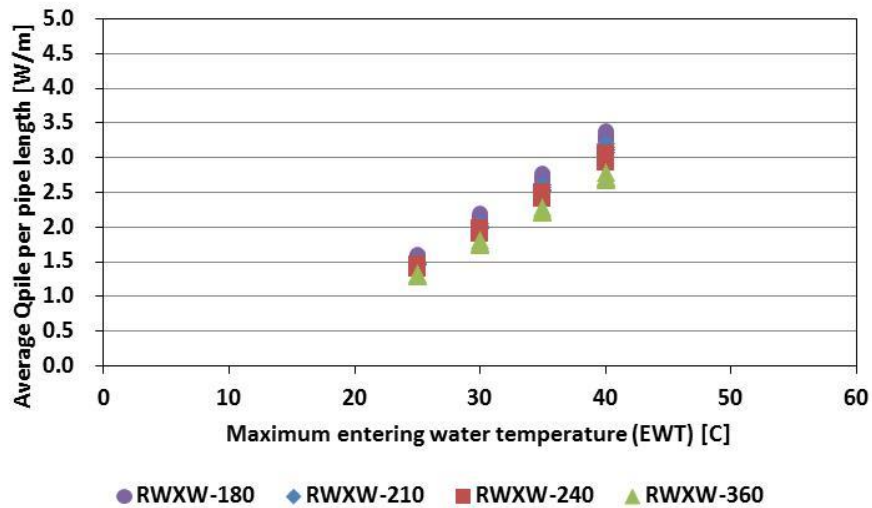


Figure 7-4: Average heat transfer rate per heat exchanger pipe length [W/m] as a function of entering water temperature for an annual average ground temperature of 7.3°C (45.1°F) representing Cheyenne, WY.

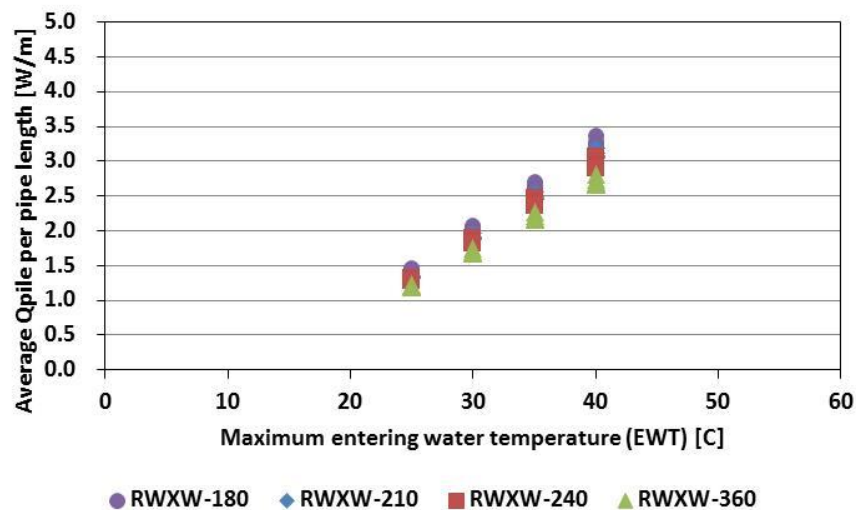


Figure 7-5: Average heat transfer rate per heat exchanger pipe length [W/m] as a function of entering water temperature for an annual average ground temperature of 9.7°C (49.5°F) representing Boulder, CO.

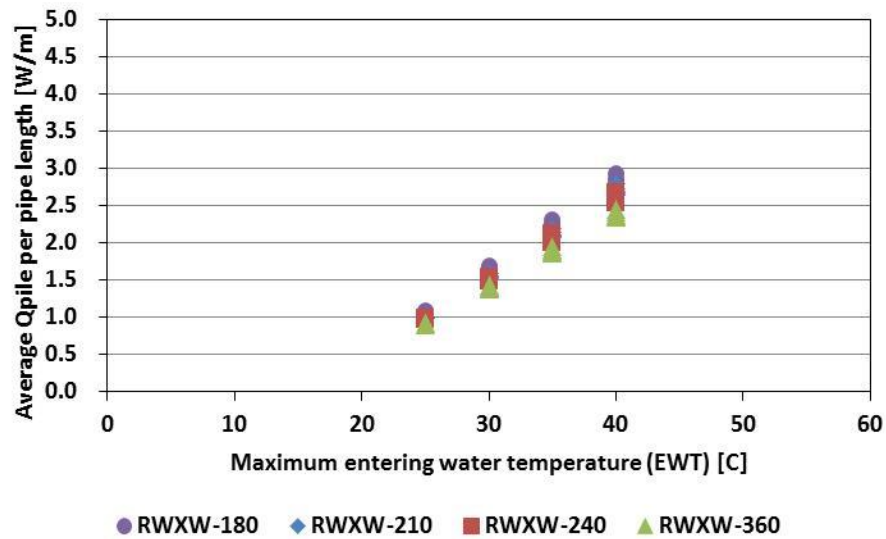


Figure 7-6: Average heat transfer rate per heat exchanger pipe length [W/m] as a function of entering water temperature for an annual average ground temperature of 12.4°C (54.3°F) representing New York, NY.

Building on the results presented in Figure 7-4 through Figure 7-6, design guidelines in the form of one chart are developed for thermo-active foundations as shown in Figure 7-7. This chart provides the required heat exchanger pipe length per water-to-water heat pump capacity and the targeted maximum entering water temperature (EWT) to a heat pump as a function of annual average ground temperature. This chart also provides the minimum efficiency of water-to-water heat pump for selected ground temperature and targeted EWT.

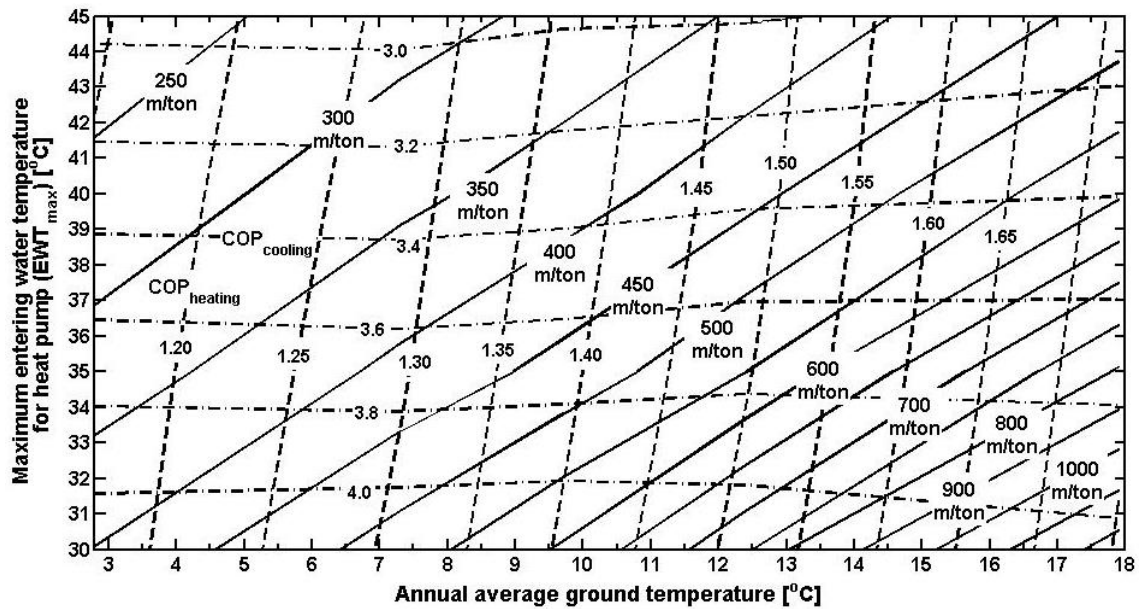


Figure 7-7: Design guide chart for thermo-active foundations ($k_{\text{soil}}=1.3 \text{ W/m-K}$, $k_{\text{conc}}=1.8 \text{ W/m-K}$)

7.4.2. Example Applications

The design chart developed in this chapter can be used to determine heat exchanger pipe length for a given heat pump capacity or to size heat pump capacity for given design limitations associated with structural or architectural requirements, such as foundation depth, and available foundation number of TAF system piles for a building. In other words, when foundation size and available number of foundations are given, the required pipe length per heat pump capacity can be selected based on building site annual ground temperature and targeted entering water temperature. Similarly when the number of foundation piles and foundation depth are given, the pipe length per ton can be used to determine a water-to-water heat pump capacity.

Medium-sized office building in Chicago, IL

For example, if a medium sized office building is located in Chicago, IL, where the annual average ground temperature is 9.8°C (49.67°F), and if the targeted maximum entering water temperature

to a heat pump is set to be 35°C (95°F), then the required heat exchanger pipe length is 469m/ton (as shown in Figure 7-9). As shown in Figure 7-8, if the example building has 77-10 m precast concrete foundation piles, then the available heat exchanger pipe length of the building is at least 1540 m when every pile has at least one loop of heat exchanger pipe. Then using the selected pipe length per ton from the chart, the required heat pump capacity can be calculated to be 3.3 ton to have the maximum EWT of 35°C (95°F), and so the expected COP for cooling mode can be 3.72.

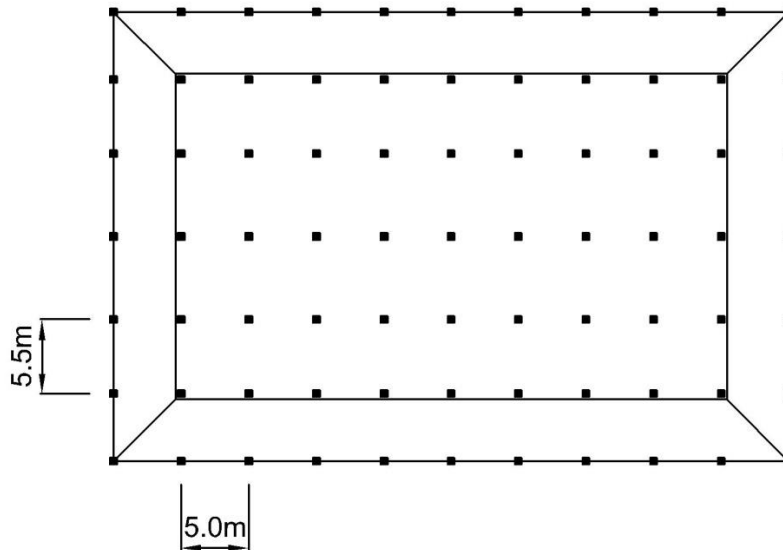


Figure 7-8: Foundation locations for the example of the medium sized office building

To verify the results obtained from the chart, the example application is modeled in EnergyPlus with relevant G-function values for Chicago climate. Since the calculated water-to-water heat pump size is 3.3-ton, the heat pump sizes of 3.14-ton and 4.29-ton can be considered for this model. As presented in Table 7-4, the heat pump capacity of 3.14-ton for this example medium sized office building with 77-10m foundation piles is less than the targeted maximum EWT, while the heat pump capacity of 4.29-ton has higher EWT than the targeted temperature.

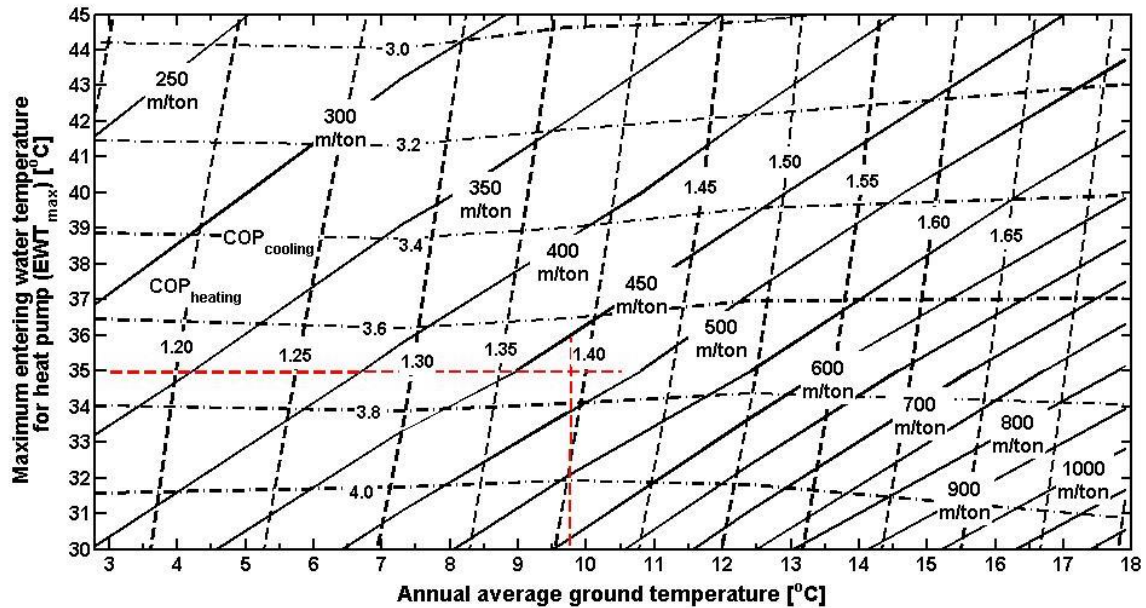


Figure 7-9: Example of using design guide chart for thermo-active foundations ($k_{soil}=1.3 \text{ W/m-K}$, $k_{conc}=1.8 \text{ W/m-K}$)

Table 7-4: Simulation results in maximum entering water temperature for Chicago, IL.

Water-to-Water Heat Pump Model	Heat Pump Capacity [Ton]	EWT_max	COP_cooling
NSW-040	3.14 ton	34.55 °C	4.0
NSW-050	4.29 ton	42.13 °C	3.3

In order to explore the correlation between water-to-water heat pump capacities and maximum entering water temperatures and minimum COPs for cooling, this chapter performs sensitivity analysis. As presented in Figure 7-10 and Figure 7-11, it is found that the correlation is linear. Based on the linear correlations between water-to-water heat pump capacities and EWT_max and COP-cooling, the EWT_max and COP_cooling for 3.3-ton water-to-water heat pump can be predicted for the example case. So, it is calculated that the predicted EWT_max is 35.74°C and the predicted COP_cooling is 3.76, and the percent errors are 2% and 1%, respectively as shown in Table 7-5.

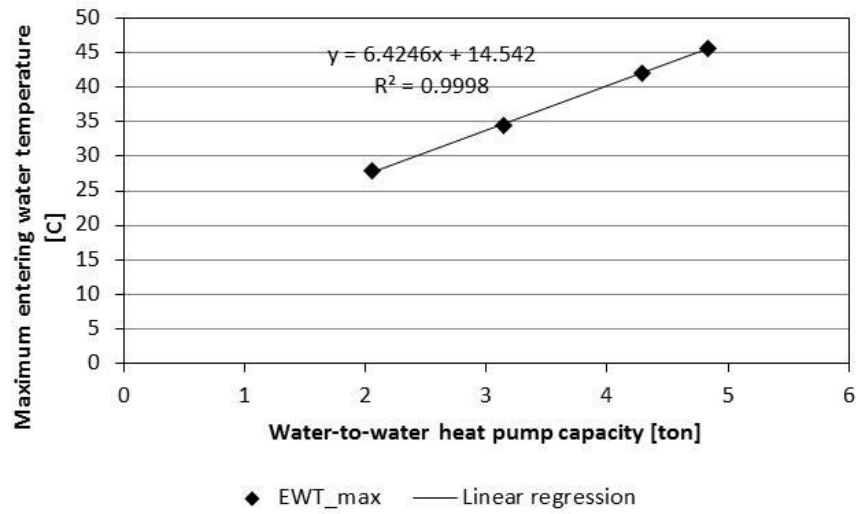


Figure 7-10: Linear relationship between water-to-water heat pump capacity and maximum EWT for the example model with 77-10m thermal piles in Chicago, IL.

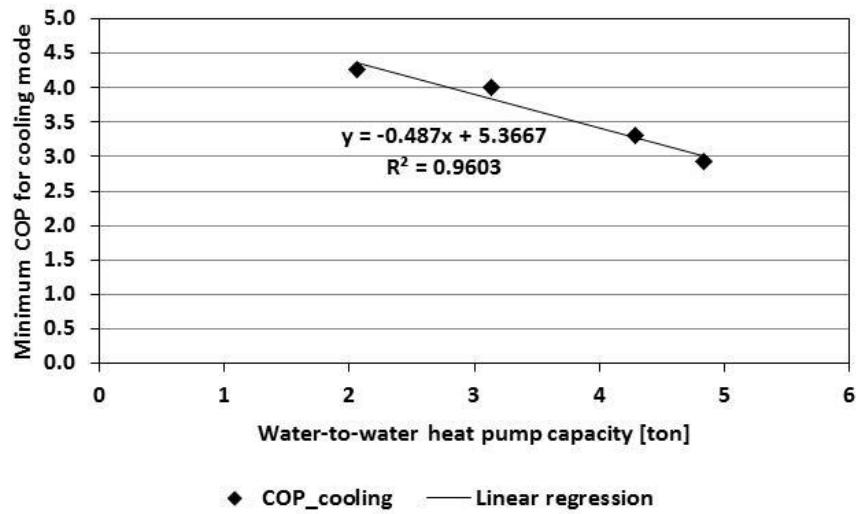


Figure 7-11: Linear relationship between water-to-water heat pump capacity and minimum COP for cooling mode for the example model with 77-10m thermal piles in Chicago, IL.

Table 7-5: Comparison of linear interpolation result of the simulations and the prediction of design guide chart

	Design Guide Chart	Simulation Results	Percent Error [%]
EWT_max	35 °C (targeted EWT_max)	35.74 °C	2.1%
COP_cooling	3.72	3.76	1.1%

Small-sized office building in New York, NY

The case study in this section is a small-sized office building with a rectangular floor plan as depicted in Figure 7-12. The building is located in New York, NY, where the annual average ground temperature is 12.4°C (54.3°F). If the targeted maximum entering water temperature to a water-to-water heat pump is assumed to be 38°C (100.4°F), then according to Figure 7-13, the required heat exchanger pipe length is 480m/ton. If the building has 24-15 m precast concrete foundation piles and if each foundation pile has one U-tube loop within each pile, then the available heat exchanger pipe length of the building is at least 720 m. Using the selected pipe length per ton from the chart (Figure 7-13), the required heat pump capacity can be estimated to be 1.5-ton for the targeted maximum EWT of 38°C (100.4°F), and the expected COP for cooling mode can be determined to be 3.52.

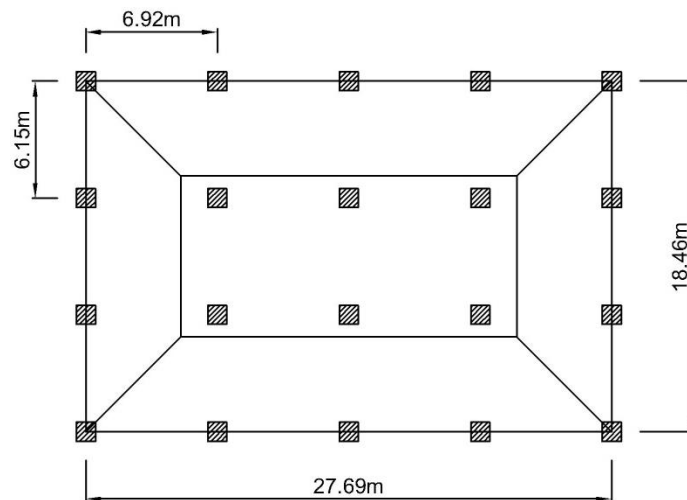


Figure 7-12: Location of foundation piles for the case study office building in New York, NY

To verify the results obtained from the chart, the office building of Figure 7-12 is modeled using EnergyPlus with relevant G-function values for New York climate. Since the calculated water-to-water heat pump size is 1.5-ton, the heat pump sizes of 1.44-ton and 2.06-ton can be considered for this model. As a result presented in Table 7-6, the heat pump capacity of 1.44-ton for the case-study of

Figure 7-12 associated with the small size office building using 24-15 m foundation piles can meet the targeted maximum EWT, while the use of 2.06-ton heat pump provides higher EWT than the targeted temperature. Based on the simulation results, the specifications obtained using the design chart of Figure 7-7 (refer also to Figure 7-13) are accurate. Indeed, the required-heat pump size is 1.5-ton for the building of Figure 7-12 with a targeted EWT of 38°C (100.4°F). If a water-to-water heat pump having a capacity higher than 1.5-ton is used, EWT would be higher than 38°C (100.4°F) as noted in Table 7-6.

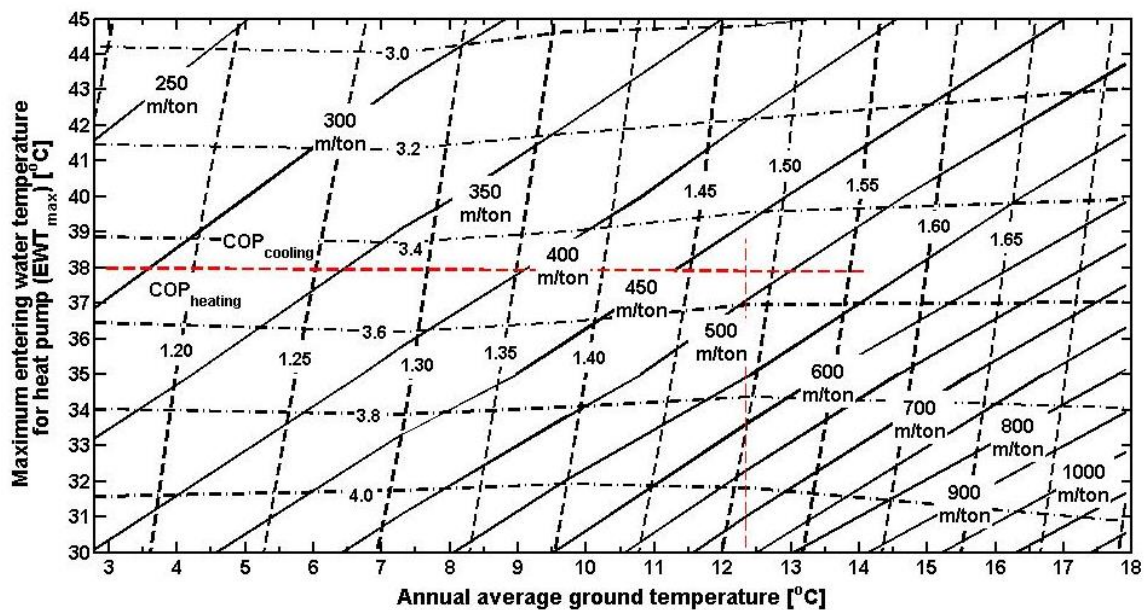


Figure 7-13: Design guide for thermo-active foundation system for small sized office building in New York, NY ($k_{soil}=1.3$ W/m-K, $k_{conc}=1.8$ W/m-K)

Table 7-6: Simulation results in maximum entering water temperature for New York, NY

Water-to-Water Heat Pump Model	Heat Pump Capacity [Ton]	EWT_max	COP_cooling
NSW-018	1.44 ton	37.65 °C	3.55
NSW-025	2.06 ton	49.02 °C	2.96

Using a linear interpolation of the simulation results indicated by Table 7-6, the EWT_{max} and COP for the water-to-water heat pump capacity of 1.5-ton can be determined. The estimated EWT_{max} for 1.5-ton heat pump is 38.71°C and the estimated COP is 3.496. The design chart specifications using Figure 7-13 have errors of 1.9% and 0.7% errors, respectively for EWT_{max} and COP (refer to Table 7-7).

Table 7-7: Comparison of linear interpolation result of the simulations and the prediction of design guide chart

	Design Guide Chart	Simulation Results	Percent Error [%]
EWT_{max}	38 °C (targeted EWT _{max})	38.71 °C	1.9%
COP_{cooling}	3.52	3.496	0.7%

Multi-family residential building in Chicago, IL.

This section considers the case of a multi-family residential building located in Chicago, IL as shown in Figure 7-14. The annual average ground temperature in Chicago, IL is 9.8°C (49.67°F). For this building, the targeted maximum entering water temperature to a heat pump is set to be 35°C (95°F). According to Figure 7-15, the required heat exchanger pipe length is 469m/ton. If the building has 28-12.5m precast concrete foundation piles as shown in Figure 7-14, then the available heat exchanger pipe length is at least 700m when every pile has one loop of heat exchanger pipe. With the selected pipe length per ton from the chart (469m/ton) and the calculated available heat exchanger pipe length, the required capacity of water-to-water heat pump can be estimated as shown in Figure 7-15. Therefore, the resulting water-to-water heat pump capacity for the building of Figure 7-14 is 1.49 ton for the maximum EWT of 35°C (95°F) in Chicago, IL (where has the ground temperature of 9.8°C or 49.67°F), and the COP for cooling is 3.72.

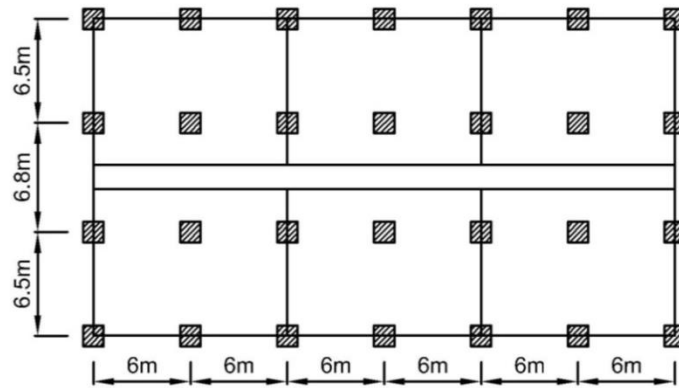


Figure 7-14: Location of foundation piles for the multi-family residential building in Chicago, IL

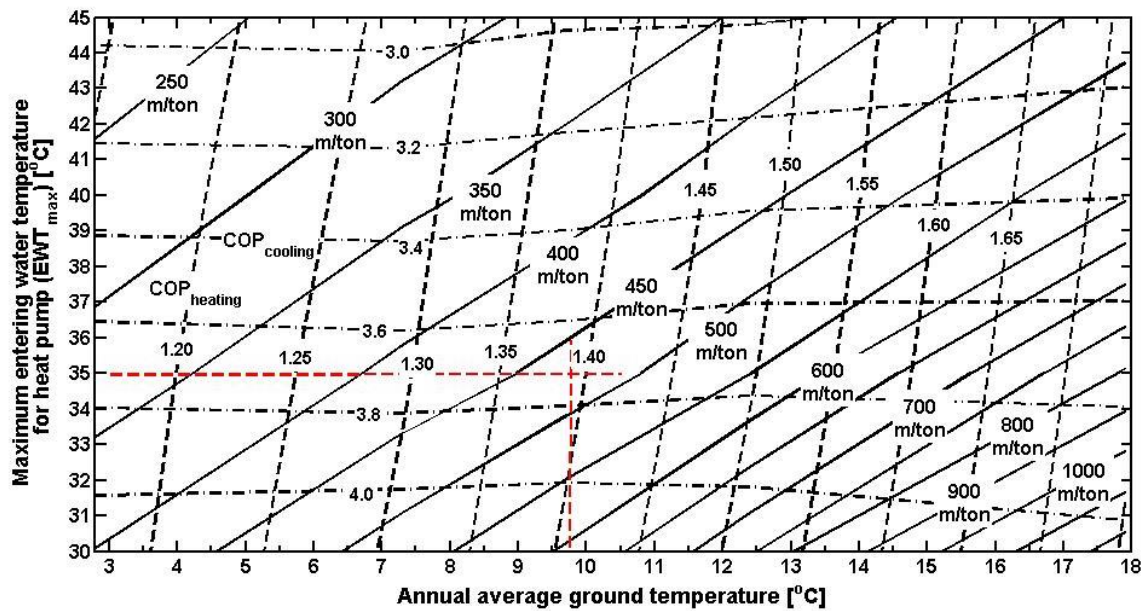


Figure 7-15: Design guide for thermo-active foundation system for the multi-family residential building in Chicago, IL
($k_{soil}=1.3 \text{ W/m-K}$, $k_{conc}=1.8 \text{ W/m-K}$)

To verify the results obtained from the chart of Figure 7-15, the multi-family residential building is modeled using EnergyPlus for Chicago, IL climate based on the calculated heat pump capacity. Since the capacity of a water-to-water heat pump is found to be 1.49-ton in the chart, heat pump sizes of 1.44-ton and 2.06-ton are simulated in the energy model. It is found that the heat pump capacity of 1.44-ton for the multi-family residential building equipped with 28-12.5m thermal foundation piles can

meet the targeted maximum EWT, while the heat pump with 2.06-ton capacity provides higher EWT than the targeted temperature as summarized in Table 7-8. Using linear interpolation of the simulated results listed in Table 7-8, the EWT_{max} and COP for the multi-family building can be estimated for the water-to-water heat pump capacity of 1.49-ton. Specifically, the EWT_{max} for 1.49-ton heat pump is determined to be 35.97, and the COP is calculated to be 3.71. The estimations of both EWT_{max} and COP have errors of 2.8% and 0.3%, respectively as outlined in Table 7-9.

Table 7-8. Using linear interpolation of the simulated results listed in Table 7-8, the EWT_{max} and COP for the multi-family building can be estimated for the water-to-water heat pump capacity of 1.49-ton. Specifically, the EWT_{max} for 1.49-ton heat pump is determined to be 35.97, and the COP is calculated to be 3.71. The estimations of both EWT_{max} and COP have errors of 2.8% and 0.3%, respectively as outlined in Table 7-9.

Table 7-8: Simulation results in maximum entering water temperature for Chicago, IL.

Water-to-Water Heat Pump Model	Heat Pump Capacity [Ton]	EWT_{max}	COP_{cooling}
NSW-018	1.44 ton	35.01 °C	3.76
NSW-025	2.06 ton	46.93 °C	3.05

Table 7-9: Comparison of linear interpolation result of the simulations and the prediction of design guide chart

	Design Guide Chart	Simulation Results	Percent Error [%]
EWT_{max}	35 °C (targeted EWT _{max})	35.97 °C	2.8%
COP_{cooling}	3.72	3.71	0.3%

7.5. Summary and conclusions

This chapter provided a set of design guidelines for thermo-active foundations for office buildings by investigating the impact of climate conditions on the minimum number of foundation piles required for TAF systems. It also estimated the proper size of the heat pump based on the foundation design. The selection criteria of the number of foundation piles are based on threshold limits of acceptable entering water temperature to a water-to-water heat pump.

The first analysis investigated the impact of climate zones on the required number of thermo-active foundation piles to meet the thermal loads of a prototypical office building. Then, the required number of thermo-active foundations is used to calculate the heat exchanger pipe length per water-to-water heat pump capacity.

Building on the results obtained for the heat exchanger pipe length per heat pump capacity for several climate conditions, this chapter develops a design chart for the thermo-active foundations. The design chart can help when determining a required heat exchanger pipe length per ton for a given building site, for a specific annual average ground temperature, and for a targeted maximum entering water temperature to a heat pump. The selected heat exchanger pipe length per ton is, then, used to determine the size of a water-to-water heat pump with respect to the design limitations of foundation piles due to structural or architectural needs. This chapter illustrated several example applications showing the usage of the design chart for different climates and for different building types. According to the results obtained from detailed simulations for the example cases, the design chart was found to provide good specifications to determine the required water-to-water heat pump size while meeting the targeted maximum EWT. Therefore, the design chart developed in this chapter has the potential to provide guidelines for designing TAF systems.

CHAPTER 8. SUMMARY AND FUTURE WORK

8.1. Summary

The main purposes of this research are: (i) developing a three-dimensional numerical model to estimate the thermal performance of thermo-active foundation (TAF) systems, (ii) adapting the existing GSHP equation of thermal response factor (G-function) calculation for TAF systems, (iii) generating thermal response factors using the new G-function calculation approach to model TAF systems in detailed building energy simulation tools, and (iv) providing guidelines for properly designing TAF systems.

Using numerical analysis, a three-dimensional finite difference model was developed as described in Chapter 3. The three-dimensional numerical model was validated utilizing measured data obtained from a laboratory experimental set-up performed by the Centrifuge Lab at the University of Colorado at Boulder. The initial RMSE between predictions and the uncalibrated model predictions was 2.32°C for the temperature field which was high but within the tolerance range of typical type-k thermocouples. Additional sensitivity analyses were performed and revealed that the thermal conductivity of foundation material had a significant impact on the predictions of the models for the temperature field. After calibration of the model, it was found that the numerical model was able to predict accurately the experimental data.

After the validation analysis, the impact of several design and operating parameters on thermal performance of TAF systems were evaluated. The results of the parametric analysis indicated that:

- The deeper the foundation pile is, the more heat is exchanged by the TAF system.

- The faster the fluid is flowing through the foundation loops, the more heat is exchanged by the TAF system with a sudden increase in heat transfer when the fluid flow shifted from laminar flow to turbulent regime.
- As the distance between the U-tube loops (shank space) becomes smaller, more thermal interactions occur and less heat transfer is exchanged by the TAF system.
- Increasing the thermal conductivities of ground and foundation material increases the heat transfer exchanged between ground and the foundation.
- However, the foundation, the flow rate, and the shank space had only minor thermal impact on the ground-coupled heat transfer through an above-grade floor.
- If the foundation pile is wide enough to hold several U-tube loops, more heat is exchanged by the TAF system.

The second achieved goal of this study was to develop an expression for computing TAF thermal response factors. The initial 'G-function' was developed by Eskilson (1987) and Yavuzturk (1999) for analyzing conventional ground-source heat pumps (GSHP). The main purpose of developing TAF-specific G-function was to take into account several features of TAF systems including (i) cross-sectional configurations of a foundation pile (i.e. circular section, square section, or rectangular section), and (ii) thermal relationships between ground surface and thermal foundation.

For taking into account cross-sectional configurations of thermo-active foundations, based on heat conduction theory, the existing GSHP G-function equation was updated by introducing a foundation shape factor (F_S). The foundation shape factor is consisted of the hydraulic diameter and

the perimeter of a foundation pile cross section ($F_S = \frac{2P}{D_H}$). This approach was verified using a mathematical approach deriving heat conduction equations for several configurations. By using the new expression, the G-function model developed for TAF systems agreed well with the reference data developed by Eskilson for long-time steps and by Yavuzturk for short-time steps.

Additionally, in order to take into account the contribution of indoor air temperature to the thermal performance of a TAF system, the G-function calculation is adjusted. So, additional boundary conditions including above-grade slab floor and indoor air temperatures are considered. Using the superposing approach, the finalized G-function can be calculated for TAF systems with considering the effects of indoor air temperatures on thermal piles. To validate the new G-function developed in this study, actual field test data were used. Using the new G-function values, the predicted outlet fluid temperatures were close to the actual field test data.

The study presented in this dissertation has integrated the G-function for TAF system into EnergyPlus, a whole-building energy simulation program, and then performed a series of simulation analyses to determine the required number of foundation piles for different heat pump capacities, and for different climate conditions. Building on the results of the simulation analysis, the required heat exchanger pipe length per heat pump capacity is determined for different targeted entering water temperatures. The results of the simulation analysis were also used to develop design guidelines for TAF systems. In particular, a design chart was developed to assist in determining the heat exchanger pipe length per heat pump capacity required to meeting a targeted maximum entering water temperature. The size of water-to-water heat pump can then be estimated using the number and depth of foundation piles. To show the application of the developed chart, an example application is considered for Chicago climate, a site not included in the development of the chart. The data obtained from the chart were

successfully used to determine the proper size of the water-to-water heat pump while meeting the maximum EWT.

8.2. Future work

The ultimate goals of the study presented in this thesis are to develop an accurate and appropriate thermal response factor of a TAF system, and to develop a comprehensive set of guidelines suitable to design and evaluate the performance for thermo-active foundation systems under various climatic and operating conditions. While the work presented in this dissertation has achieved these goals, the design guidelines need to be improved and extended to consider other design parameters, including:

- Various building sizes and building types
- Various climate conditions, including non-U.S. climate locations
- For some climate conditions where has imbalance cooling/heating loads
- The effect of thermal properties of ground and pile materials
- Heat and moisture transfer in ground medium

In addition, the research presented in this paper has several assumptions to evaluate energy performances of TAF system integrated into EnergyPlus. Especially, one of the assumptions is the single-pile approximation which neglects thermal interferences between thermal piles. Based on this assumption, this paper developed G-functions for a single thermal pile and applied it for multiple thermal piles which assuming to have enough distances between piles to avoid thermal interferences. However, for the better and accurate analysis and design guidelines, it needs to explore the effect of multi-thermal piles with respect to following considerations:

- G-function calculations designed for any placement of multi-thermal piles
- Considering the effect of locations of multi-thermal piles on G-function calculations; locations of corner, edge, or center
- Effect of multi-thermal piles on the design guidelines and on the energy performances of TAFs

REFERENCES

- A.D. Chiasson, C.C. Yavuzturk, D.W. Johnson, T.P. Filburn** Optimization of the Ground Thermal Response in Hybrid Geothermal Heat Pump Systems [Journal]. - [s.l.] : ASHRAE Transactions, 2010. - Vols. Vol. 116 Issue 1, p512-524. 13p.
- Adrian Bejan, Allan D. Kraus** Heat Transfer Handbook, (pp.167, 221) [Book]. - [s.l.] : John Wiley & Sons, Inc., 2003.
- Alaska Center for Energy and Power Cold Climate Housing Research Center** Ground-Source Heat Pumps in Cold Climates [Report]. - [s.l.] : A report for the Denali Commission, 2011.
- ASHRAE Research** ASHRAE Handbook: HVAC Applications - Chapter 32 [Book]. - 2007.
- ASHRAE Research** ASHRAE Handbook: HVAC Systems and Equipments - Chapter 26 [Book]. - 2008.
- Byung Chang Kwag, Moncef Krarti** 3D Numerical Analysis of Thermal Performance of Thermoactive Foundations for Commercial Buildings [Journal]. - [s.l.] : ASME, 2014.
- Byung Chang Kwag, Moncef Krarti** Development of a Response Factor Model for Thermo-Active Building Foundation [Conference] // ASME 2014 International Mechanical Engineering Congress & Exposition. - Montreal, Quebec, Canada : [s.n.], 2014. - Vols. 6b, IMECE2014-36350, doi:10.1115/IMECE2014-36350.
- Byung Chang Kwag, Moncef Krarti** Performance of Thermoactive Foundations for Commercial Buildings [Conference] // ASME 2012 International Mechanical Engineering Congress & Exposition. - Houston, Texas : ASME, IMECE2012-93121, 2012.
- Byung Chang Kwag, Moncef Krarti** Performance of Thermoactive Foundations for Commercial Buildings [Journal]. - [s.l.] : Journal of Solar Energy Engineering, 2013. - Vols. 135(4), 040907 (10 pages); Paper No: SOL-13-1016; doi:10.1115/1.4025587.
- Cenk Yavuzturk, Jeffrey D. Spitler** A Short Time Step Response Factor Model for Vertical Ground Loop Heat Exchangers [Journal]. - [s.l.] : ASHRAE Transactions, 1999. - Part 2, pp.465-474 : Vol. 105.
- Cenk Yavuzturk, Jeffrey D. Spitler, Simon J. Rees** A Transient Two-Dimensional Finite Volume Model for the Simulation of Vertical U-Tube Ground Heat Exchangers [Journal]. - [s.l.] : ASHRAE Transactions, 1999. - Part 2, pp.475-485 : Vol. 105.
- Christian Kaltreider** Heat Transfer Analysis of Thermo-active Foundations [Journal]. - 2011.
- Christopher J. Wood, Hao Liu, Saffa B. Riffat** An investigation of the heat pump performance and ground temperature of a piled foundation heat exchanger system for a residential building [Journal]. - [s.l.] : Energy, 2010. - pp.4932-4940 : Vol. 35.

- D. Adam, R. Markiewicz** Energy from earth-coupled structures, foundations, tunnels and sewers [Journal]. - [s.l.] : Geotechnique, 2009. - No 3, pp.229-236 : Vol. 59.
- D. Bozis, K. Papakostas, N. Kyriakis** On the evaluation of design parameters effects on the heat transfer efficiency of energy piles [Journal]. - [s.l.] : Energy and Buildings, 2011. - pp.1020-1029 : Vol. 43.
- Daniel E. Fisher, Simon J. Rees** Modeling ground source heat pump systems in a building energy simulation program (ENERGYPLUS) [Conference] // Building Simulation 2005, Ninth International IBPSA Conference. - Montreal, Canada : [s.n.], 2005.
- David P. Hart, Rick Couvillion** Earth-coupled Heat Transfer: Offers Engineers and Other Practitioners of Applied Physics the Information to Solve Heat Transfer Problems as They Apply to Earth-coupling [Book]. - [s.l.] : National Water Well Association, 1986.
- ENERGYPLUS TM** EnergyPlus Engineering Reference - pp.768-777. - 2010.
- F. Loveridge** The thermal performance of foundation piles used as heat exchangers in ground energy systems [Report]. - [s.l.] : University of Southampton, Faculty of Engineering and the Environment, Doctoral Thesis, 2012 a.
- F. Loveridge, W. Powrie** Pile heat exchangers: thermal behavior and interactions [Conference] // Institution of Civil Engineers, Geotechnical Engineering. - 2012 b. - Vols. 166, Issue GE2.
- F. Loveridge, W. Powrie** Temperature response functions (G-functions) for single pile heat exchangers [Journal]. - [s.l.] : Energy, 2013. - Vols. 57. pp.554-564.
- F.M. Rad, A.S. Fung, W.H. Leong** Combined solar thermal and ground source heat pump system [Conference] // 11th International IBPSA Conference. - Glasgow, Scotland : [s.n.], 2009.
- Frank Kreith, Mark S. Bohn** Principles of Heat Transfer, Sixth Edition - Chapter 3, Chapter 4 [Book].
- G. Phetteplace** Geothermal Heat Pumps [Journal]. - [s.l.] : ASEC, 2007. - 1(32), pp.32-38 : Vol. 133.
- H. Brandl** Energy foundations and other thermo-active ground structures [Journal]. - [s.l.] : Geotechnique, 2006. - No. 2, pp.81-122 : Vol. 56.
- H.S. Carslaw, J.C. Jaeger** CONDUCTION OF HEAT IN SOILDS, 2nd Edition [Book]. - [s.l.] : OXFORD, 1959.
- H.Y. Zeng, N.R. Diao, Z.H. Fang** A Finite Line-Source Model for Boreholes in Geothermal Heat Exchangers [Journal]. - [s.l.] : Heat Transfer - Asian Research, 2002. - Vols. 31, pp.559-567.
- Jalaloddin, Akio miyara, Koutaro Tsubaki, Shuntaro Inoue, Kentaro Yoshida** Experimental study of several types of ground heat exchanger using a steel pile foundation [Journal]. - [s.l.] : Renewable Energy, 2011. - Vols. 36, pp.764-771.
- James J. Hirsch** DOE-2.2 - Building Energy Use and Cost Analysis Program: Dictionary - pp.299-305. - [s.l.] : E. O. Lawrence Berkeley National Laboratory, 2009. - Vol. 2.

Jeffrey D. Spitler GLHEPRO – A DESIGN TOOL FOR COMMERCIAL BUILDING GROUND LOOP HEAT EXCHANGERS [Conference] // 4th International Conference on Heat Pumps in Cold Climate. - Aylmer, Quebec : [s.n.], 2000.

John A. Shonder, Patrick J. Hughes Increasing confidence in geothermal heat pump design methods [Conference] // Proc. 2nd Stockton Geothermal Conference. - 1998.

John S. McCartney Centrifuge Modeling of Soil-Structure Interaction in Geothermal Foundations [Report]. - 2010.

Jonathan J. Giardina Evaluation of ground coupled heat pumps for the state of Wisconsin [Conference]. - 1995.

Jun Gao, Xu Zhang, Jun Liu, Kuishan Li, Jie Yang Numerical and experimental assessment of thermal performance of vertical energy piles: An application [Journal]. - [s.l.] : Applied Energy, 2008. - Issue 10, pp.901-910 : Vol. 85.

Kentaro Sekine, Ryoza Ooka, Mutsumi Yokoi, Yoshiro Shiba, SuckHo Hwang Development of a Ground-Source Heat Pump System with Ground Heat Exchanger Utilizing the Cast-in-Place Concrete Pile Foundations of Buildings [Journal]. - [s.l.] : ASHRAE Transactions, 2007. - Vols. 113, pp.558-566.

L.R. Ingersoll, O.J. Zobel, A.C. Ingersoll Heat conduction with engineering, geological and other applications [Book]. - [s.l.] : University of Wisconsin Press, 1954.

Louis Lamarche, Benoit Beauchamp A new contribution to the finite line-source model for geothermal boreholes [Journal]. - [s.l.] : ENERGY and BUILDINGS, 2007. - Vols. 39, pp.188-198.

Louis Lamarche, Benoit Beauchamp New solutions for the short-time analysis of geothermal vertical boreholes [Journal]. - [s.l.] : International Journal of HEAT and MASS TRANSFER, 2007. - Vols. 50, pp.1408-1419.

Lyesse Laloui, Mathieu Nuth, Laurent Vulliet Experimental and numerical investigations of the behaviour of a heat exchanger pile [Journal]. - [s.l.] : International Journal for Numerical and Analytical Methods in Geomechanics, 2006. - Vols. 30, pp.763-781.

M. Krarti, C. Lopez-Alonzo, D.E. Claridge, J.F. Kreider Analytical Model to Predict Annual Soil Surface Temperature Variation [Journal]. - [s.l.] : Journal of Solar Energy Engineering by ASME, 1995. - Vols. 117, pp.91-99.

Melissa Ann Stewart, John Scott McCartney Centrifuge Modeling of Soil-Structure Interaction in Energy Foundations [Journal]. - [s.l.] : Journal of Geotechnical and Geoenvironmental Engineering, 2012.

Metka Pesl, Darko Goricanec, Jurij Krope Response Functions and Thermal Influence for Various Multiple Borehole Configurations in Ground Coupled Heat Pump Systems [Journal]. - [s.l.] : WSEAS TRANSACTIONS on HEAT and MASS TRANSFER, 2007. - 3, pp.61-71 : Vol. 2.

Mikael Philippe, Michel Bernier, Dominique Marchio Validity ranges of three analytical solutions to heat transfer in the vicinity of single boreholes [Journal]. - [s.l.] : Geothermics. - Vols. 38, pp.407-413.

Moncef Krarti Energy Audit of Building Systems: An Engineering Approach, Second Edition - Chapter 9 [Book]. - [s.l.] : Francis and Taylor, CRC Press, Boca Raton, Florida, 2010.

Natural Resources Canada's Office of Energy Efficiency (OEE) Heating and Cooling With a Heat Pump [Report]. - [s.l.] : Natural Resources Canada, 2004.

Oronzio Manca, Vincenzo Naso Solution to steady-state three-dimensional conduction for a rectangular surface heat source on a semi-infinite body [Journal]. - [s.l.] : International Communications in Heat and Mass Transfer, 1994. - 6, pp.799-808 : Vol. 21.

P.J. Bourne-Webb, B. Amatya, K. Soga, T. Amis, C. Davidson, P. Payne Energy pile test at Lambeth College, London: geotechnical and thermodynamic aspects of pile response to heat cycles [Journal]. - [s.l.] : Geotechnique, 2009. - 3, pp.237-248 : Vol. 59.

S. P. Rottmayer, W. A. Beckman, and J. W. Mitchell Simulation of a Single Vertical U-Tube Ground Heat Exchanger in an Infinite Medium [Journal]. - [s.l.] : ASHRAE Transactions, 1997. - Part 2, pp.651-659 : Vol. 103.

S.L. Abdelaziz, C.G. Olgun, J.R. Martin II Design and Operational Considerations of Geothermal Energy Piles [Conference] // Geo-Frontiers 2011: Advances in Geotechnical Engineering: ASCE Geotechnical Special Publication. - 2011. - Vols. No.211, pp.450-459.

Scott Hackel, Amanda Pertzborn Hybrid Ground-Source Heat Pump Installations: Experiences, Improvements and Tools [Report]. - [s.l.] : Energy Center of Wisconsin, 2011.

Signhild Gehlin, Bo Nordell Thermal response tests of boreholes - results from in situ measurements [Conference] // The Second Stockton International Geothermal Conference. - March 16 and 17, 1998.

Steve Kavanaugh An Instruction Guide for Using a Design Tool for Vertical Ground-Coupled, Groundwater and Surface Water Heat Pumps Systems - Ground Source Heat Pump System Designer, GshpCalc Version 5.0. - 2010.

Steve Kavanaugh, K. Rafferty Ground source heat pumps - Design of Geothermal Systems for Commercial and Institutional Buildings [Book]. - [s.l.] : ASHRAE, 1997.

T. Kusuda, P. R. Achenbach Earth temperature and Thermal Diffusivity at Selected Stations in the United States [Journal]. - [s.l.] : ASHRAE Transactions, 1965. - Part 1 : Vol. 71.

Tatyana V. Bandos, Alvaro Montero, Esther Fernandez, Juan Luis G. Santander, Jose Maria Isidro, Jezabel Perez, Pedro J. Fernandez de Cordoba, Javier F. Urchueguia Finite line-source model for borehole heat exchangers: effect of vertical temperature variations [Journal]. - [s.l.] : Geothermics, 2009. - Vols. 38, pp.263-270.

Thomas Ray Young Development, Verification, and Design Analysis of the Borehole Fluid Thermal Mass Model for Approximating Short Term Borehole Thermal Response // MS Thesis. - [s.l.] : Oklahoma State University, 2001.

U.S. Department of Energy's Energy Efficiency & Renewable Energy (EERE) Commercial Prototype Building Models [Online]. - July 2013. - <http://www.energycodes.gov/commercial-prototype-building-models>.

U.S. Department of Energy's Energy Efficiency & Renewable Energy (EERE) Guide to Geothermal Heat Pumps [Online]. - 2011. - http://energy.gov/sites/prod/files/guide_to_geothermal_heat_pumps.pdf.

U.S. Department of Energy's Energy Efficiency & Renewable Energy (EERE) Residential Prototype Building Models [Online]. - July 2013. - http://www.energycodes.gov/development/residential/iecc_models.

U.S. Energy Information Administration (EIA) Electricity rate of Colorado [Online]. - October 2014. - <http://www.eia.gov/state/rankings/?sid=CO#series/31>.

U.S. Energy Information Administration (EIA) Natural gas rate of Colorado [Online]. - October 2014. - <http://www.eia.gov/state/rankings/?sid=CO#series/28>.

V.V. Dharaiya, S.G. Kandlikar Numerical Investigation of Heat Transfer in Rectangular Microchannels Under H2 Boundary Condition During Developing and Fully Developed Laminar Flow [Journal]. - [s.l.] : Journal of Heat Transfer by ASME, 2012. - 020911-1-10 : Vol. 134.

WaterFurnace Inc. Heat Pump Product Catalog - Hydronic NSW, Hydronic NDW [Online]. - 2012. - <http://www.waterfurnace.com/literature/envision/SC1007WN.pdf>.

William H. Beyer CRC Standard Mathematical Tables, 26th Edition (pp.301, eq.157) [Book]. - [s.l.] : CRC Press, Inc., 1981.

Wojciech Kozak, Joachim Seifert, Wolfgang Richter Influence of ground heat exchanger modelling on the predicted efficiency of the heat pump system [Conference] // Building Simulation 2009. - Glasgow, Scotland : Eleventh International IBPSA Conference, 2009.

Yasuhiro Hamada, Hisashi Saitoh, Makoto Nakamura, Hideki Kubota, Kiyoshi Ochifuji Field performance of an energy pile system for space heating [Journal]. - [s.l.] : Energy and Buildings, 2007. - Vols. 39, pp.517-524.

Yunus A. Cengel, Michael A. Boles Thermodynamics And Engineering Approach, 5th Edition - Chapter 11 [Book]. - [s.l.] : McGraw-Hill Book Company, 2005.